

ALEXANDER ROTH

COLLECTIVE EFFECTS AND SUPERRADIANCE IN
ATOMIC ENSEMBLES

COLLECTIVE EFFECTS AND SUPERRADIANCE IN ATOMIC
ENSEMBLES

Von der Fakultät für Mathematik und Physik
der Gottfried Wilhelm Leibniz Universität Hannover
zur Erlangung des akademischen Grades

Doktor der Naturwissenschaften
Dr. rer. nat.

genehmigte Dissertation
von

M. Sc. Alexander Roth

geboren am 8.4.1989 in Trier, Deutschland

2018

Referent: Prof. Dr. Klemens Hammerer
(Universität Hannover, Institut für Theoretische Physik und Albert-Einstein-Institut)

Korreferent: Prof. Dr. Tobias J. Osborne
(Universität Hannover, Institut für Theoretische Physik)

Vorsitzender der Prüfungskommission: apl. Prof. Dr. Milutin Kovacev
(Universität Hannover, Institut für Quantenoptik)

Tag der Promotion: 7.9.2018

For my parents, my wife and my two daughters



ABSTRACT

This thesis contributes to the field of collective effects in atomic ensembles. We explore synchronization of superradiant lasers in different coupling configurations and study superradiance in off-resonantly probed atomic ensembles, where we take into account the complete level structure of alkali metal atoms. In the first part we introduce the superradiant laser and extend the discussion of synchronization of symmetrically coupled superradiant lasers to unidirectional coupled superradiant lasers. We show that synchronization is also present when we replace the superradiant laser couplings with classical channels, meaning the synchronization can be considered a classical effect.

In the second part we generalize a widely used approximation method taking into account lower order atom-atom correlations — the cumulant expansion method — to a basis independent formalism. We implement this formalism in a Python program allowing us to numerically calculate the n -atom reduced density matrix and two-time correlation functions for ensembles of multi-level atoms. This method allows us to study the stationary state of an ensemble of off-resonantly probed alkali metal atoms with a ground-state manifold consisting of many hyperfine levels. We show that collective effects in light-matter interaction depends on the tensor-polarizability of atoms and therefore cannot be explained on the basis of two-level-approximations.

keywords: collective effects, atomic ensembles, superradiant lasers, synchronization, unidirectional coupled superradiant lasers, atom-atom correlation, cumulant expansion method, two-time correlation functions, light-matter interaction, tensor-polarizability

ZUSAMMENFASSUNG

Diese Arbeit leistet einen Beitrag zum Verständnis von kollektiven Effekten in atomaren Ensembles. Wir untersuchen die Synchronisation von superradianten Lasern in verschiedenen Kopplungskonfigurationen und das Verhalten von einem off-resonant getriebenen atomaren Ensemble bei dem wir alle Niveaus der Alkalimetallatome berücksichtigen. In dem ersten Teil der Arbeit geben wir eine Einführung zu dem superradianten Laser und erweitern die Diskussion der Synchronisation von symmetrisch gekoppelten superradianten Lasern auf Synchronisation mit gerichteter Kopplung. Wir können zeigen, dass die Synchronisation als klassische Synchronisation betrachtet werden kann, da diese bei beiden Konfigurationen ebenfalls mit Kopplung durch einen klassischen Kanal vorhanden ist.

Im zweiten Teil der Arbeit verallgemeinern wir die bekannte Kumulanten Approximationsmethode, welche niedrige Ordnungen von Atom-Atom Korrelationen berücksichtigt, zu einem basis-unabhängigem Formalismus. Durch eine eigens programmierte Implementierung in Python können wir mit diesem Formalismus die n -atom reduzierte Dichtematrix numerisch evolvieren und sogar Zweizeitenkorrelationsfunktionen von Ensembles mit Mehrniveau-Atomen berechnen. Diese Methode wenden wir an um den stationären Zustand eines Ensembles aus off-resonant getriebenen Alkalimetallatomen mit mehreren Grundzustands-Hyperfineniveaus zu untersuchen. Wir zeigen dass die kollektiven Effekte der Atom-Licht-Wechselwirkung von der Tensorpolarisierbarkeit der Atome abhängt und deshalb nicht anhand von Zweiniveauapproximationen erklärt werden kann.

Schlagnworte: kollektive Effekte, atomare Ensembles, superradianter Laser, Kumulanten Approximationsmethode, Atom-Atom Korrelationen, Zweizeitenkorrelationsfunktionen, Tensorpolarisierbarkeit, Mehrniveau-Atome, Synchronisation

ACKNOWLEDGMENTS

I owe a tremendous professional and personal thank you to my advisor, Klemens Hammerer. He gave me the opportunity to learn and work in his group, where he had always an open door and could always find time to teach me new methods, to discuss problems, come up with new ideas, and to share his intuition into the underlying physical principles. He also introduced me to the topic of steady state superradiance, which led us to develop a new numerical method allowing me to merge my passion for physics and programming. Especially I thank him for the welcoming, friendly and open atmosphere in his group, that made it a pleasure to share problems and successes alike. This is one of the things I will miss most after leaving his group.

I thank my second supervisor and referee, Tobias Osborne, for many fruitful discussions and taking the time to referee this thesis. I also want to thank Reinhard Werner for the discussions and feedback of our new density matrix cumulant formalism.

I thank Rodrigo Thomas of the group of Eugene Polzik for countless discussions about the experimental setup.

I thank all of my current and former colleagues at Hannover and Mainz: Sahand Mahmoodian, Jonas Lammers, and Julian Großmann especially not only for many discussions about physics, but also for giving me feedback for my papers and thesis. I thank Kirill Tikhonov for working with me on the generalized superradiant laser, Ondřej Černotík for his help in learning about opto-mechanics, Niels Lörch for the introduction to machine learning, and Hashem Zoubi for insights into phase-transitions.

I thank Birgit Gemmeke for all her friendly and quick help for everything involving bureaucracy at the institute and making it look easy.

I thank all members and collegiates of the Research Training Group 1991 for the great time learning from each other.

I would like to thank the computer cluster team at the Leibniz University of Hannover for their support and the research training group 1991 for funding.

I could not be more grateful for all the help from my parents, my sister, and especially my wife Minyi Hu. She supported me in the bright and the dark times of research and together we managed to build our own family with two wonderful daughters: Amelie and Sophie.

CONTENTS

1	SUPERRADIANT LASER	5
1.1	Introduction and setup	5
1.2	Adiabatic elimination	6
1.2.1	Projector method	6
1.2.2	Application of the projector method	7
1.3	Approximation methods	8
1.4	Cumulant expansion	8
1.5	Spectrum	10
2	SYNCHRONIZATION OF SUPERRADIANT LASERS	13
2.1	Introduction	13
2.2	Synchronization through quantum channels	14
2.2.1	Synchronization of two atomic ensembles in a common cavity	14
2.2.2	Two atomic ensembles in separate cascaded cavities	17
2.3	Synchronization through classical channels	22
2.3.1	Unidirectional synchronization	22
2.3.2	Bidirectional synchronization	25
2.4	Summary	29
3	<i>n</i> -TH ORDER CORRELATIONS IN SYMMETRIC SYSTEMS	31
3.1	Introduction	31
3.2	Symmetric master equation	32
3.3	Density matrix cumulants	34
3.3.1	Symmetric density matrices and their truncation .	36
3.4	Two-time correlation functions in cumulant expansion . .	37
3.4.1	Generating function of two-time correlations . . .	39
3.4.2	Truncation of two-time correlations at second order	40
3.5	Examples	41
3.5.1	Steady state	42
3.5.2	Time evolution	42
3.6	Fundamental problems	44
3.6.1	Estimation of approximation errors	44
3.6.2	Problems	45
3.7	Summary	45
4	COLLECTIVE EFFECTS IN ATOMIC ENSEMBLES INTERACTING WITH LIGHT	47
4.1	Introduction	47
4.2	Generalized superradiant laser	48
4.2.1	Steady State	49
4.2.2	Spectrum	50
4.3	Three-level atom	53
4.3.1	Steady state expectation values	55
4.3.2	Spectrum	57
4.4	Alkali metal atoms with off-resonant probe beam	59
4.4.1	Introduction and definitions	59
4.4.2	Full atom-light interaction	62
4.4.3	Elimination of the spontaneous emission modes .	64

4.4.4	Replacing free space by a single mode cavity . . .	65
4.4.5	Elimination of the excited atom levels	66
4.4.6	Elimination of the cavity mode	69
4.4.7	Analysis	72
4.4.8	Results	76
4.5	Summary	78
5	CONCLUSION AND OUTLOOK	81
I	APPENDIX	
A	SUPERRADIANT LASER	85
A.1	The projector method	85
B	SYNCHRONIZATION OF SUPERRADIANT LASERS	89
B.1	Complete derivation for the bidirectional synchronization using a classical channel	89
C	COLLECTIVE EFFECTS IN ATOMIC ENSEMBLES INTERACTING WITH LIGHT	93
C.1	Scattering elimination relations	93
C.2	Gauging the electric field of the cavity	94
C.2.1	Free space	94
C.2.2	Cavity	95
C.2.3	Comparison	97
	BIBLIOGRAPHY	99

INTRODUCTION

The laws of quantum mechanics govern all known physical systems. While quantum mechanics fundamentally prevents certain operations, such as precise simultaneous measurements of non-commuting operators, it allows preparing states and performing measurements not possible in classical mechanics. The field of quantum metrology aims to use exactly this fact to enhance technically feasible measurement precisions up to the absolute limit dictated by quantum mechanics. Besides quantum metrology theoretical and experimental efforts are also pushing the boundary of what is technically possible in quantum computation and quantum communication.

Quantum computation promises polynomial and even exponential speed-up of certain algorithms, most famously the polynomial time factorization algorithm by Shor [1]. The challenges in quantum computation are to find a physical system that (1) can address many qubits individually, (2) allows controlled and coherent interactions between qubits, (3) minimizes decoherent effects on the qubits, and (4) is theoretically and technically scalable to microscopic lengths. Fulfilling all these criteria is an ongoing effort with many different candidates such as superconducting qubits [2, 3] or trapped ions [4, 5].

Quantum communication aims to create a worldwide network of quantum teleportation stations [6], allowing to communicate using quantum mechanical states, analogous to what the world wide web has done for classical information. While this quantum internet [7] would be crucial to link future quantum computers to a network, the first – more modest – goal is to use entanglement to facilitate the creation of secret keys between two parties with security guaranteed by quantum mechanics. These secret keys can then be used to encrypt classical information and communicate securely via the world wide web. The fundamental problem of quantum communication lies in the technical problem of exponential amplitude damping of light in glass fibers, the best known method for earthbound long-distance light communication. A whole class of protocols, called quantum repeaters [8], deals with overcoming this exponential loss and distributing entanglement between distant teleportation stations. Many repeater protocols use on the one hand light to bridge the long distances between stations and on the other hand non-moving quantum systems serving as quantum memories, such as ions [9], atoms [10], or atomic ensembles [11–13]. Using quantum memories at repeater stations allows overcoming the exponential scaling with distance and turns it into a polynomial scaling. The quantum memory-light interaction is therefore a crucial part of quantum repeaters.

The first protocols for quantum repeaters, such as the DLCZ protocol [11], were based on probabilistic events, such as a photodetection. Recently however there has been interest in dissipative protocols allowing a deterministic quantum state engineering [14] and even full quantum computation [15]. Dissipative protocols have the advantage that the desired state — engineered to be the steady state — is created without any

measurements lowering the technical requirements. It is therefore natural to consider dissipative protocols involving atomic ground states, such as hyperfine states, as a quantum memory. The atoms can either interact with the light strongly, in a cavity with high quality factor, or weakly as a dense atomic ensemble in a low quality factor cavity or even in free space. For strong coupling the atoms and cavity form together a joint quantum system, that behaves significantly different than the individual components. For the full understanding of such a system a diagonalization is very helpful, but not always feasible. For weak coupling the atoms and cavity evolve dominantly independently with the interaction being a weak disturbance. This weak interaction between light, which typically has a short coherence time compared to the atomic ground states, and atoms can create significant correlations between the atoms themselves, giving rise to collective effects such as superradiance.

In this thesis we focus on the description of identical atoms coupling weakly and identically to light. The identical coupling of each atom to the light mode(s) therefore associates a creation or destruction of a photon to a collective atomic jump. In the simplest possible case of N excited two-level atoms and collective decay, one can observe superradiance [16, 17]. Dicke described it as: *“For want of a better term, a gas which is radiating strongly because of coherence will be called superradiant.”* The pure states of collective excitation the two-level atoms takes on are called Dicke states. Recently superradiance has received renewed interest, because of the theoretical prediction of a new kind of laser – the superradiant laser [18]. While its power output is just enough to be technically usable, it makes up with its supernarrow linewidth of the order of mHz. In the superradiant laser each atom is continuously repumped with the same rate as the collectively enhanced decay. The laser operates in a regime where the repumping continuously destroys — and the collective decay continuously creates — atom-atom correlations. This laser operated in steady state, with its frequency identical to the atomic frequency, can serve as a new kind of atomic clock, also called an active atomic clock. Steady-state superradiance however is a collective phenomenon not only relevant for atomic clocks, but for all weakly coupled systems having a competition between local and collective evolution.

This thesis contributes to collective effects due to superradiance in atomic ensembles and focuses on two different topics: Synchronization of superradiant lasers in Chapter 2 and steady-state superradiance in multi-level atoms as relevant for quantum communication protocols in Chapter 4. Master equations governing ensembles of multi-level atoms are however not feasible to solve with the previously used analytical methods. To be able to make predictions for these ensembles we generalized the analytical basis-dependent approximation method to a basis-independent formalism in Chapter 3, allowing us to not only take into account the multiple levels, but also increase precision arbitrarily high. We apply this method in Chapter 4 to an off-resonantly probed ensemble of Caesium atoms to study the collective effects and dependence on various parameters. In the following we give a short overview over the thesis structure. All Chapters were created by me, Alexander Roth, under the supervision of Klemens Hammerer. Kirill Tikhonov developed the analytical formulas

of the generalized superradiant laser in Section 4.2 together with me and Klemens Hammerer. Kirill also created the Figures 1.2, 1.3, 4.2, 4.3, 4.4, and 4.5. All other figures were created by me.

CHAPTER 1 briefly reviews the superradiant laser developed in [18].

We introduce the master equation with atom-cavity interaction and adiabatically eliminate the cavity mode using the projector method, which is used multiple times throughout the thesis. From the resulting atom-only master equation we derive the differential equation system of moments up to second order and apply the moment factorization [19] based on approximately vanishing cumulants. This equation system can be solved analytically for the steady state, resulting in the solutions of the polarization and atom-atom correlations.

CHAPTER 2 develops the synchronization behavior of superradiant lasers in different configurations. This is very important for future applications of the superradiant laser as atomic clocks, where one can link many superradiant lasers together to a network for greater stability against local disturbances. For the simplest configuration of two frequency detuned ensembles in a single cavity Xu et al. showed that frequency synchronization occurs over a large detuning regime [19]. We analyze the situation for unidirectional quantum-coupling, i.e., the output of one superradiant laser is fed into another, for classical unidirectional coupling involving a measurement, and for classical bi-directional coupling involving two measurements. We show synchronization appears for all of these cases, even though each configuration has its own subtleties. The unidirectional quantum and classical coupling synchronize also in a large parameter regime, however the behavior in the parameter regime outside complete synchronization is fundamentally different than in the symmetric coupling. The fact that synchronization appears for the unidirectional and for the symmetric classical coupling shows that the synchronization of superradiant lasers can be regarded as a classical phenomenon.

The contents of this have been published in [20].

CHAPTER 3 develops a general method to decompose the density matrix into orders of atom-atom correlations, which we name density matrix cumulants. Density matrix cumulants of order k contain all k -order cumulants capturing all correlations of k subsystems. This novel formalism to capture cumulants in a basis independent fashion allows to derive a general approximation method for a large class of permutation-invariant master equations with unitary interactions of up to two atoms and collective decay. This method we implement in a comprehensive and flexible Python program, which can integrate all master equations of this class for arbitrary parameters. We demonstrate at the example of the superradiant laser, that we can include correlations up to sixth order, meaning correlations involving up to six atoms. We also demonstrate that we can get not only the steady state, but the full time-evolution

and show the superradiant burst exists even in the presence of significant dephasing.

The contents of this chapter are going to be published in [21].

CHAPTER 4 is separated into three sections for better readability: Section 4.2 is introducing an ensemble of two-level systems with continuous single-atom jumps and collective jumps, both from excited to ground state (down) and from ground to excited state (up) – which we name the generalized superradiant laser. When this generalized superradiant laser operates in the superradiant regime the spectrum shows two ultranarrow Lorentz peaks. Their amplitude and width depends on the rate imbalance of collective down and up jumps. In Sec. 4.3 we introduce an off-resonantly probed atom with a three levels in the ground-state manifold, serving as a simple, yet powerful model system, to understand the behavior of Caesium atoms. We show that the angle of linear polarization of the probe laser controls the rate imbalance of collective down and up jumps of the two transitions. In Sec. 4.4 we derive the master equation governing the evolution of the off-resonantly probed room-temperature Caesium gas, inspired by the experiments of Eugene Polzik [12, 22–24]. The off-resonant probe laser induces coherent and incoherent two-photon transitions in the ground-state manifold, both dependent on the angle of linear polarization of the probe laser. With the implementation of the density matrix cumulants and approximation method in Chapter 3 we integrate this master equation numerically until a steady state is reached.

The contents of this chapter are going to be published in [25].

SUPERRADIANT LASER

1.1 INTRODUCTION AND SETUP

Atomic clocks based on optical transitions already achieve record precisions with fractional uncertainties of 10^{-18} [26] and offer great potential for further improvements [27]. Notably, current optical clocks are limited in precision by the instability of the laser used for interrogating the atomic reference system rather than by the linewidth of the clock transition [28]. In order to overcome this limitation the concept of an active atomic clock – also called superradiant laser has been suggested where a lattice of cold atoms with ultra-narrow clock transition itself serves as a laser gain medium resulting in radiation with extremely narrow linewidth in the mHz regime [18, 29–32]. This would remedy the need to reference an external laser to an atomic clock transition.

An active clock laser operates in a regime with inverted timescales as compared to a normal laser [18]: In the usual case atoms are pumped incoherently faster than the laser cavity decays. The cavity amplitude then amplifies through stimulated emission only those frequencies which fit within the cavity linewidth. In an active clock laser the atoms are pumped incoherently much slower than the cavity decays. Due to the long lifetime of atomic coherences, correlations between the atoms build up leading to a collectively enhanced, superradiant emission into the cavity. The correlations between the atoms result in a linewidth of the output light which is on the order of the one of the atomic transition itself.

In this Chapter we want to introduce a brief theoretical description and most important theoretical predictions of the superradiant laser. The setup (see Fig. 1.1) consists of N two-level atoms placed in a cavity with linewidth κ . Each atom has the two states $|g\rangle$, $|e\rangle$ with the transition frequency ν . The transition $|g\rangle \leftrightarrow |e\rangle$ couples to the cavity mode \hat{a} with a single photon Rabi frequency $\Omega/2$. The cavity frequency is set to be resonant with the atom transition frequency ν . Atoms also decay from $|e\rangle$

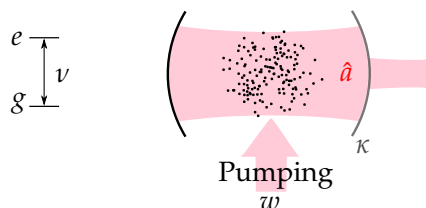


Figure 1.1: An ensemble of two level systems coupled to a cavity mode with annihilation operator \hat{a} . The frequency ν is the transition frequency between the states $|e\rangle$ and $|g\rangle$. The atoms are pumped incoherently from $|g\rangle$ to $|e\rangle$ via a third fast decaying level (not shown in level scheme) at rate w and decay from $|e\rangle$ to $|g\rangle$ predominantly through the cavity. The cavity decays at rate κ .

to $|g\rangle$ into free space with rate γ_s and are incoherently repumped from $|g\rangle$ to $|e\rangle$ with the rate w through an already eliminated third level (not shown in Fig. 1.1). In a frame rotating at the cavity frequency the system is described by the Lindblad master equation

$$\dot{\rho} = \frac{\Omega}{2i} [\hat{a}^\dagger \hat{f}^- + \hat{a} \hat{f}^+, \rho] + \kappa \mathcal{D}[\hat{a}] \rho + \sum_{j=1}^N \left(\gamma_s \mathcal{D}[\hat{\sigma}_j^-] + w \mathcal{D}[\hat{\sigma}_j^+] \right) \rho \quad (1.1)$$

where $\hat{\sigma}_j^z = |e\rangle \langle e|_j - |g\rangle \langle g|_j$, $\hat{\sigma}_j^+ = |e\rangle \langle g|_j$, and $\hat{\sigma}_j^- = |g\rangle \langle e|_j$ for atom $j \in \{1, \dots, N\}$. We used the definitions of the collective spin operators $\hat{f}^\pm := \sum_{i=1}^N \hat{\sigma}_i^\pm$, $\hat{f}^z := \frac{1}{2} \sum_{i=1}^N \hat{\sigma}_i^z$, and the Lindblad superoperator $\mathcal{D}[A] \rho := A\rho A^\dagger - \frac{1}{2}[A^\dagger A, \rho]_+$ where $[\cdot, \cdot]_+$ denotes the anti-commutator.

1.2 ADIABATIC ELIMINATION

The cavity is assumed to decay fast, meaning $\kappa \gg w, \Omega/2$, which allows for an adiabatic elimination of the cavity mode \hat{a} . While there are several methods for adiabatic elimination in Schrödinger and in Heisenberg picture, we briefly introduce a very general method in Schrödinger picture, which we will use countless times throughout the thesis.

1.2.1 Projector method

The *projector method* [33] is a formalism to eliminate a system B (in our case it will mostly be a cavity mode) of a master equation of the form

$$\dot{\rho}_{AB} = (L_A + L_B + L_{AB}) \rho_{AB}$$

where L_A is a superoperator acting on system A , L_B is a superoperator acting on system B , and L_{AB} is a superoperator acting on both systems. We start with defining the projector P defined by

$$P\rho_{AB}(t) = \text{Tr}_B [\rho_{AB}(t)] \otimes \rho_B^{\text{ss}}(t)$$

and the complement $Q = \mathbb{1} - P$. Crucial in the adiabatic elimination is the *weak coupling* assumption, meaning the evolution of L_{AB} is much slower than the evolution L_B of system B . Additional to the weak coupling assumption, one requires to assume (i) that there is one unique steady state of the system B fulfilling $L_B \rho_B^{\text{ss}}(t) = 0$, and (ii) the interaction term fulfills $PL_{AB}P = 0$.

After an instructive calculation (see appendix A.1) we derive the evolution of system A only

$$\begin{aligned} \dot{\rho}_A(t) = & L_A \rho_A(t) \\ & + \text{Tr}_B \left[L_{AB} \int_0^\infty d\tau e^{(L_A + L_B)\tau} Q L_{AB} e^{-L_A \tau} \rho_A(t) \otimes \rho_B^{\text{ss}}(t) \right]. \end{aligned} \quad (1.2)$$

We want to point out that this equation, though an evolution equation of ρ_A , is not always corresponding to a completely positive map, and

therefore can lead to unphysical states ρ_A after integration. In general one has to be able to either make a Rotating Wave Approximation, or L_A has to vanish [34, p. 132,133].

1.2.2 Application of the projector method

We can now directly apply equation (1.2) to the situation of the super-radiant laser, because (i) $L_B(\rho) = \kappa \mathcal{D}[\hat{a}]\rho$ has a unique steady state (the vacuum state), (ii) the interaction fulfills $PL_{AB}P = 0$, and the systems couple weakly, meaning $\kappa \gg \Omega/2$. In the first step we can approximate the integrand

$$e^{(L_A+L_B)\tau} Q L_{AB} e^{-L_A\tau} \rho_A(t) \otimes \rho_B^{ss}(t) \approx e^{L_B\tau} Q L_{AB} \rho_A(t) \otimes \rho_B^{ss}(t).$$

This is a good approximation because the fast decay rate κ implies that the integrand only contributes significantly for $\tau < 1/\kappa$. For these short times $\tau < 1/\kappa$ the term $e^{-L_A\tau}$ is approximately the identity because L_A evolves on the much slower timescale $w \ll \kappa$. This gives

$$\begin{aligned} & \dot{\rho}_A(t) - L_A \rho_A(t) \\ & \approx \text{Tr}_B \left[L_{AB} \int_0^\infty d\tau e^{L_B\tau} Q L_{AB} \rho_A(t) \otimes \rho_B^{ss}(t) \right] \\ & = \frac{\Omega}{2i} \text{Tr}_B \left[L_{AB} \int_0^\infty d\tau e^{L_B\tau} \left(\hat{f}^- \rho_A(t) \otimes \hat{a}^\dagger \rho_B^{ss} - \text{h.c.} \right) \right] \\ & = \frac{\Omega}{2i} \text{Tr}_B \left[L_{AB} \int_0^\infty d\tau \hat{f}^- \rho_A(t) \otimes e^{L_B\tau} \hat{a}^\dagger \rho_B^{ss} - \text{h.c.} \right] \\ & = -\frac{\Omega^2}{4} [\hat{f}^+, \hat{f}^- \rho_A(t)] \int_0^\infty d\tau e^{-\frac{\kappa}{2}\tau} + \text{h.c.} \\ & = -\frac{\Omega^2}{2\kappa} [\hat{f}^+, \hat{f}^- \rho_A(t)] + \text{h.c.} \\ & = \gamma \mathcal{D}[\hat{f}^-] \rho_A(t) \end{aligned}$$

where we defined $\gamma = \Omega^2/\kappa$. The adiabatic elimination translated the Lindblad term of the cavity decay $\kappa \mathcal{D}[\hat{a}]\rho$ to a collective decay of the atoms $\gamma \mathcal{D}[\hat{f}^-]\rho$ with the effective atomic decay rate γ . The decay into the cavity mode is enhanced by a factor of N and dominates the decay process [29], i.e., $\gamma N \gg \gamma_s$ giving the master equation

$$\dot{\rho} = \gamma \mathcal{D}[\hat{f}^-] \rho + \sum_{j=1}^N w \mathcal{D}[\hat{\sigma}_j^+] \rho. \quad (1.3)$$

This adiabatic elimination with the projector method above is effectively equivalent to a much simpler adiabatic elimination method using operator relation

$$\hat{a} \simeq -\frac{i\Omega}{\kappa} \hat{f}^-, \quad (1.4)$$

which can be derived from the Quantum Langevin equation of the cavity mode \hat{a} and removing quantum fluctuations. The projector method is however more useful for us, since it allows to handle also very complicated situations, as occurring in the later chapters, in a straight forward and mathematical rigorous manner.

1.3 APPROXIMATION METHODS

The dimensionality of the density matrix in master equation (1.3) is daunting: 4^N for N atoms where N in experiments where superradiant effects are involved is e.g. 10^6 [30], 10^8 [22], and 10^{16} [35]. The dimensionality of the density matrix alone is far beyond anything a computer can handle and it is therefore necessary to approximate the exact evolution (1.3). Depending on the relation of both parameters γ and w different approximation methods apply:

$w \gg N\gamma$: The incoherent pumping term dominates even collectively enhanced decay. The steady state will be necessarily close to a product state of N atoms. If the initial condition is not a strongly correlated state, we can approximate that the density matrix can be written as $\rho_N = \otimes_{j=1}^N \rho_j$, where ρ_j is the reduced density matrix of atom j . One can then derive a nonlinear mean-field evolution equation. While the mean-field, meaning expectation values of single atom-operators are taken into account, this method neglects all atom-atom correlations in the state and evolution.

$w \ll \gamma$: The collective term dominates even without any correlations in the initial state. This is the case if we do not have continuous processes, but for example polarize the atoms first with a strong pumping only and then switch on the collective interaction without any pumping. We can then do a Holstein–Primakoff transformation to $\hat{b} := (N/2 + J^z)^{-1/2} J^+$ and approximation $\hat{b} \approx (N/2 + \langle J^z \rangle)^{-1/2} J^+$ for highly polarized atoms giving a nonlinear evolution equation of the mode \hat{b} . This nonlinearity can however be removed if the spins are so highly polarized that one can assume $\langle J^z \rangle \approx N/2$.

$w > \gamma$: Pumping and collective decay are of similar order of magnitude and we cannot neglect either term. The steady state is assumed to have up to k -atom correlations with $k \ll N$ with relevant dynamics for the lower-order moments. This is the regime where the cumulant expansion and approximation can be applied and which we will introduce in the following section.

1.4 CUMULANT EXPANSION

The cumulant expansion effectively labels the basis vectors of the operator space by their correlations. This has the advantage, that one can truncate the basis at a certain number atoms involved in correlations. This truncation is of course only a good approximation if the state one wants to work with, such as the steady state of (1.3), has only insignificant amplitudes

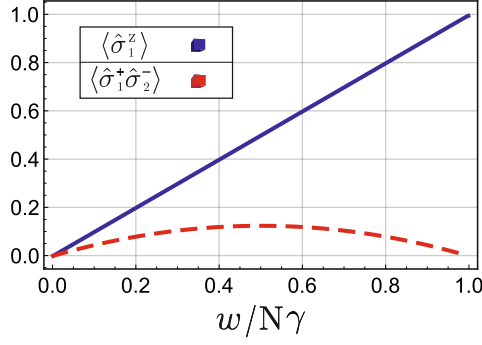


Figure 1.2: The polarization $\langle \sigma_1^z \rangle$, and atom-atom correlation $\langle \sigma_1^+ \sigma_2^- \rangle$ versus the single-atom pump rate w . The plot shows the characteristic linearly increasing polarization and inverted parabola for the correlations.

of truncated basis vectors. In fact in Chapter 3 we will develop a method to do this labeling according to correlations in a basis independent way. For now however we will present the cumulant expansion method in a certain basis as it was used in the derivation of the superradiant laser [18, 19].

Using the master equation (1.3) we calculate the moment dynamics

$$\begin{aligned} \frac{d}{dt} \langle \hat{\sigma}_1^z \rangle &= - \langle \hat{\sigma}_1^z \rangle (\gamma + w) - 2\gamma (N - 1) \langle \hat{\sigma}_1^+ \hat{\sigma}_2^- \rangle - \gamma + w \\ \frac{d}{dt} \langle \hat{\sigma}_1^+ \hat{\sigma}_2^- \rangle &= - (\langle \hat{\sigma}_1^+ \hat{\sigma}_2^- \rangle (\gamma + w) - \gamma \langle \hat{\sigma}_1^+ \hat{\sigma}_2^- \hat{\sigma}_3^z \rangle (N - 2)) \\ &\quad + \frac{\gamma}{2} (\langle \hat{\sigma}_1^z \hat{\sigma}_2^z \rangle + \langle \hat{\sigma}_1^z \rangle) \end{aligned} \quad (1.5)$$

where we used the permutation invariance to relabel atoms, e.g., $\langle \hat{\sigma}_1^z \hat{\sigma}_2^z \rangle = \langle \hat{\sigma}_i^z \hat{\sigma}_j^z \rangle$ for $i \neq j$. While the differential equation system (1.5) is linear, it is not closed. In fact moments of order k will couple to moments of order $k + 1$, creating a hierarchy of moments. The number of equations in this hierarchy scales exponentially in N for inhomogeneous systems and is still scaling polynomially in N for symmetric systems. This exponential improvement is possible due to the Schur basis [36] labeling the basis elements with their respective Young tableau [37] symmetry properties. One can then pick out the fully symmetric basis elements to describe the symmetric states. While this is an exponential improvement, the polynomially large basis of $(N^3 + 6N^2 + 11N + g)/6$ elements [38] is still intractable for realistic atom numbers, e.g., $N = 10^8$, and the scaling gets worse for more than two-level atoms.

To truncate this hierarchy we are in need to approximate the moments $\langle \hat{\sigma}_1^z \hat{\sigma}_2^z \rangle$ and $\langle \hat{\sigma}_1^+ \hat{\sigma}_2^- \hat{\sigma}_3^z \rangle$. As mentioned above we expect the steady state to be in some sense close to a product state, meaning the higher order correlations are insignificant. Quantum and classical correlations between subsystems, such as atoms, are captured in joint cumulants, which we will just call cumulants. It is therefore natural to assume the cumulants of

the moments $\langle \hat{\sigma}_1^z \hat{\sigma}_2^z \rangle$ and $\langle \hat{\sigma}_1^+ \hat{\sigma}_2^- \hat{\sigma}_3^z \rangle$ vanish approximately [19, 29] giving the relations

$$\begin{aligned} 0 &\approx \langle \hat{\sigma}_1^z \hat{\sigma}_2^z \rangle_c = \langle \hat{\sigma}_1^z \hat{\sigma}_2^z \rangle - \langle \hat{\sigma}_1^z \rangle \langle \hat{\sigma}_2^z \rangle, \\ 0 &\approx \langle \hat{\sigma}_1^+ \hat{\sigma}_2^- \hat{\sigma}_3^z \rangle_c = \langle \hat{\sigma}_1^+ \hat{\sigma}_2^- \hat{\sigma}_3^z \rangle - \langle \hat{\sigma}_1^+ \hat{\sigma}_2^- \rangle \langle \hat{\sigma}_3^z \rangle \end{aligned}$$

where we used the J^z symmetry of the master equation, resulting in $\langle \hat{\sigma}_i^\pm \rangle = 0$ for the steady state and every atom i . This approximation allows to close (1.5) resulting in the nonlinear differential equation system

$$\begin{aligned} \frac{d}{dt} \langle \hat{\sigma}_1^z \rangle &= -\langle \hat{\sigma}_1^z \rangle (\gamma + w) - 2\gamma (N - 1) \langle \hat{\sigma}_1^+ \hat{\sigma}_2^- \rangle - \gamma + w \\ \frac{d}{dt} \langle \hat{\sigma}_1^+ \hat{\sigma}_2^- \rangle &= -\langle \hat{\sigma}_1^+ \hat{\sigma}_2^- \rangle (\gamma + w - \gamma \langle \hat{\sigma}_1^z \rangle (N - 2)) \\ &\quad + \frac{\gamma}{2} \langle \hat{\sigma}_1^z \rangle (\langle \hat{\sigma}_1^z \rangle + 1). \end{aligned} \quad (1.6)$$

In the steady state, meaning all time derivatives of moments vanish, we can analytically solve this equation system giving a quadratic equation. The solution of the polarization and atom-atom correlations are plotted in Fig. 1.2.

Correlations can build up only in the superradiant regime

$$\gamma < w < N\gamma. \quad (1.7)$$

At the lower boundary the pumping w overcomes the single atom decay rate γ , creating a population inversion, and at the upper boundary the pumping w overcomes even the collectively enhanced decay rate $N\gamma$ [19, 29].

1.5 SPECTRUM

The spectrum $S(\omega)$ can be related to the atomic operators

$$\begin{aligned} S(\omega) &= \frac{\kappa}{2\pi} \int d\tau e^{-i\omega\tau} \langle \hat{a}^\dagger(\tau) \hat{a}(0) \rangle \\ &\approx \frac{N\Omega^2}{2\pi\kappa} \int d\tau e^{-i\omega\tau} \{ (N - 1) \langle \hat{\sigma}_1^+(\tau) \hat{\sigma}_2^-(0) \rangle + \langle \hat{\sigma}_1^+(\tau) \hat{\sigma}_1^-(0) \rangle \} \end{aligned} \quad (1.8)$$

where we consider vacuum cavity input and used the operator relation (1.4) of the adiabatic elimination. The spectrum (1.8) is written without the shot noise contribution following [39, (2.4-5)]. The atomic two-time correlations functions can be derived by applying the Quantum Regression Theorem [40, Sec. 3.2] on the moment evolution

$$\frac{d}{dt} \langle \hat{\sigma}_1^+ \rangle = -\frac{1}{2} (\gamma + w) \langle \hat{\sigma}_1^+ \rangle + \frac{\gamma}{2} (N - 1) \langle \hat{\sigma}_1^+ \hat{\sigma}_2^z \rangle \quad (1.9)$$

for the steady state $t = 0$ and an arbitrary atom j resulting in

$$\frac{d}{d\tau} \langle \hat{\sigma}_1^+(\tau) \hat{\sigma}_j^-(0) \rangle = -\frac{\Gamma}{2} \langle \hat{\sigma}_1^+(\tau) \hat{\sigma}_j^-(0) \rangle, \quad (1.10)$$

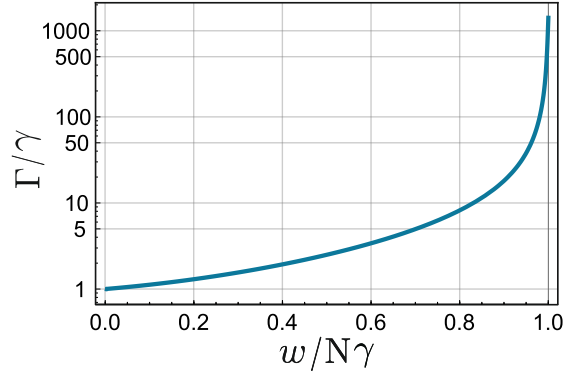


Figure 1.3: Linewidth Γ of the emitted light of the cavity versus the pumping strength w . In most of the superradiant regime and especially at the optimal pumping strength $w = N\gamma/2$ is the linewidth of the order of the effective atomic decay rate γ itself.

for the linewidth $\Gamma = \gamma + w - \gamma(N-1)\langle\hat{\sigma}_1^z\rangle$. We factorized the two-time correlation function $\langle(\hat{\sigma}_1^+\hat{\sigma}_2^z)(\tau)\hat{\sigma}_j^-(0)\rangle \approx \langle\hat{\sigma}_1^+(\tau)\hat{\sigma}_j^-(0)\rangle\langle\hat{\sigma}_1^z\rangle$ according to [19] and will explain this factorization in a general and systematic way in Sec. 3.4. The linewidth Γ , plotted in Fig. 1.3, can be approximated to leading order $1/N$ as

$$\frac{\Gamma}{\gamma} \approx \frac{1}{W(1-W)} + \frac{W}{1-W} - W - \frac{1}{W}$$

where we defined the dimensionless pumping rate $W := w/N\gamma$. For low pumping rates $w \ll N\gamma$ the linewidth can be approximated as $\Gamma/\gamma = 1 + w/N\gamma$. The Fourier transform in the Spectrum (1.8) converts the exponential solution of (1.10) into two Lorentz peaks. The dominant Lorentz peak will be the one created by the first term, as long as the steady state has correlations $\langle\hat{\sigma}_1^+\hat{\sigma}_2^-\rangle \gg 1/N$. The remarkable property is that the linewidth Γ is of the order of the effective atomic decay rate γ of the atoms themselves (see Fig. 1.3), which can in principle be ultra-narrow as in alkaline-earth-metal atoms [41].

2.1 INTRODUCTION

The superradiant laser, introduced in the previous Chapter, has an additional remarkable property: Recently it was shown by Xu et al. [19] and experimentally demonstrated by Weiner et al. [42] that two frequency-detuned atomic ensembles coupling to the same cavity mode operated in the superradiant regime synchronize in a large detuning range; they radiate at the mean frequency while preserving the narrow linewidth. For larger detuning the ensembles will cross through a phase transition separating the synchronized from the unsynchronized phase and then behave like two independent superradiant lasers at their natural frequency. The synchronization dynamics of superradiant lasers serving as active atomic clocks receives particular importance in the perspective of quantum networks of atomic clocks as envisioned in [43] for enhanced positioning, navigation and geodesy. However, the results of [19, 42] cannot be directly applied to the context of synchronization of remote atomic clocks as the two atomic ensembles are coupled to a common cavity mode.

In this Chapter we extend the analysis of [19] and consider two remote superradiant lasers coupled through an optical channel in the cascaded configuration of a master and a slave laser. We determine the phase diagram of synchronization and determine the parallels and differences to the case of a setup with symmetric coupling studied in [19, 42].

Additionally we consider the question whether the synchronization in the symmetric and cascaded configuration are due to *classical* synchronization or *quantum* synchronization. There has not yet been a clear measure to distinguish both, even though synchronization of quantum system has been the topic of several papers [44–48]. We will test both configurations by replacing the quantum channel (the light mode) with an idealized classical channel (measurement and feedback by a laser) and will find that in both cases that the classical channel only introduces noise, but does not inhibit synchronization, such that it can be regarded as classical synchronization.

The Chapter is organized as indicated in the following table:

	Symmetric coupling	Cascaded setup
Quantum channel	Review of [19], Sec. 2.2.1	Sec. 2.2.2
Classical channel	Sec. 2.3.2	Sec. 2.3.1

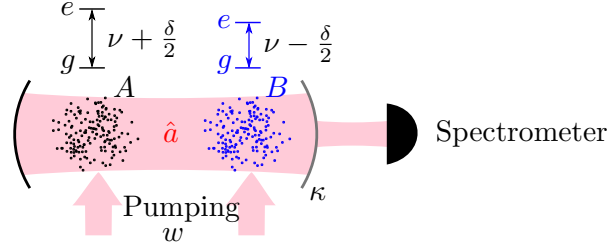


Figure 2.1: Two ensembles of two level systems (A and B) coupling to the same cavity mode \hat{a} , as considered in [19]. The frequencies of the transitions $|g\rangle \leftrightarrow |e\rangle$ are detuned by $\pm\delta/2$ from the cavity resonance at frequency ν for ensemble A and B respectively. Atoms are pumped incoherently from $|g\rangle$ to $|e\rangle$ via a third fast decaying level (not shown in level scheme) at rate w and decay from $|e\rangle$ to $|g\rangle$ predominantly through the cavity. The cavity decays at rate κ .

2.2 SYNCHRONIZATION THROUGH QUANTUM CHANNELS

2.2.1 Synchronization of two atomic ensembles in a common cavity

In this section we will briefly review the setup, methods, and results of Xu et al. [19]. We aim to present a sufficient level of detail in order to provide a self-contained derivation of the results going beyond the work of Xu et al. in the later sections. The setup in Fig. 2.1 consists of two ensembles of atoms A and B, each containing N atoms, placed in the same cavity. Atoms are assumed to have two relevant internal levels $|g\rangle$ and $|e\rangle$. The transition frequencies of atoms in ensemble A and B have a relative frequency detuning of δ while all atoms within each ensemble are assumed to be frequency degenerate. The transition $|g\rangle \leftrightarrow |e\rangle$ couples to the cavity mode \hat{a} with a single photon Rabi frequency $\Omega/2$. Ensemble A is detuned from the cavity resonance by $\delta/2$ and ensemble B by $-\delta/2$. The cavity linewidth is κ , and we will ultimately assume the bad cavity limit such that the assumptions regarding the detuning of atoms from cavity resonance are insignificant. Atoms decay from $|e\rangle$ to $|g\rangle$ into free space with rate γ_s and dephase with rate T_2^{-1} , and at the same time they are incoherently repumped from $|g\rangle$ to $|e\rangle$ with the rate w (e.g. through an already eliminated third level). In a rotating frame at the cavity frequency the system is described by the Lindblad master equation

$$\begin{aligned} \dot{\rho} = & -i \left[\frac{\delta}{2} (\hat{J}_A^z - \hat{J}_B^z) + \frac{\Omega}{2} (\hat{a}^\dagger (\hat{J}_A^- + \hat{J}_B^-) + \text{h.c.}) \right], \rho \\ & + \kappa \mathcal{D}[\hat{a}] \rho + \sum_{\substack{T=A,B \\ j=1\dots N}} \left(\gamma_s \mathcal{D}[\hat{\sigma}_{T,j}^-] + w \mathcal{D}[\hat{\sigma}_{T,j}^+] \right) \rho. \end{aligned} \quad (2.1)$$

where we remind that $\hat{\sigma}_{T,j}^z$ and $\hat{\sigma}_{T,j}^\pm$ are the usual Pauli matrices for the $|g\rangle \leftrightarrow |e\rangle$ transition for atom $j \in \{1 \dots N\}$ in ensemble $T \in \{A, B\}$. We also use the collective spin operators $\hat{J}_T^\pm := \sum_{i=1}^N \hat{\sigma}_{T,i}^\pm$, $\hat{J}_T^z := \frac{1}{2} \sum_{i=1}^N \hat{\sigma}_{T,i}^z$, and the Lindblad superoperator $\mathcal{D}[A] \rho := A \rho A^\dagger - \frac{1}{2} [A^\dagger A, \rho]_+$. Steady state superradiance is achieved with a dominating cavity decay $\kappa \gg w$, which is inverted compared to an ordinary laser where the pumping dominates $w \gg \kappa$. The fast decay of the cavity with rate κ compared to

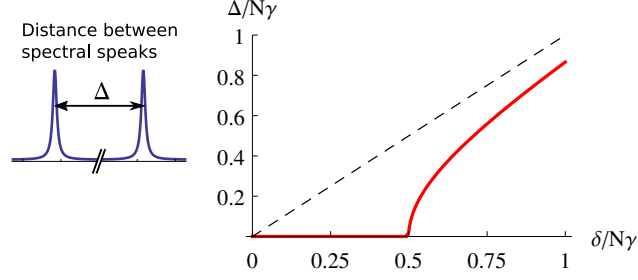


Figure 2.2: Effective detuning Δ between the spectral peaks of light emerging from the laser cavity versus detuning δ between the bare transition frequencies of the two ensembles. For $\delta < w$, the rate of incoherent pumping of atoms, the two peaks coalesce signifying synchronization of atoms. The dashed line is $\Delta = \delta$ and is approached asymptotically for $\delta \gg w$.

all other timescales in the system allows for an adiabatic elimination of the cavity mode

$$\hat{a} \simeq -\frac{i\Omega}{\kappa + i\delta} \hat{J}_A^- - \frac{i\Omega}{\kappa - i\delta} \hat{J}_B^- \approx -\frac{i\Omega}{\kappa} (\hat{J}_A^- + \hat{J}_B^-), \quad (2.2)$$

where we used the approximation that the detuning $\delta \ll \kappa$ is small compared to the cavity linewidth. After adiabatic elimination the decay of the cavity $\kappa \mathcal{D}[\hat{a}] \rho$ translates to a collective decay of the atoms $\gamma \mathcal{D}[\hat{J}^-] \rho$ at rate $\gamma = \Omega^2/\kappa$. The decay into the cavity mode is enhanced by a factor of N and dominates the decay process [29], i.e. $\gamma N \gg \gamma_s, T_2^{-1}$, allowing us to drop the emission into free space and the dephasing

$$\dot{\rho} = -\frac{i\delta}{2} [\hat{J}_A^z - \hat{J}_B^z, \rho] + \gamma \mathcal{D}[\hat{J}_A^- + \hat{J}_B^-] \rho + \sum_{\substack{T=A,B \\ j=1\dots N}} w \mathcal{D}[\hat{\sigma}_{T,j}^+] \rho. \quad (2.3)$$

We can use the permutation symmetry of the master equation to drop unnecessary indices $\langle \hat{\sigma}^{\pm,z} \rangle = \langle \hat{\sigma}_{A,i}^{\pm,z} \rangle$, $\langle \hat{\sigma}_1^+ \hat{\sigma}_2^- \rangle = \langle \hat{\sigma}_{A,i}^+ \hat{\sigma}_{A,j}^- \rangle = \langle \hat{\sigma}_{B,i}^+ \hat{\sigma}_{B,j}^- \rangle \forall i \neq j$ and $\langle \hat{\sigma}_A^+ \hat{\sigma}_B^- \rangle = \langle \hat{\sigma}_{A,n}^+ \hat{\sigma}_{B,m}^- \rangle \forall n, m$ and solve the dynamics analogous to Chapter 1. As in Chapter 1 holds $\langle \hat{\sigma}_{T,i}^\pm \rangle = 0$ for $T \in \{A, B\}$ and we proceed with the approximation $\langle \hat{\sigma}_{A,1}^z \hat{\sigma}_{A,2}^z \rangle \approx \langle \hat{\sigma}^z \rangle^2$, which holds true outside of the regime of very weak pumping $w < \gamma, T_2^{-1}, \gamma_s$ [19]. The mean polarization in stationary state in leading order $1/N$ is found to be

$$\langle \hat{\sigma}^z \rangle = \begin{cases} \min\left(\frac{w^2 + \delta^2}{2wN\gamma}, 1\right), & 0 \leq \delta < w \\ \min\left(\frac{w}{N\gamma}, 1\right), & \delta \geq w \end{cases}. \quad (2.4)$$

The synchronization of the two ensembles is witnessed by the spectrum of light emitted from the cavity which is given by the Fourier transform of the two-time correlation function $\langle \hat{a}^\dagger(\tau) \hat{a}(0) \rangle$ of the intra-cavity field. In view of Eq. (2.2) this requires evaluation of the two-time correlations of atomic dipoles, which can be done by means of the quantum regres-

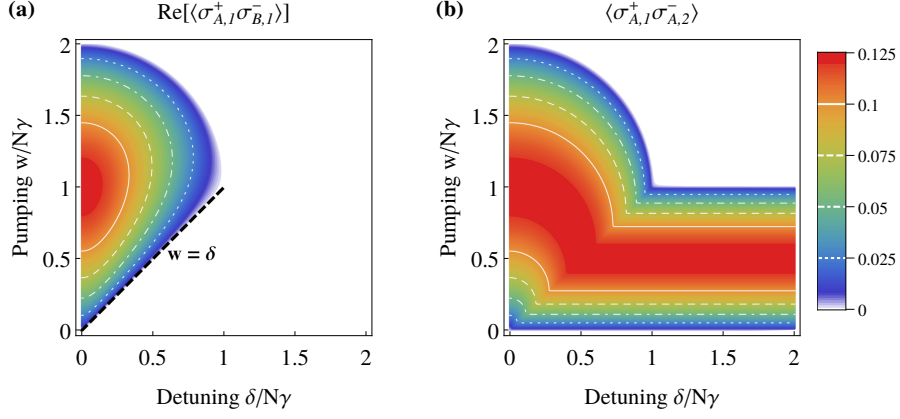


Figure 2.3: (a) Non-vanishing inter-ensemble correlations $\text{Re} [\langle \hat{\sigma}_A^+ \hat{\sigma}_B^- \rangle]$ outline the synchronized parameter regime. The dashed line $w = \delta$ separates the synchronized from the unsynchronized superradiant regime. (b) shows the intra-ensemble correlations $\langle \hat{\sigma}_1^+ \hat{\sigma}_2^- \rangle$ equal for both ensembles. For detuning smaller than the incoherent pumping rate $\delta < w$ both ensembles are synchronized and the critical pumping rate is moved from $w = N\gamma$ for $\delta > w\zeta$ to $w = 2N\gamma$ for $\delta = 0$. Both plots use $N\gamma = 10^6 \text{Hz}$.

sion theorem. For later reference we explicitly state the corresponding equations of motion for atomic two-time correlation functions,

$$\frac{d}{d\tau} \begin{pmatrix} \langle \hat{\sigma}_A^+(\tau) \hat{\sigma}_B^-(0) \rangle \\ \langle \hat{\sigma}_1^+(\tau) \hat{\sigma}_2^-(0) \rangle \end{pmatrix} = \frac{1}{2} \begin{pmatrix} X & Y \\ Y & X^* \end{pmatrix} \begin{pmatrix} \langle \hat{\sigma}_A^+(\tau) \hat{\sigma}_B^-(0) \rangle \\ \langle \hat{\sigma}_1^+(\tau) \hat{\sigma}_2^-(0) \rangle \end{pmatrix} \quad (2.5)$$

where $X = \gamma(N-1)\langle \hat{\sigma}^z \rangle - \gamma - w + i\delta$, and $Y = N\gamma\langle \hat{\sigma}^z \rangle$, cf. Eq. (8) in [19]. The two-time correlation functions, the solution of (2.5), consist of linear combinations of $\exp(-(\Gamma_0 \pm x_0)\tau/2)$, where $\Gamma_0 := w - \gamma(N-1)\langle \hat{\sigma}^z \rangle + \gamma$, and $x_0 := \sqrt{(N\gamma\langle \hat{\sigma}^z \rangle)^2 - \delta^2}$. For $\delta \gg w$ this corresponds to two components oscillating at frequencies $\pm\delta/2$ and decaying at rate Γ_0 . The spectrum thus consists of two separate peaks of width Γ_0 at the bare transitions frequency $\nu \pm \delta/2$ of each ensemble. For smaller detuning δ the coupled dynamics of the two ensembles of atoms first exhibits frequency pulling giving rise to an effective detuning $\Delta < \delta$ between the two peaks as long as $\delta > w$, cf. Fig. 2.2. For $\delta < w$ the two peaks merge and the two ensembles radiate at the same frequency signifying synchronization. The corresponding widths are given by

$$\Gamma/\gamma = \begin{cases} \frac{w^2 + \delta^2}{2wN\gamma} + 1, & 0 \leq \delta < w \\ \frac{w}{N\gamma} + 1, & \delta \geq w \end{cases} \quad (2.6)$$

for small pumping w inside the superradiant regime, which is upper bounded by $\langle \hat{\sigma}^z \rangle < 1$ using (2.4).

Synchronization of the two active atomic clocks physically means that the collective atomic dipoles oscillate in phase. This corresponds to a large non-zero average value of $\langle \vec{\sigma}_A^\perp \cdot \vec{\sigma}_B^\perp \rangle$ where $\sigma_{A(B)}^\perp$ denotes the spin component transverse to the mean polarization along z for ensemble

$A(B)$ (each of which is zero on average in steady state, $\langle \sigma_{A(B)}^\perp \rangle = 0$). It is straight forward to check that $\langle \vec{\sigma}_A^\perp \cdot \vec{\sigma}_B^\perp \rangle = 4 \operatorname{Re} [\langle \hat{\sigma}_A^+ \hat{\sigma}_B^- \rangle]$ such that these inter-ensemble correlations can also be directly used as a measure for synchronization [49]. It is instructive to directly look at this quantity in its dependence on the pumping w and the bare detuning δ , see Fig. 2.3a. The regime of synchronization is clearly visible as the regime of non-vanishing inter-ensemble correlations. This regime is bounded by $w = \delta$ and the quarter circle $(w - N\gamma)^2 + \delta^2 = (N\gamma)^2$, which can be derived from (2.4). The synchronization can be understood as nothing else but the transition from two independent superradiant ensembles $\delta \gg w$ to one superradiant ensemble with $2N$ particles for $\delta = 0$. For $\delta \gg w$ the superradiance is visible in non-vanishing intra-ensemble correlations $\langle \vec{\sigma}_1^\perp \cdot \vec{\sigma}_2^\perp \rangle = 4 \langle \hat{\sigma}_1^+ \hat{\sigma}_2^- \rangle$ (see Fig. 2.3b) and their independence in vanishing inter-ensemble correlations. Decreasing δ into the synchronized regime inter-ensemble correlations build up, approaching the intra-ensemble correlations, until $\delta = 0$ where there is no difference between both ensembles and $\langle \hat{\sigma}_A^+ \hat{\sigma}_B^- \rangle = \langle \hat{\sigma}_1^+ \hat{\sigma}_2^- \rangle$. The additional inter-ensemble correlations in the synchronized regime make the collective spin $\vec{J}_A + \vec{J}_B$ more robust against noise and move the critical pumping rate for the phase transition between superradiant emission and chaotic light to $w = 2N\gamma$ for $\delta = 0$.

The overall photon flux emerging from the cavity is, for large N ,

$$\langle \hat{a}_{\text{out}}^\dagger \hat{a}_{\text{out}} \rangle \approx 2\gamma N^2 (\langle \hat{\sigma}_1^+ \hat{\sigma}_2^- \rangle + \operatorname{Re} [\langle \hat{\sigma}_A^+ \hat{\sigma}_B^- \rangle]),$$

which follows from Eq. (2.2) and the input-output relation $\hat{a}_{\text{out}} = \hat{a}_{\text{in}} + \sqrt{\kappa} \hat{a}$ [33]. For $\delta = 0$ the photon flux scales proportional to $(2N)^2$, as one would expect of one ensemble with $2N$ atoms, and scales with $2N^2$ for two independent ensembles each with N atoms.

2.2.2 Two atomic ensembles in separate cascaded cavities

Next we are going to consider an alternative setup where the two atomic ensembles are kept in separate cavities which are coupled unidirectionally: Light emerging from the cavity containing ensemble A is channeled to the second cavity containing ensemble B , but no light of the latter cavity reaches the first one, cf. Fig. 2.4. This setup is inherently different from the symmetric configuration in the previous section, and it is unclear if or which synchronization behavior still occurs. What is clear is that the properties of light emitted by ensemble A will be completely unaffected by ensemble B downstream. It is therefore advantageous to assume that the transition frequency of atoms in ensemble A is ν and the one of atoms in ensemble B is $\nu - \delta$ as indicated in Fig. 2.4. The cavity frequencies are assumed to be equal to ν , but this assumption is insignificant in the bad cavity limit.

The dynamics in this setup is described by means of a cascaded systems master equation [33]. In a rotating frame it is given by

$$\begin{aligned} \dot{\rho} = & -i \left[\frac{\Omega}{2} \left(J_A^+ \hat{a} + J_A^- \hat{a}^\dagger + J_B^+ \hat{b} + J_B^- \hat{b}^\dagger \right) - \delta J_B^z, \rho \right] \\ & + w \sum_{\substack{T=A,B \\ i=1\dots N}} \mathcal{D} \left[\hat{\sigma}_{T,i}^+ \right] \rho + \frac{\kappa}{2} \left[\hat{a}^\dagger \hat{b} - \hat{b}^\dagger \hat{a}, \rho \right] + \kappa \mathcal{D} \left[\hat{a} + \hat{b} \right] \rho, \end{aligned} \quad (2.7)$$

The atomic ensembles A and B are coupled to their respective cavity modes \hat{a} and \hat{b} with single-photon Rabi frequency $\Omega/2$, and are pumped incoherently at the rate w to their excited states $|e\rangle$. We dropped already the spontaneous emission into free space and the dephasing, knowing the enhanced decay into the cavity modes \hat{a} and \hat{b} dominate the decay processes, as in the previous section. The last two terms describe the cascaded, unidirectional coupling and decay of the cavity modes at rate κ , cf. [33].

As in section 2.2.1 the cavity decay is assumed to be the fastest timescale in the system $\kappa \gg \Omega, w$, allowing us to adiabatically eliminate the cavity fields which yields here

$$\hat{a} \simeq \frac{\Omega}{i\kappa} J_A^-, \quad \hat{b} \simeq \frac{\Omega}{i\kappa} (J_B^- - 2J_A^-). \quad (2.8)$$

The effective master equation for atoms is

$$\begin{aligned} \dot{\rho} = & i\delta [J_B^z, \rho] + w \sum_{T,j} \mathcal{D} [\hat{\sigma}_{T,i}^+] \rho \\ & - \frac{\gamma}{2} [J_A^+ J_B^- - J_B^+ J_A^-, \rho] + \gamma \mathcal{D} [J_A^- - J_B^-] \rho \end{aligned} \quad (2.9)$$

with $\gamma = \Omega^2/\kappa$. Comparing this equation to (2.3) in the previous section we see that the decay of the two ensembles still happens collectively, despite the relative sign. The additional effective Hamiltonian term describes unidirectional character of the coupling as in Eq. (2.7).

The master equation implies the following equations of motion for the expectation values

$$\begin{aligned} \partial_t \langle \hat{\sigma}_A^z \rangle &= -\langle \hat{\sigma}_A^z \rangle (\gamma + w) - 2\gamma (N-1) \langle \hat{\sigma}_A^+ \hat{\sigma}_A^- \rangle - \gamma + w \\ \partial_t \langle \hat{\sigma}_A^+ \hat{\sigma}_A^- \rangle &= -\langle \hat{\sigma}_A^+ \hat{\sigma}_A^- \rangle (\gamma + w - \gamma \langle \hat{\sigma}_A^z \rangle (N-2)) \\ &\quad + \frac{\gamma}{2} \langle \hat{\sigma}_A^z \rangle (\langle \hat{\sigma}_A^z \rangle + 1) \\ \partial_t \langle \hat{\sigma}_B^z \rangle &= -\langle \hat{\sigma}_B^z \rangle (\gamma + w) - 2\gamma (N-1) \langle \hat{\sigma}_B^+ \hat{\sigma}_B^- \rangle \\ &\quad - \gamma + w + 4\gamma N \text{Re} [\langle \hat{\sigma}_A^+ \hat{\sigma}_B^- \rangle] \\ \partial_t \langle \hat{\sigma}_B^+ \hat{\sigma}_B^- \rangle &= -\langle \hat{\sigma}_B^+ \hat{\sigma}_B^- \rangle (\gamma + w - \gamma \langle \hat{\sigma}_B^z \rangle (N-2)) \\ &\quad + \frac{\gamma}{2} \langle \hat{\sigma}_B^z \rangle (\langle \hat{\sigma}_B^z \rangle + 1) - 2\gamma N \langle \hat{\sigma}_B^z \rangle \text{Re} [\langle \hat{\sigma}_A^+ \hat{\sigma}_B^- \rangle] \\ \partial_t \langle \hat{\sigma}_A^+ \hat{\sigma}_B^- \rangle &= \langle \hat{\sigma}_A^+ \hat{\sigma}_B^- \rangle \gamma (N-1) (\langle \hat{\sigma}_A^z \rangle + \langle \hat{\sigma}_B^z \rangle) / 2 \\ &\quad + \langle \hat{\sigma}_A^+ \hat{\sigma}_B^- \rangle (i\delta - \gamma - w) - \frac{\gamma}{2} \langle \hat{\sigma}_B^z \rangle \langle \hat{\sigma}_A^z \rangle \\ &\quad - \frac{\gamma}{2} \langle \hat{\sigma}_B^z \rangle (2 \langle \hat{\sigma}_A^+ \hat{\sigma}_A^- \rangle (N-1) + 1), \end{aligned} \quad (2.10)$$

where we used the symmetry of (2.9) to introduce the abbreviations $\langle \hat{\sigma}_A^z \rangle := \langle \hat{\sigma}_{A,i}^z \rangle$, $\langle \hat{\sigma}_B^z \rangle := \langle \hat{\sigma}_{B,i}^z \rangle$, $\langle \hat{\sigma}_A^+ \hat{\sigma}_A^- \rangle = \langle \hat{\sigma}_{A,i}^+ \hat{\sigma}_{A,j}^- \rangle$, $\langle \hat{\sigma}_B^+ \hat{\sigma}_B^- \rangle = \langle \hat{\sigma}_{B,i}^+ \hat{\sigma}_{B,j}^- \rangle$ for $i \neq j$, and $\langle \hat{\sigma}_A^+ \hat{\sigma}_B^- \rangle = \langle \hat{\sigma}_{A,m}^+ \hat{\sigma}_{B,n}^- \rangle$. Note that the symmetry between A and B is broken in the cascaded setup. In (2.10) we also factorized occurrences of the mean field $\langle \hat{\sigma}_{A(B)}^z \rangle$, which we validated using small system numerical solutions of (2.7) using QuTiP [50]. The steady state solution can be obtained by setting all time-derivatives on the left hand sides equal to zero and solving the algebraic equations. The first two

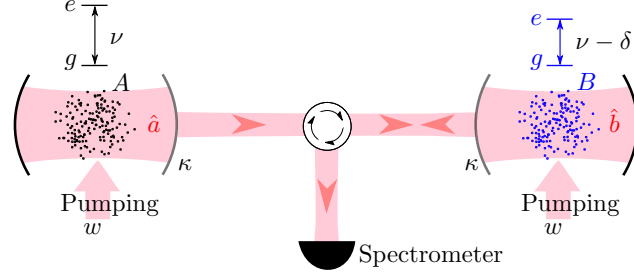


Figure 2.4: Two ensembles of two level systems (A and B) coupling to the cavity modes \hat{a}, \hat{b} respectively. The transition frequencies $|g\rangle \leftrightarrow |e\rangle$ of ensemble A and the cavity frequencies \hat{a}, \hat{b} are ν , while ensemble B 's transition frequency is detuned by $-\delta$. Atoms are pumped incoherently from $|g\rangle$ to $|e\rangle$ via a third fast decaying level (not shown in level scheme) at rate w and decay from $|e\rangle$ to $|g\rangle$ predominantly through the cavity. The cavities decay with rate κ and the output of cavity \hat{a} is directly injected into cavity \hat{b} . The output of cavity \hat{b} is diverted into a spectrometer and not into cavity \hat{a} using a lossless Faraday rotator.

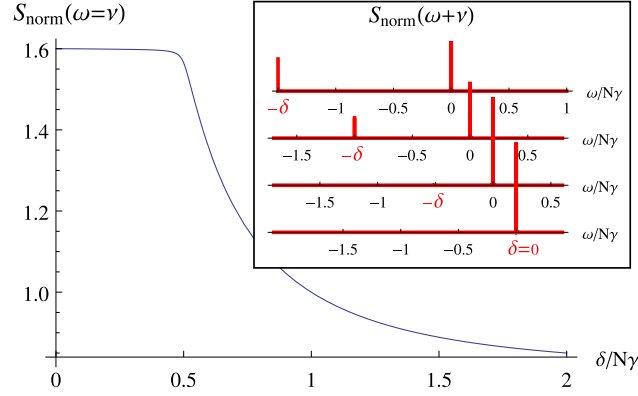


Figure 2.5: (Main plot): $S_{\text{norm}}(\omega = \nu)$ is the photon flux at the resonance frequency ν of ensemble A . Since ensemble A is independent of δ any change with δ comes from ensemble B also at frequency ν . For decreasing δ ensemble B radiates stronger on the injected frequency ν and less at its resonance frequency $\nu - \delta$. For $\delta < w$ ensemble B radiates dominantly on the injected frequency ν and decreasing δ further does not change this, resulting in the plateau of $S_{\text{norm}}(\omega = \nu)$. (Inset): The normalized spectrum $S_{\text{norm}}(\omega)$ for multiple detunings $\delta/N\gamma = 1.5, 1, 0.5, 0$ shows a suppression of the peak at $\nu - \delta$ for decreasing detuning δ , while the Lorentz peak at ν rises until ensemble B is radiating dominantly at ν . Both plots use for the parameters $N\gamma = 10$ kHz and $w = 0.5N\gamma$.

equations involving only ensemble A can be solved independently of ensemble B , as expected in view of the cascaded setup. The remaining equations can be reduced to a polynomial equation of fourth order, which can be solved exactly and used for analytical results up to leading order in $1/N$. In order to obtain numerical results it is easier and faster to solve the system (2.10) numerically and select the stable solution by linearizing (2.10) around each solution.

The spectrum follows again from the Fourier transform of the two-time correlation functions which we calculate using the quantum regression theorem,

$$\frac{d}{d\tau} \begin{pmatrix} \langle \hat{\sigma}_A^+(\tau) \hat{\sigma}_T^-(0) \rangle \\ \langle \hat{\sigma}_B^+(\tau) \hat{\sigma}_T^-(0) \rangle \end{pmatrix} = \frac{1}{2} \begin{pmatrix} X & 0 \\ Y & X' \end{pmatrix} \begin{pmatrix} \langle \hat{\sigma}_A^+(\tau) \hat{\sigma}_T^-(0) \rangle \\ \langle \hat{\sigma}_B^+(\tau) \hat{\sigma}_T^-(0) \rangle \end{pmatrix} \quad (2.11)$$

with $T = A, B$ and

$$\begin{aligned} X &= \gamma(N-1) \langle \hat{\sigma}_A^z \rangle - \gamma - w \\ X' &= \gamma(N-1) \langle \hat{\sigma}_B^z \rangle - \gamma - w - 2i\delta \\ Y &= -2N\gamma \langle \hat{\sigma}_B^z \rangle. \end{aligned}$$

The normalized spectrum of the field emerging from cavity \hat{b} is

$$S_{\text{norm}}(\omega) := \frac{1}{2\pi I} \int d\tau \exp(-i\omega\tau) \langle \hat{b}_{\text{out}}^\dagger(\tau) \hat{b}_{\text{out}}(0) \rangle$$

which can be evaluated using the input-output relation for cascaded systems [33]

$$\hat{b}_{\text{out}} = \hat{a}_{\text{in}} + \sqrt{\kappa}(\hat{a} + \hat{b}). \quad (2.12)$$

and Eq. (2.8). The normalization factor is $I = \langle \hat{b}_{\text{out}}^\dagger \hat{b}_{\text{out}} \rangle$. The peaks in $S_{\text{norm}}(\omega)$ are always located at the bare transition frequencies ν and $\nu - \delta$ of ensemble A and B respectively which does not hint at synchronization effects. Synchronization becomes visible in the regime $\delta < w < N\gamma$ via a change of relative peak heights, as illustrated in Fig. 2.5 Inset, which is qualitatively different from the frequency pulling in section 2.2.1. For fixed pumping w in the superradiant regime [18] $\gamma < w < N\gamma$ we can distinguish different regimes for δ

- $\delta \gg w$ Ensembles A and B radiate only at their own resonance frequency $\nu, \nu - \delta$ respectively with equal intensity.
- $\delta \geq w$ Ensemble A is unaffected by any change in δ and radiates at ν , but ensemble B radiates at two frequencies ν and $\nu - \delta$. This leads to an increasing total intensity at frequency ν , cf. Fig. 2.5.
- $\delta < w$ Ensemble A still radiates with the same intensity at frequency ν and ensemble B now also dominantly radiates at frequency ν , while radiation at its own resonance frequency becomes negligible (for large N). Ensemble B is synchronized to ensemble A resulting in a plateau of $S_{\text{norm}}(\nu)$, cf. Fig. 2.5.

While the peak value of the normalized spectrum at frequency ν shows a plateau in the synchronized regime $\delta < w$, the integrated unnormalized spectrum, that is the total power output is still increasing for smaller detuning, similar to the finding in section 2.2.1. In leading order in N^2 the total photon flux is given by

$$\langle \hat{b}_{\text{out}}^\dagger \hat{b}_{\text{out}} \rangle \approx \gamma N^2 \left(\sum_{T=A,B} \langle \hat{\sigma}_{T,1}^+ \hat{\sigma}_{T,2}^- \rangle + 2 \text{Re} [-\langle \hat{\sigma}_A^+ \hat{\sigma}_B^- \rangle] \right).$$

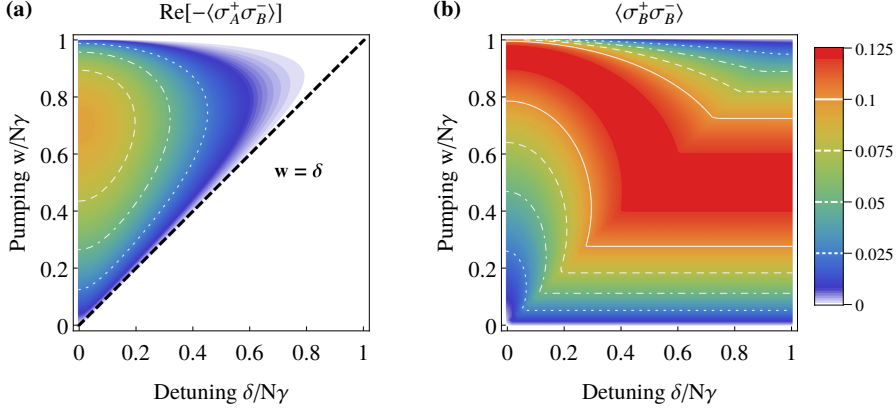


Figure 2.6: (a) Non-vanishing inter-ensemble correlations $\text{Re}[-\langle\hat{\sigma}_A^+\hat{\sigma}_B^-\rangle]$ outline the synchronized parameter regime. The dashed line $w = \delta$ separates the synchronized from the unsynchronized superradiant regime. (b) shows the intra-ensemble correlations $\langle\hat{\sigma}_B^+\hat{\sigma}_B^-\rangle$ of the slave ensemble B . For detuning smaller than the incoherent pumping rate $\delta < w$ the slave ensemble B is synchronized to the master ensemble A . Here $N\gamma = 10^6\text{Hz}$.

The photon flux increases for smaller detuning δ due to increasing correlations $\text{Re}[-\langle\hat{\sigma}_A^+\hat{\sigma}_B^-\rangle]$ between the two ensembles as shown in Fig. 2.6a. In Sec. 2.2.1 the synchronized regime stretched out beyond $w = N\gamma$ up to $w = 2N\gamma$ for vanishing detunings, cf. Fig. 2.3 due to the fact that the two ensembles radiate in this regime as one ensemble containing $2N$ atoms. This is not the case in the cascaded system, see Fig. 2.6. For $w > N\gamma$ ensemble A (containing N atoms) will stop emitting superradiantly and for $w \gg N\gamma$ will radiate chaotic light [29]. The correlations $\langle\hat{\sigma}_B^+\hat{\sigma}_B^-\rangle$ shown in Fig. 2.6b indicate that if the first cavity would still radiate superradiantly (e.g. N larger in the first cavity), then the synchronized regime could also stretch beyond $w = N\gamma$.

Analyzing the Lorentz peaks in the spectrum reveals that the peaks at ν and $\nu - \delta$ have a width

$$\frac{\Gamma_\nu}{\gamma} = \frac{w}{N\gamma} + 1, \quad (2.13)$$

$$\frac{\Gamma_{\nu-\delta}}{\gamma} = \begin{cases} O(N), & \delta \leq w \\ \frac{w}{N\gamma} + 1, & \delta > w \end{cases}, \quad (2.14)$$

which is valid up to order $1/N$ for small pumping w inside the superradiant regime. Most significantly we see that the linewidth at $\nu - \delta$ for $\delta \leq w$ scales with N and as a result the peak effectively vanishes for large N . This shows that ensemble B cannot sustain radiating at its resonance frequency and radiates instead at the frequency of ensemble A . The independence of Γ_ν of δ is also significant, since it means that in the synchronized regime ensemble B is amplifying the input signal without increasing the linewidth.

2.3 SYNCHRONIZATION THROUGH CLASSICAL CHANNELS

2.3.1 *Unidirectional synchronization*

One can ask the question whether the synchronization in Sec. 2.2.2 is dominated by quantum mechanics and requires a quantum channel in between both cavities or whether the same or a similar result can be achieved by synchronizing the two clocks through a classical channel. Synchronization or locking of the two superradiant laser through a classical channel means that classical information is transmitted between the two systems, rather than quantum states of light as was considered in the previous section.

In this section we are going to answer this questions for a highly idealized classical channel: We will consider phase sensitive measurements (heterodyne detection) of the output field of one laser cavity, transmission of the classical measurement result (the photocurrent), and injection of an appropriate coherent field to the second cavity. Thus, we assume a continuous-time feedback strategy where the measured amplitude and phase of the field of the first cavity is recreated with appropriate feedback gains as a seed for the second cavity as illustrated in Fig. 2.7. This measure and prepare strategy simulates the direct injection of Sec. 2.2.2. Both heterodyne measurement and laser are idealizations adding no technical noise, but will add quantum noise due to the gain of classical information. From a quantum information point of view we have replaced the quantum channel between both cavities by a classical channel and local operations. We will show that this introduces a certain level of additional noise due to the measurement, but will not change the synchronization behavior.

This result has to be understood as an upper bound to the quality of classical synchronization achievable through a classical channel. Any real classical procedure will actually perform worse, as it will add technical noise in phase sensitive detection and feedback. This will be especially relevant when attempting to synchronize superradiant lasers exhibiting unprecedentedly low linewidths.

To describe the system we use an unconditional feedback master equation using continuous-time heterodyne measurements developed in [51, 52]

$$\begin{aligned} \dot{\rho} = & -i[H, \rho] - \frac{i}{4} [(\hat{F}_+ + i\hat{F}_-) \hat{s} + h.c., \rho] \\ & + \frac{1}{2} \mathcal{D} [\hat{s} - i\hat{F}_+] \rho + \frac{1}{2} \mathcal{D} [\hat{s} - \hat{F}_-] \rho. \end{aligned} \quad (2.15)$$

The operator \hat{s} describes the type of measurement being performed which, for the case of a heterodyne detection, is given by $\hat{s} = \sqrt{\kappa} \hat{a}$. The heterodyne detection provides two photocurrents I_{\pm} for the phase and the amplitude quadrature which can be used for the feedback operation. We consider Markovian and linear feedback, that is, the photocurrents are each multiplied by suitable gains and, in the case considered here, fed back as a coherent driving field to the second cavity. The feedback due to the two photocurrents I_{\pm} is described by Hermitian operators \hat{F}_{\pm} which are given by $\hat{F}_{\pm} = g_{\pm} \hat{b} + g_{\pm}^* \hat{b}^{\dagger}$ with gain coefficients $g_{+} = -i\sqrt{\kappa}$ and

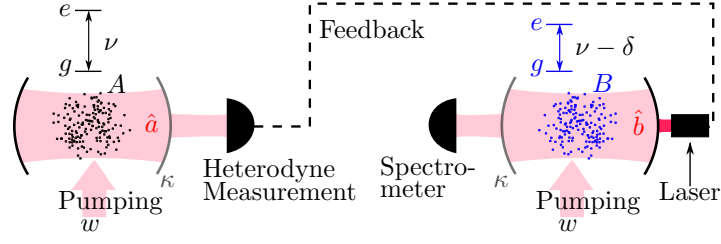


Figure 2.7: Two ensembles of two level systems (A and B) coupling to the cavity modes \hat{a}, \hat{b} respectively. The transition frequencies $|g\rangle \leftrightarrow |e\rangle$ of ensemble A and the cavity frequencies \hat{a}, \hat{b} are ν , while ensemble B 's transition frequency is detuned by $-\delta$. Atoms are pumped incoherently from $|g\rangle$ to $|e\rangle$ via a third fast decaying level (not shown in level scheme) at rate w and decay from $|e\rangle$ to $|g\rangle$ predominantly through the cavity. The cavities decay with rate κ and the output of cavity \hat{a} is measured via an ideal heterodyne detection and then recreated with an ideal laser with a certain gain and fed into cavity \hat{b} . The measurement and feedback via the laser are a classical simulation of the direct injection in Sec. 2.2.2.

$g_- = -\sqrt{\kappa}$. We choose this particular feedback strategy as it reproduces an unidirectional coupling identical to the one found in Eq. (2.7) when inserted to the feedback master equation in (2.15),

$$\begin{aligned} \dot{\rho} = & -i \left[\frac{\Omega}{2} \left(J_A^+ \hat{a} + J_A^- \hat{a}^\dagger + J_B^+ \hat{b} + J_B^- \hat{b}^\dagger \right) - \delta J_B^z, \rho \right] \\ & + w \sum_{\substack{T=A,B \\ i=1\dots N}} \mathcal{D} \left[\hat{\sigma}_{T,i}^+ \right] \rho + \frac{\kappa}{2} \left[\hat{a}^\dagger \hat{b} - h.c., \rho \right] + \kappa \mathcal{D} \left[\hat{a} + \hat{b} \right] \rho \\ & + \kappa \mathcal{D} \left[\hat{b} \right] \rho + \kappa \mathcal{D} \left[\hat{b}^\dagger \right] \rho. \end{aligned}$$

We added the incoherent atom pumping with rate w and the decay of cavity field \hat{b} with rate κ . The coherent dynamics is given by the atom-cavity interaction at rate $\Omega/2$, and the detuning of the atomic transitions $-\delta$, as in the previous section. The only difference to (2.7) are the last two cooling and heating terms indicating additional noise due to the measurement.

The cavity fields can again be adiabatically eliminated considering the subtlety that cavity \hat{b} is now driven with rate κ by the Lindblad terms to a thermal state with 1 mean photon. The adiabatic elimination translates the decays of the cavity modes to a collective decay of the atoms at rate $\gamma = \Omega^2/\kappa$

$$\begin{aligned} \dot{\rho} = & i\delta [J_B^z, \rho] + \gamma \mathcal{D} [J_A^- - J_B^-] \rho + \frac{\gamma}{2} [J_B^+ J_A^- - h.c., \rho] \\ & + w \sum_{\substack{T=A,B \\ i=1\dots N}} \mathcal{D} \left[\hat{\sigma}_{T,i}^+ \right] \rho + \gamma \mathcal{D} [J_B^-] \rho + \gamma \mathcal{D} [J_B^+] \rho. \end{aligned}$$

The corresponding dynamics of the expectation values is

$$\begin{aligned}
\partial_t \langle \hat{\sigma}_A^z \rangle &= -\langle \hat{\sigma}_A^z \rangle (\gamma + w) - 2\gamma (N - 1) \langle \hat{\sigma}_A^+ \hat{\sigma}_A^- \rangle - \gamma + w \\
\partial_t \langle \hat{\sigma}_A^+ \hat{\sigma}_A^- \rangle &= -\langle \hat{\sigma}_A^+ \hat{\sigma}_A^- \rangle (\gamma + w - \gamma \langle \hat{\sigma}_A^z \rangle (N - 2)) \\
&\quad + \frac{\gamma}{2} \langle \hat{\sigma}_A^z \rangle (\langle \hat{\sigma}_A^z \rangle + 1) \\
\partial_t \langle \hat{\sigma}_B^z \rangle &= -\langle \hat{\sigma}_B^z \rangle (\gamma u + w) - 2\gamma (N - 1) \langle \hat{\sigma}_B^+ \hat{\sigma}_B^- \rangle \\
&\quad - \gamma + w + 4\gamma N \operatorname{Re} [\langle \hat{\sigma}_A^+ \hat{\sigma}_B^- \rangle] \\
\partial_t \langle \hat{\sigma}_B^+ \hat{\sigma}_B^- \rangle &= -\langle \hat{\sigma}_B^+ \hat{\sigma}_B^- \rangle (u\gamma + w - \gamma \langle \hat{\sigma}_B^z \rangle (N - 2)) \\
&\quad + \frac{\gamma}{2} \langle \hat{\sigma}_B^z \rangle (u \langle \hat{\sigma}_B^z \rangle + 1) - 2\gamma N \langle \hat{\sigma}_B^z \rangle \operatorname{Re} [\langle \hat{\sigma}_A^+ \hat{\sigma}_B^- \rangle] \\
\partial_t \langle \hat{\sigma}_A^+ \hat{\sigma}_B^- \rangle &= \langle \hat{\sigma}_A^+ \hat{\sigma}_B^- \rangle \gamma (N - 1) (\langle \hat{\sigma}_A^z \rangle + \langle \hat{\sigma}_B^z \rangle) / 2 \\
&\quad + \langle \hat{\sigma}_A^+ \hat{\sigma}_B^- \rangle (i\delta - v\gamma - w) - \frac{\gamma}{2} \langle \hat{\sigma}_B^z \rangle \langle \hat{\sigma}_A^z \rangle \\
&\quad - \frac{\gamma}{2} \langle \hat{\sigma}_B^z \rangle (2 \langle \hat{\sigma}_A^+ \hat{\sigma}_A^- \rangle (N - 1) + 1), \tag{2.16}
\end{aligned}$$

where $u = 3$ and $v = 2$. This is almost identical to the dynamics found for the cascaded system considered in the previous section, Eqs. (2.10) and (2.11), which are identical the set of equations in (2.16) when the parameters u and v are set to $u = 1$ and $v = 1$. Importantly, u and v never occur multiplied with N, w, δ and therefore do not contribute significantly to the dynamics in the limit of large N . This is also visible in the steady state results in Figs. 2.8 and showing no visible difference to Fig. 2.6.

To evaluate whether ensemble B synchronizes with ensemble A , just like in Sec. 2.2.2, we extract from the two-time correlation functions the components $\exp(-\Gamma_v \tau / 2)$ and $\exp(-(\Gamma_{v-\delta} / 2 + i\delta) \tau)$. Using the solutions for $\langle \hat{\sigma}_A^z \rangle$ and $\langle \hat{\sigma}_B^z \rangle$, which are identical to Sec. 2.2.2 up to leading order in $1/N$, we calculate the width of these Lorentzian peaks, giving for small pumping w inside the superradiant regime

$$\frac{\Gamma_v}{\gamma} = \frac{w}{N\gamma} + 1, \quad \frac{\Gamma_{v-\delta}}{\gamma} = \begin{cases} O(N), & \delta \leq w \\ \frac{w}{N\gamma} + 3, & \delta > w \end{cases}.$$

Just as in Sec. 2.2.2 we see that the peak at $v - \delta$ for $\delta \leq w$ gets extremely broad for large N and thus effectively vanishes. Again this means that the resonance frequency of ensemble B is suppressed and ensemble B synchronizes to the frequency of ensemble A . Remarkable is that even though there is now a classical channel between both cavities, ensemble B amplifies the input signal in the synchronized regime without increasing the linewidth Γ_v . In the unsynchronized regime $\delta > w$ the linewidth $\Gamma_{v-\delta}$ is larger than in the quantum coupled setup (2.14). Due to the chosen gain in the feedback operators $\hat{F}_\pm = g_\pm \hat{b} + g_\pm^* \hat{b}^\dagger$ the output spectrum of cavity \hat{b} has now a larger Lorentz peak at v than at $v - \delta$ for large detuning $\delta \gg w$. This stronger feedback gain is necessary to simulate the same amplitude of cavity field \hat{a} being injected into cavity \hat{b} as in Sec. 2.2.2.

From the dynamics of the expectation values (2.16) and from the correlation functions in the steady state Fig. 2.8 we see that there is no significant difference in the synchronization between the quantum and

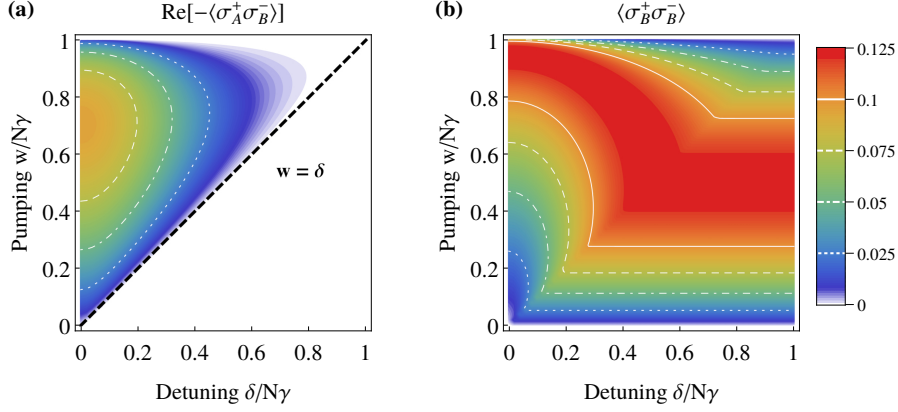


Figure 2.8: (a) Non-vanishing inter-ensemble correlations $\text{Re}[-\langle\hat{\sigma}_A^+\hat{\sigma}_B^-\rangle]$ outline the synchronized parameter regime. The dashed line $w = \delta$ separates the synchronized from the unsynchronized superradiant regime and is identical to Sec. 2.2.2. (b) shows the intra-ensemble correlations $\langle\hat{\sigma}_B^+\hat{\sigma}_B^-\rangle$ of the slave ensemble B. Here $N\gamma = 10^6\text{Hz}$.

the classically coupled setups considered in the previous and this section, respectively. This holds in the limit of large N , that is far above threshold of the superradiant laser where the emitted field is essentially classical. However, it is important to remember that our analysis is based on an ideal heterodyne detection and feedback operations, and that any realistic classical synchronization will perform worse.

2.3.2 Bidirectional synchronization

In view of the results of the previous section it is worthwhile considering the question whether the synchronization in Sec. 2.2.1 was dependent on the coupling to the same quantum mechanical cavity mode, or if this synchronization also occurs when we replace this quantum coupling with a classical, bidirectional coupling. In order to address this question we consider the setup in Fig. 2.9. Both cavity fields decay with rate $\tilde{\kappa}$ and are measured with ideal heterodyne measurements. The measurement results are then used by an ideal lasers to recreate the measured coherent state with a certain gain, giving rise to a symmetric coupling between both cavities using classical channels. Just like in the previous section the heterodyne measurements and lasers are idealizations adding no technical noise and the continuous-time feedback is instantaneous – i.e. Markovian. This setup is a strategy to simulate the coupling to the same cavity mode in Sec. 2.2.1 with a classical (but not necessarily technically feasible) bi-directional coupling. In this section we will leave out some details and refer to appendix B.1 for the complete derivation.

To describe this system we use the same unconditional feedback master equation (2.15) twice. Once with the measurement operator $\hat{s}_{\hat{a}} = \sqrt{\tilde{\kappa}}\hat{a}$ and feedback operators $\hat{F}_{\pm}^{\hat{b}} = g_{\pm}\hat{b} + g_{\pm}^*\hat{b}^{\dagger}$ acting on field \hat{b} , and then with the measurement operator $\hat{s}_{\hat{b}} = \sqrt{\tilde{\kappa}}\hat{b}$ and feedback operator $\hat{F}_{\pm}^{\hat{a}} = g_{\pm}\hat{a} + g_{\pm}^*\hat{a}^{\dagger}$ acting on field \hat{a} , where $g_+ := g_-/i$. Without loss of generality we can introduce the feedback strength ξ with $g_- := -\xi\sqrt{\tilde{\kappa}}$ and restrict the

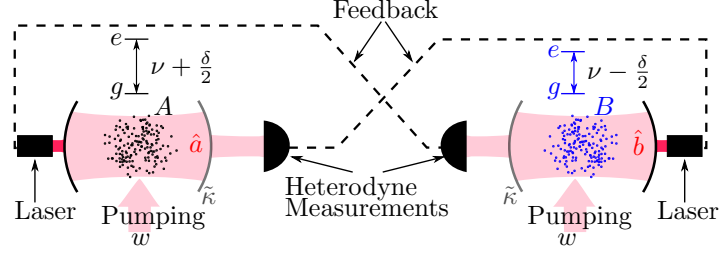


Figure 2.9: Two ensembles of two level systems (A and B) coupling to the cavity modes \hat{a}, \hat{b} respectively. The frequencies of the transitions $|g\rangle \leftrightarrow |e\rangle$ are detuned by $\pm\delta/2$ from the cavity resonance at frequency ν for ensemble A and B respectively. Atoms are pumped incoherently from $|g\rangle$ to $|e\rangle$ via a third fast decaying level (not shown in level scheme) at rate w and decay from $|e\rangle$ to $|g\rangle$ predominantly through the cavity. The cavities decay with rate $\tilde{\kappa}$ and the output of both cavities is measured via an ideal heterodyne detection and then recreated with an ideal laser with a certain gain and fed into the opposite cavity. The measurements and feedbacks via the lasers are symmetric such that this simulates the coupling to the same cavity mode as in Sec. 2.2.1.

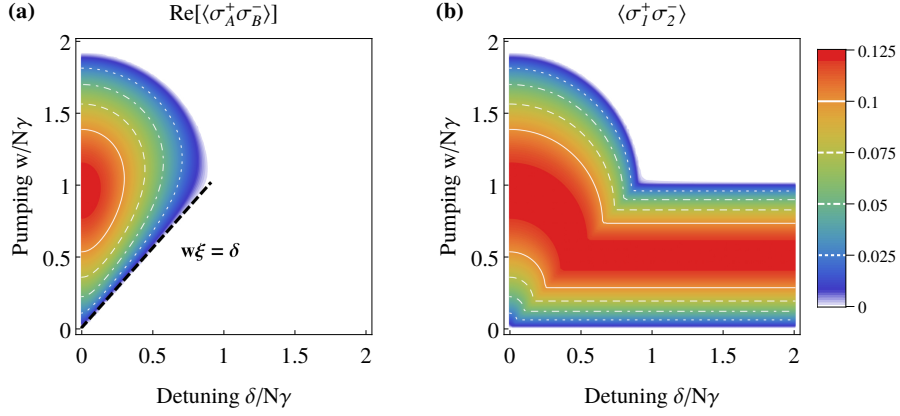


Figure 2.10: (a) Non-vanishing inter-ensemble correlations $\text{Re}[\langle\hat{\sigma}_A^+\hat{\sigma}_B^-\rangle]$ outline the synchronized parameter regime. This regime is reduced compared to Fig. 2.3, and the dashed line $w\zeta = \delta$ separates the synchronized from the unsynchronized superradiant regime. (b) shows the intra-ensemble correlations $\langle\hat{\sigma}_1^+\hat{\sigma}_2^-\rangle$ equal for both ensembles. For detuning smaller than the incoherent pumping rate times the feedback strength $\delta < w\zeta$ both ensembles are synchronized and the critical pumping rate is moved from $w = N\gamma$ for $\delta > w\zeta$ to $w = (1 + \zeta)N\gamma$ for $\delta = 0$. Both plots use $N\gamma = 10^6\text{Hz}$.

feedback strength to $\zeta \in [0, 1)$, such that the resulting equations form a stable system for the cavity fields. If ζ would be allowed to be equal to unity or larger, the measurement & feedback would increase the amplitude of the cavity fields and there would be no steady state with

finite amplitudes. We can proceed with adiabatically eliminating the cavity fields, which gives the master equation for the atoms only

$$\begin{aligned} \dot{\rho} = & \frac{\delta}{2i} [J_A^z - J_B^z, \rho] + \sum_{\substack{T \in \{A, B\} \\ i \in \{1..N\}}} w \mathcal{D} [\hat{\sigma}_{T,i}^+] \rho + \sum_{s=\pm} \frac{\Omega^2}{2\kappa_s} \times \\ & \times \left((1 + \bar{n}_s) \mathcal{D} [J_A^- - sJ_B^-] + \bar{n}_s \mathcal{D} [J_A^+ - sJ_B^+] \right) \rho, \end{aligned} \quad (2.17)$$

where $\kappa_{\pm} := \bar{\kappa} (1 \pm \zeta)$ and $\bar{n}_{\pm} := \bar{\zeta}^2 / (4(1 \pm \zeta))$.

For $\zeta = 0$ the second Lindblad terms drop out and the first Lindblad terms can be transformed to show independent decay for both ensembles. For $\zeta \neq 0$ the Lindblad terms cannot be separated for both ensembles and for increasing ζ both ensembles couple more and more strongly. Comparing the dynamics of $\langle \hat{\sigma}_A^+ \rangle$ with the completely uncoupled case and the completely coupled case in Sec. 2.2.1 we choose the cavity decays $\bar{\kappa}$ dependent on the feedback strength ζ such that both cases are simulated best:

$$\bar{\kappa}(\zeta) := \frac{\kappa}{(1 - \zeta)(1 + \zeta)}. \quad (2.18)$$

From master equation (2.17) with the parameterization (2.18) we can calculate the dynamics of the expectation values

$$\begin{aligned} \partial_t \langle \hat{\sigma}^z \rangle &= w(1 - \langle \hat{\sigma}^z \rangle) - \gamma - \langle \hat{\sigma}^z \rangle \gamma \zeta \\ &\quad - 2\gamma (\langle \hat{\sigma}_1^+ \hat{\sigma}_2^- \rangle (N-1) + \zeta N \operatorname{Re} [\langle \hat{\sigma}_A^+ \hat{\sigma}_B^- \rangle]) \\ \partial_t \langle \hat{\sigma}_1^+ \hat{\sigma}_2^- \rangle &= \langle \hat{\sigma}_1^+ \hat{\sigma}_2^- \rangle (-w + \gamma(N-2) \langle \hat{\sigma}^z \rangle - \gamma \zeta) \\ &\quad + \frac{\gamma}{2} \langle \hat{\sigma}^z \rangle (1 + \zeta \langle \hat{\sigma}^z \rangle + 2N\zeta \operatorname{Re} [\langle \hat{\sigma}_A^+ \hat{\sigma}_B^- \rangle]) \\ \partial_t \langle \hat{\sigma}_A^+ \hat{\sigma}_B^- \rangle &= \langle \hat{\sigma}_A^+ \hat{\sigma}_B^- \rangle (\gamma(N-1) \langle \hat{\sigma}^z \rangle - \gamma \zeta - w + i\delta) \\ &\quad + \frac{\gamma}{2} \bar{\zeta} \langle \hat{\sigma}^z \rangle \left(2 \langle \hat{\sigma}^z \rangle \zeta (\bar{\zeta}^4 - \bar{\zeta}^2 + 2)^{-1} + 1 \right) \\ &\quad + \gamma \zeta \langle \hat{\sigma}^z \rangle \langle \hat{\sigma}_1^+ \hat{\sigma}_2^- \rangle (N-1) \end{aligned} \quad (2.19)$$

with $\zeta := (\bar{\zeta}^4 - \bar{\zeta}^2 + 2) / (2(1 - \bar{\zeta}^2))$ and factorized $\langle \hat{\sigma}^z \rangle$ from all occurring correlation functions, giving a closed system of equations. We could use the same short notation for the expectation values as in Sec. 2.2.1, since the effective coupling in (2.17) is symmetric for both ensembles and even recover the equations of [19], when disregarding the relation between ζ and $\bar{\zeta}$ and setting $\zeta = \bar{\zeta} = 1$. The steady state can now simply be calculated setting all time-derivatives equal to zero. These algebraic equations can be solved numerically or analytically, while filtering out the stable solution. Fig. 2.10 show the expectation values responsible for inter- and intra- ensemble correlations in the steady state and they are very similar to Fig. 2.3 in Sec. 2.2.1. The only difference is a by $\bar{\zeta}$ reduced synchronization regime, visible in non-vanishing inter-ensemble correlations $\langle \hat{\sigma}_A^+ \hat{\sigma}_B^- \rangle$. The synchronized regime for leading order in $1/N$ is bounded by $w\bar{\zeta} = \delta$ and the quarter circle $(w - N\gamma)^2 + \delta^2 = (\bar{\zeta}N\gamma)^2$ (see Fig. 2.10a).

Analog to Sec. 2.2.1 we can extract the half-width $\Gamma/2$ of the Lorentz peaks in the spectrum from the two-time correlation functions and use

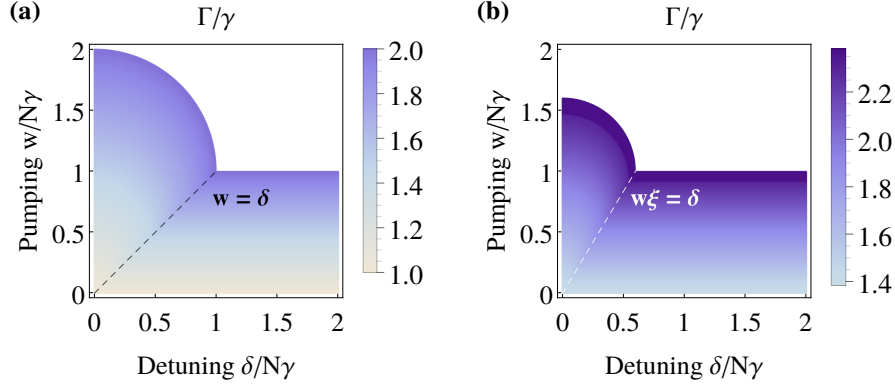


Figure 2.11: The dimensionless linewidth Γ/γ for quantum (a) Eq. (2.6) and classical (b) Eq. (2.20) coupling with $\zeta = 0.6$ for leading order in $1/N$. The linewidth for classical coupling (b) is always larger than the quantum coupling, due to noise term ζ increasing with coupling strength ζ . In the regime far above a critical pumping the atoms radiate chaotically [29] with a linewidth scaling with $O(N)$, which is not plotted here and typically many orders of magnitude larger than the linewidth in the superradiant regime.

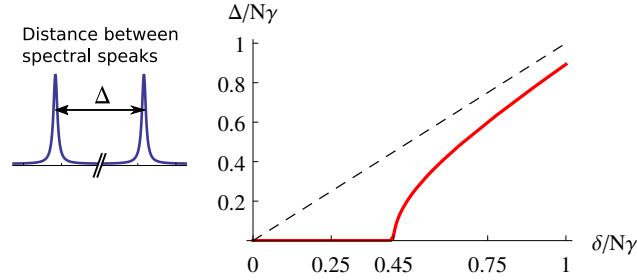


Figure 2.12: Pole distance Δ of the output spectrum versus the detuning δ with the critical detuning at $w\xi$, and the parameters $N\gamma = 10^6$ Hz, $w = 0.5N\gamma$, and $\zeta = 0.9$. The dashed line is $\Delta = \delta$.

the analytical solution for $\langle \hat{\sigma}^z \rangle$ (see (B.6)) up to leading order in $1/N$ to derive

$$\Gamma/\gamma = \zeta + \begin{cases} \frac{w - \sqrt{w^2 \zeta^2 - \delta^2 (1 - \zeta^2)}}{N\gamma(1 - \zeta^2)}, & 0 \leq \delta < w\xi \\ \frac{w}{N\gamma}, & \delta \geq w\xi \end{cases}, \quad (2.20)$$

which is valid for small pumping w inside the superradiant regime. This linewidth is plotted in Fig. 2.11b and compared with (2.6) from Sec. 2.2.1 plotted in Fig. 2.11a. The linewidth using the classical coupling is larger than the linewidth using the quantum coupled setup, due to the measurement induced noise term ζ . This noise term ζ also prevents one to take the limit $\zeta \rightarrow 1$ to approach the same synchronization regime as in Sec. 2.2.1, since ζ diverges in this limit.

The striking feature of the setup in Sec. 2.2.1 was clear synchronization visible in the distance of the Lorentzian peaks Δ plotted versus the bare detuning δ , which is also reproduced here with a smaller critical detuning $w\xi$ (see Fig. 2.12).

The results presented here show that the synchronization of superradiant lasers [19, 42] is not dominated by quantum effects, but a classical synchronization of quantum systems. However this classical coupling setup has a reduced synchronization regime and an increased linewidth, even with the ideal measurements and lasers assumed for the feedback. For any experimental realization the lasers for the feedback would need an even lower linewidth than the superradiant lasers. This setup is therefore of more theoretical interest to help defining the border between synchronization of quantum systems using classical channels and quantum systems using quantum channels.

2.4 SUMMARY

We discussed if and how synchronization occurs in a cascaded setup of master & slave superradiant atomic ensembles, or active atomic clocks. Additionally we simulated the symmetric coupling and the cascaded coupling with idealized classical coupling channels.

The cascaded setup in Sec. 2.2.2 shows synchronization of the slave ensemble to the injected frequency. The main difference to Sec. 2.2.1 is that the synchronization is not apparent in the distance Δ of the Lorentz peaks, but in the Lorentz peak heights. In the synchronized regime the slave ensemble radiates only at the injected frequency, while its Lorentz peak at the resonance frequency effectively vanishes.

In Sec. 2.3.1 we replaced the direct injection of the light with a measurement and feedback, introducing a classical channel in between both cavities. The resulting steady state equations reveal only minor changes, which do not scale with the system size, resulting in basically identical steady state results and the same synchronization far above laser threshold.

n -TH ORDER CORRELATIONS IN SYMMETRIC SYSTEMS

3.1 INTRODUCTION

In the previous two Chapters we extracted the essential information from a master equation of N subsystem using the cumulant expansion method involving the following steps:

- (i) Deriving the moment system from a master equation.
- (ii) Setting the cumulants of order $n + 1$ to zero, which effectively factorizes the $n + 1$ order moments to moments of order $\leq n$.
- (iii) Solving the nonlinear moment differential equation system analytically or numerically.
- (iv) Applying the Quantum Regression Theorem to the moment system and factorizing the two-time correlations to calculate the spectrum.

The crucial part is the cumulant expansion [53–55] in step (ii). To use the cumulant expansion, one needs to derive the evolution equations of the moments, which grow exponentially with truncation order, yet there is in principle no more information in the moment system, than in the master equation itself. This method has the additional disadvantage that it is only feasible for small subsystem dimension, as for example two-level systems, because the required moments grow polynomially fast with subsystem dimension. Nonetheless it is a widely used method and carries names like: Expectation value based cluster expansion [56, 57], Cluster Variation Method [58, 59], cluster expansion [60], Bogoliubov-Born-Green-Kirkwood-Yvon trajectories [61, 62], or mean-field method including pair-correlations [63].

In this Chapter we generalize the cumulant expansion method such that we only need the following steps for N subsystems, e.g., atoms, with d levels:

- (i) Defining a cutoff order $n + 1$.
- (ii) Solving a nonlinear density matrix evolution equation numerically
- (iii) Numerically calculating a matrix of dimension d^8 and doing a matrix inverse repeatedly to calculate the spectrum.

Contrary to the basis dependent method in the previous Chapters, the formalism introduced in this Chapter is feasible for

- arbitrary subsystem algebras of finite dimension and
- arbitrary cutoff order

such that the reduced density matrix of dimensionality d^{2n} in sparse format fits into the available memory.

The Chapter is structured the following way:

SEC. 3.2 We define the symmetric master equation and motivate the nonlinear approximation as a use case for the density matrix cumulants.

SEC. 3.3 We define density matrix cumulants.

SEC. 3.4 We show how two-time correlations and the spectrum can be derived.

SEC. 3.5 We demonstrated the method for example systems.

SEC. 3.6 We point out fundamental problems inherent in the cumulant expansion.

3.2 SYMMETRIC MASTER EQUATION

We consider a system composed of N identical subsystems whose Hilbert space is $\mathcal{H}_N = \mathcal{H}_1^{\otimes N}$ where \mathcal{H}_1 denotes the Hilbert space of one subsystem. In the following we restrict the discussion to finite dimensional Hilbert spaces $\dim(\mathcal{H}_1) = d$, though most conclusions will hold also for infinite dimensional spaces. The state of the compound system is described by the N -particle density matrix ρ_N whose dynamics is, by assumption, governed by a symmetric Lindblad Master equation of the form ($\hbar = 1$)

$$\begin{aligned} \dot{\rho}_N &= \frac{1}{i} \sum_{i=1}^N [H_i, \rho_N] + \sum_{i=1}^N \mathcal{D}[O_i] \rho_N \\ &\quad + \frac{1}{i} \sum_{i,j=1}^N [W_i^\dagger W_j, \rho_N] + \mathcal{D} \left[\sum_{i=1}^N V_i \right] \rho_N \\ &=: L_N(\rho_N). \end{aligned} \tag{3.1}$$

Here operators H_i, O_i, W_i, V_i are arbitrary single particle operators acting on the i -th subsystem. We make the crucial assumption that these operators act identically on their respective system, that is, for all permutation operators P_{ij} we have $H_i = P_{ij} H_j P_{ij}$ and equivalent relations for O_i, W_i, V_i . Lindblad superoperators describing incoherent dynamics are defined by $\mathcal{D}[A] \rho := A \rho A^\dagger - \frac{1}{2} [A^\dagger A, \rho]_+ = -\frac{1}{2} [A^\dagger, A \rho] + h.c.$ where A is referred to as jump operator. Thus, the master equation comprises local Hamiltonians (H_i), pair interactions ($W_i^\dagger W_j$), and decay channels with both local (O_i) and collective ($\sum_i V_i$) jump operators. While we assume here a single type of pair interaction, local and collective decay, the formalism is easily generalized to more general models. The overall N -particle Liouvillian L_N is symmetric under particle exchange, that is $L_N(P_{ij} \rho_N P_{ij}) = P_{ij} L_N(\rho_N) P_{ij}$. We also assume that the state of the compound system is symmetric, $P_{ij} \rho_N P_{ij} = \rho_N$.

Despite the high degree of symmetry integration of the Master equation becomes unfeasible for a large number N of subsystems. However, in many cases the relevant physical quantities are n -particle correlations

of the form $\langle A_1^{\alpha_1} \otimes \cdots \otimes A_n^{\alpha_n} \rangle$ where $n < N$ and observables A_i^α refer to subsystem i . Later on we will use that $\{A_i^\alpha\}_{\alpha=1}^D$ represents a basis in the space of linear operators $\mathcal{B}(\mathcal{H}_1)$ ¹. Any such correlations follows from the reduced density matrix ρ_n for n -subsystems,

$$\left\langle \bigotimes_{i=1}^n A_i^{\alpha_i} \right\rangle = \text{Tr}_N \left[\rho_N \bigotimes_{i=1}^n A_i^{\alpha_i} \right] = \text{Tr}_n \left[\rho_n \bigotimes_{i=1}^n A_i^{\alpha_i} \right] \quad (3.2)$$

where

$$\rho_n = \text{Tr}_{\{n+1, \dots, N\}} [\rho_N],$$

and $\text{Tr}_{\{n+1, \dots, N\}}$ denotes the partial trace over the set of subsystems indicated in the subscript. The trace over all up to the n -th subsystem is denoted by $\text{Tr}_n = \text{Tr}_{\{1, \dots, n\}}$. Note that the correlations considered in (3.2) are not necessarily symmetric, but that due to the assumed symmetry of the state it is irrelevant which subset of $N - n$ particles is traced out. Without loss of generality we chose to track the state ρ_n of the first n subsystems.

Taking the partial trace $\text{Tr}_{\{n+1, \dots, N\}}$ of the Master equation (3.1) and exploiting the symmetry of the state ρ_N one arrives at the equation of motion for the reduced density matrix

$$\begin{aligned} \dot{\rho}_n = L_n(\rho_n) + (N - n) \sum_{i=1}^n \left\{ \frac{1}{i} \left[W_i^\dagger, \text{Tr}_{\{n+1\}} [W_{n+1} \rho_{n+1}] \right] \right. \\ \left. - \frac{1}{2} \left[V_i^\dagger, \text{Tr}_{\{n+1\}} [V_{n+1} \rho_{n+1}] \right] + h.c. \right\} \end{aligned} \quad (3.3)$$

$$=: \mathcal{L}_n(\rho_{n+1}) \quad (3.4)$$

The first term on the right hand side describes the evolution of the first n subsystems as defined by Eq. (3.1), and the second term describes the coupling to the $N - n$ other subsystems. Due to the permutation invariance this coupling can be fully described by the reduced density matrix ρ_{n+1} for the first $n + 1$ subsystems. Thus, the master equation for ρ_n is not closed, because the ρ_{n+1} contains more information than ρ_n – namely information on correlations involving $n + 1$ subsystem – and can therefore not be derived from ρ_n .

The core idea in the cumulant expansion, explained in the next section, is to systematically neglect *only* the $n + 1$ -particle correlations in the density matrix ρ_{n+1} in such a way that the approximate, truncated $n + 1$ -particle density matrix $\rho_{n+1}^{\text{trunc}}$ can be determined from the n -particle state ρ_n . We will see that this systematic approximation yields $\rho_{n+1}^{\text{trunc}}(\rho_n)$ as a, in general, highly nonlinear function of ρ_n giving a closed, but nonlinear differential equation

$$\begin{aligned} \dot{\rho}_n = L_n(\rho_n) + (N - n) \sum_{i=1}^n \left\{ \frac{1}{i} \left[W_i^\dagger, \text{Tr}_{\{n+1\}} [W_{n+1} \rho_{n+1}^{\text{trunc}}(\rho_n)] \right] \right. \\ \left. - \frac{1}{2} \left[V_i^\dagger, \text{Tr}_{\{n+1\}} [V_{n+1} \rho_{n+1}^{\text{trunc}}(\rho_n)] \right] + h.c. \right\}. \end{aligned} \quad (3.5)$$

¹ For a d -dimensional Hilbert space \mathcal{H}_1 we have $D = d^2$

3.3 DENSITY MATRIX CUMULANTS

We start by recalling the formal definition of cumulants and collecting some properties (see [64, 65] and [66, p. 2.290]) which are of importance in the present context. While we are ultimately interested in moments of the form (3.2) with respect to symmetric states ρ_N , we are taking a slightly more general approach in this section and consider general moments of the form $\langle \bigotimes_{i \in \mathbb{A}} A_i^{\alpha_i} \rangle$ for any subset $\mathbb{A} \subseteq \{1, \dots, N\}$ without making any assumption regarding the symmetry of the state.

The *moment generating function*

$$\chi(\{r_j^\alpha\}) := \text{Tr} \left[e^{\sum_{j,\alpha} r_j^\alpha A_j^\alpha} \rho_N \right] \quad (3.6)$$

where $r_j^\alpha \in \mathbb{R}$ ($j = 1, \dots, N, \alpha = 1, \dots, D$) can be used to calculate correlations by taking derivatives and evaluating at $r_j^\alpha = 0$. Slightly more general, for any subset $\mathbb{A} \subseteq \{1, \dots, N\}$ of systems the means of $|\mathbb{A}|$ -particle correlations follow from

$$\left\langle \bigotimes_{i \in \mathbb{A}} A_i^{\alpha_i} \right\rangle = \left(\prod_{i \in \mathbb{A}} \frac{\partial}{\partial r_i^{\alpha_i}} \right) \chi(\{r_j^\alpha\}) \Big|_{r_j^\alpha=0}.$$

Note that we can restrict the derivatives to involve at most one of the parameters $\{r_j^\alpha\}_{\alpha=1}^D$ per particle since we assumed the $\{A_j^\alpha\}_{\alpha=1}^D$ to constitute an operator basis.

The *cumulant generating function* is $\ln \chi(\{r_j^\alpha\})$ and the *cumulants* of $|\mathbb{A}|$ -particle correlations are

$$\left\langle \bigotimes_{i \in \mathbb{A}} A_i^{\alpha_i} \right\rangle_c = \left(\prod_{i \in \mathbb{A}} \frac{\partial}{\partial r_i^{\alpha_i}} \right) \ln \chi(\{r_j^\alpha\}) \Big|_{r_j^\alpha=0}. \quad (3.7)$$

For illustration and later use we write out explicitly the lowest cumulants in terms of moments, that is

$$\begin{aligned} \langle A_1^{\alpha_1} \rangle_c &= \langle A_1^{\alpha_1} \rangle \\ \langle A_1^{\alpha_1} A_2^{\alpha_2} \rangle_c &= \langle A_1^{\alpha_1} A_2^{\alpha_2} \rangle - \langle A_1^{\alpha_1} \rangle \langle A_2^{\alpha_2} \rangle \\ \langle A_1^{\alpha_1} A_2^{\alpha_2} A_3^{\alpha_3} \rangle_c &= \langle A_1^{\alpha_1} A_2^{\alpha_2} A_3^{\alpha_3} \rangle - \langle A_1^{\alpha_1} A_2^{\alpha_2} \rangle \langle A_3^{\alpha_3} \rangle \\ &\quad - \langle A_1^{\alpha_1} A_3^{\alpha_3} \rangle \langle A_2^{\alpha_2} \rangle - \langle A_2^{\alpha_2} A_3^{\alpha_3} \rangle \langle A_1^{\alpha_1} \rangle \\ &\quad + 2 \langle A_1^{\alpha_1} \rangle \langle A_2^{\alpha_2} \rangle \langle A_3^{\alpha_3} \rangle \end{aligned}$$

for, respectively, $\mathbb{A} = \{1\}$, $\mathbb{A} = \{1, 2\}$, and $\mathbb{A} = \{1, 2, 3\}$. In the general case the connection between cumulants and moments (see [67, (2.9)]) is given by

$$\left\langle \bigotimes_{i \in \mathbb{A}} A_i^{\alpha_i} \right\rangle_c = \sum_{\pi \in \pi_{\mathbb{A}}} f(|\pi|) \prod_{\mathbb{B} \in \pi} \left\langle \bigotimes_{i \in \mathbb{B}} A_i^{\alpha_i} \right\rangle \quad (3.8)$$

where

$$f(|\pi|) := (|\pi| - 1)! (-1)^{|\pi|-1},$$

$|\pi|$ denotes the cardinality of the set π , and $\pi_{\mathbb{A}}$ denotes the set of all possible partitions of \mathbb{A} . E.g. for $\mathbb{A} = \{1, 2, 3\}$ the set $\pi_{\mathbb{A}}$ is composed of the elements $\{1, 2, 3\}$, $\{\{1, 2\}, \{3\}\}$, $\{\{1\}, \{2, 3\}\}$, $\{\{1, 3\}, \{2\}\}$, $\{\{1\}, \{2\}, \{3\}\}$.

We now define $\tau_{\mathbb{A}}$ as the operator on the space of particles in \mathbb{A} from which $|\mathbb{A}|$ -particle cumulants can be calculated simply by taking the trace, that is

$$\left\langle \bigotimes_{i \in \mathbb{A}} A_i^{\alpha_i} \right\rangle_c = \text{Tr}_{\mathbb{A}} \left[\tau_{\mathbb{A}} \bigotimes_{i \in \mathbb{A}} A_i^{\alpha_i} \right]. \quad (3.9)$$

We will refer to $\tau_{\mathbb{A}}$ as the *density matrix cumulant* for the ensemble of subsystems in \mathbb{A} . From Eq. (3.8) one can read off that this operator is given by

$$\tau_{\mathbb{A}} := \sum_{\pi \in \pi_{\mathbb{A}}} f(|\pi|) \bigotimes_{\mathbb{B} \in \pi} \rho_{\mathbb{B}} \quad (3.10)$$

where $\rho_{\mathbb{B}}$ denotes the reduced density operator for the subsystems contained in \mathbb{B} . It is straight forward to check that inserting (3.10) in (3.9) yields (3.8). For illustration we write down again the lowest orders, that is,

$$\begin{aligned} \tau_{\{1\}} &= \rho_{\{1\}}, \\ \tau_{\{1,2\}} &= \rho_{\{1,2\}} - \rho_{\{1\}} \otimes \rho_{\{2\}}, \\ \tau_{\{1,2,3\}} &= \rho_{\{1,2,3\}} - \rho_{\{1,2\}} \otimes \rho_{\{3\}} - \rho_{\{1,3\}} \otimes \rho_{\{2\}} \\ &\quad - \rho_{\{1\}} \otimes \rho_{\{2,3\}} + 2\rho_{\{1\}} \otimes \rho_{\{2\}} \otimes \rho_{\{3\}}. \end{aligned} \quad (3.11)$$

The connection to the lowest order cumulants is obvious.

The density matrix $\rho_{\mathbb{A}}$ can be reconstructed from the density matrix cumulants in the same way as moments can be expressed through cumulants. The inverse relation to (3.8) is

$$\left\langle \bigotimes_{i \in \mathbb{A}} A_i^{\alpha_i} \right\rangle = \sum_{\pi \in \pi_{\mathbb{A}}} \prod_{\mathbb{B} \in \pi} \left\langle \bigotimes_{i \in \mathbb{B}} A_i^{\alpha_i} \right\rangle_c. \quad (3.12)$$

from which we conclude

$$\rho_{\mathbb{A}} = \sum_{\pi \in \pi_{\mathbb{A}}} \bigotimes_{\mathbb{B} \in \pi} \tau_{\mathbb{B}}. \quad (3.13)$$

For the lowest orders this is

$$\begin{aligned} \rho_{\{1\}} &= \tau_{\{1\}} \\ \rho_{\{1,2\}} &= \tau_{\{1,2\}} + \tau_{\{1\}} \otimes \tau_{\{2\}} \\ \rho_{\{1,2,3\}} &= \tau_{\{1,2,3\}} + \tau_{\{1,2\}} \otimes \tau_{\{3\}} + \tau_{\{1,3\}} \otimes \tau_{\{2\}} \\ &\quad + \tau_{\{1\}} \otimes \tau_{\{2,3\}} + \tau_{\{1\}} \otimes \tau_{\{2\}} \otimes \tau_{\{3\}}. \end{aligned}$$

We collect a number of properties of density matrix cumulants:

- (i) Density matrix cumulants are Hermitean.

- (ii) Operators $\tau_{\mathbb{A}}$ for $|\mathbb{A}| = 1$ correspond to single particle reduced density operators, that is

$$\tau_{\{i\}} = \rho_{\{i\}} \quad \forall i.$$

- (iii) Operators $\tau_{\mathbb{A}}$ for $|\mathbb{A}| > 1$ are traceless and (partial-trace)-less, that is

$$\text{Tr}_{\mathbb{B}} [\tau_{\mathbb{A}}] = 0 \quad \forall \mathbb{B} \subseteq \mathbb{A}, \mathbb{B} \neq \emptyset. \quad (3.14)$$

Cumulants of second and higher order are invariant under affine transformations (see [67, p. 2.4]). This implies in particular that $\langle \bigotimes_{i \in \mathbb{A}} A_i^{\alpha_i} \rangle_c$ is not changed when we replace any of the operators by $A_i^{\alpha_i} + \mathbb{1}_i$, which directly entails (3.14). For example, the cumulant is unchanged in the replacement $A_1^{\alpha_1} \rightarrow A_1^{\alpha_1} + \mathbb{1}_1$, that is, $\langle \bigotimes_{i \in \mathbb{A}} A_i^{\alpha_i} \rangle_c = \langle (A_1^{\alpha_1} + \mathbb{1}_1) \bigotimes_{i \in \mathbb{A} \setminus \{1\}} A_i^{\alpha_i} \rangle_c$, which implies

$$\begin{aligned} 0 &= \left\langle \bigotimes_{i \in \mathbb{A} \setminus \{1\}} A_i^{\alpha_i} \right\rangle_c = \text{Tr}_{\mathbb{A}} \left[\left(\bigotimes_{i \in \mathbb{A} \setminus \{1\}} A_i^{\alpha_i} \right) \tau_{\mathbb{A}} \right] \\ &= \text{Tr}_{\mathbb{A} \setminus \{1\}} \left[\left(\bigotimes_{i \in \mathbb{A} \setminus \{1\}} A_i^{\alpha_i} \right) \text{Tr}_1 [\tau_{\mathbb{A}}] \right] \quad \forall A_i^{\alpha_i}. \end{aligned}$$

Therefore $\text{Tr}_1 [\tau_{\mathbb{A}}] = 0$. The restriction $|\mathbb{A}| > 1$ is due to the fact that affine transformations do change first order cumulants.

- (iv) For $\mathbb{A} \supseteq \mathbb{B} \supseteq \mathbb{C}$ the density matrix cumulants $\tau_{\mathbb{C}}$ constructed from $\rho_{\mathbb{A}}$ are the same as those constructed from the reduced density matrix $\rho_{\mathbb{B}}$. This follows directly from the definition (3.10) of density matrix cumulants through tensor products of reduced density operators.

3.3.1 Symmetric density matrices and their truncation

The concept of density matrix cumulants is general and applies to all density matrices irrespective of their symmetry. Here we will pick up the discussion of Sec. 3.2 and consider the important special case of symmetric (permutation invariant) density matrices ρ_N of N systems. We remind the reader that we denote by ρ_n the reduced density operator for the first n subsystems. Similarly we will use τ_n for the density matrix cumulant of n -th order referring to the first n subsystems. By π_n we denote the set of partitions of $\{1, \dots, n\}$. We also note that for symmetric states both the reduced density matrix $\rho_{\mathbb{A}}$ and the density matrix cumulants $\tau_{\mathbb{A}}$ for $|\mathbb{A}| < N$ can be constructed from, respectively, ρ_n and τ_n for $n = |\mathbb{A}|$ by relabeling subsystems.

We now come back to the equation of motion for the reduced density operator ρ_n in Eq. (3.4). The challenge is to turn this equation into a closed equation of motion for ρ_n using a suitable approximation for ρ_{n+1} . The n -th order cumulant expansion consists in removing $n + 1$ -th order cumulants from the state ρ_{n+1} maintaining only cumulants of lower order

which, as discussed above, are fully determined by the reduced density operator ρ_n . Accordingly, we define the *truncated density operator* for $n + 1$ subsystems

$$\begin{aligned}\rho_{n+1}^{\text{trunc}} &:= \rho_{n+1} - \tau_{n+1} \\ &= \sum_{\pi \in \pi_{n+1}} \bigotimes_{\mathbb{B} \in \pi} \tau_{\mathbb{B}} - \tau_{n+1} \\ &= \sum_{\substack{\pi \in \pi_{n+1} \\ |\pi| > 1}} \bigotimes_{\mathbb{B} \in \pi} \tau_{\mathbb{B}}\end{aligned}\quad (3.15)$$

By construction the truncated operator involves only density matrix cumulants $\tau_{\mathbb{B}}$ with $|\mathbb{B}| \leq n$ and therefore, is fully determined by ρ_n . Since the density matrix cumulants in general depend in a nonlinear way on the density matrix the same is true for the truncated density operator $\rho_{n+1}^{\text{trunc}}(\rho_n)$ in (3.15). We note that the construction of $\rho_{n+1}^{\text{trunc}}$ can be seen alternatively as an *extension* of ρ_n to $n + 1$ subsystems in a symmetric fashion, fulfilling $\rho_n = \text{Tr}_{\{k\}}[\rho_{n+1}^{\text{trunc}}]$ for all $k \in \{1, \dots, n + 1\}$.

For example, the truncated density matrices for $n = 1$ and $n = 2$ are given by, respectively,

$$\begin{aligned}\rho_2^{\text{trunc}} &= \rho_1 \otimes \rho_2 \\ \rho_3^{\text{trunc}} &= \tau_{\{1,2\}} \otimes \tau_{\{3\}} + \tau_{\{1,3\}} \otimes \tau_{\{2\}} + \tau_{\{1\}} \otimes \tau_{\{2,3\}} \\ &\quad + \tau_{\{1\}} \otimes \tau_{\{2\}} \otimes \tau_{\{3\}} \\ &= \rho_{\{1,2\}} \otimes \rho_{\{3\}} + \rho_{\{1,3\}} \otimes \rho_{\{2\}} + \rho_{\{1\}} \otimes \rho_{\{2,3\}} \\ &\quad - 2\rho_{\{1\}} \otimes \rho_{\{2\}} \otimes \rho_{\{3\}}\end{aligned}$$

where we reinserted the definition of density matrix cumulants (3.10).

Inserting (3.15) in (3.5) yields a closed nonlinear master equation for the reduced n -particle density operator ρ_n in n -th order cumulant expansion. The master equation can be integrated in time with suitable initial conditions or can be solved for the steady state, as will be illustrated in Sec. 3.5 at the example of superradiant systems. The time evolution and stationary values of correlation functions of the form (3.2) involving up to n particles follow from ρ_n .

We emphasize that the master equation (3.5) and the truncated density operator (3.15) are given in a basis independent form which makes it straight forward to derive the corresponding (nonlinear) system of differential equations for moments up to a desired order n and local dimension d . In particular, it is thus a suitable starting point for systematic investigations regarding convergence of cluster expansions for growing truncation order n .

3.4 TWO-TIME CORRELATION FUNCTIONS IN CUMULANT EXPANSION

The previous section presented an approach for determining n -particle single-time correlation functions as given in Eq. (3.2) in a cumulant expansion of the density matrix which systematically truncated cumulants involving $n + 1$ or more particles. In this section we will extend this approach to two-time correlation functions.

As a motivation we consider the example of cavity QED where a collective decay with jump operator $\sum_{i=1}^N V_i$ as in (3.1) is due to collective emission of photons leaking through the cavity. The first order coherence function of emitted light, and per Fourier transform its spectrum, then follow from the two-time correlation function of the collective jump operator

$$\begin{aligned} & \sum_{i,j=1}^N \langle V_i(t+\tau)V_j(t) \rangle \\ &= N(N-1)\langle V_2(t+\tau)V_1(t) \rangle + N\langle V_1(t+\tau)V_1(t) \rangle. \end{aligned}$$

In this section we will show how the cumulant expansion on the level of the density matrix can be adapted and used to derive systematic approximations to two-time correlation functions of this type. While we concentrate here to the most relevant case of two-time 2-particle correlation functions we emphasize that it is straight forward to extend the approach developed in the following to higher order correlation functions.

Thanks to the permutation symmetry it is sufficient to consider 1- and 2-particle correlation functions of the form $\langle A_i^\alpha(\tau)A_1^\beta \rangle$ for $i = 1, 2$. We follow the notation introduced in the previous section, and denote by $\{A_i^\alpha\}$ a basis in the space of linear operators $\mathcal{B}(\mathcal{H}_1)$ of the i -th subsystem. Formally the two-time 2-particle correlation function is given by

$$\langle A_i^\alpha(t+\tau)A_1^\beta(t) \rangle = \text{Tr}_N \left[A_i^\alpha e^{L_N \tau} \left(A_1^\beta \rho_N(t) \right) \right] \quad (3.16)$$

where $\rho_N(t)$ solves the master equation (3.1) and L_N is the full N -particle Liouvillian. Stationary correlation functions are attained in the long time limit with respect to t when $\rho_N(t)$ is effectively replaced by the steady state of the master equation (3.1). In the following we will suppress the argument t keeping in mind that all quantities have an implicit time dependence on t via ρ_N .

Two time correlation functions of the form (3.16) can be calculated in principle without approximation using the quantum regression theorem. In a form suitable for our purpose this theorem states the following: For fixed A_1^β and arbitrary A_i^α two time correlations follow from the operator

$$\omega_N(\tau) := e^{L_N \tau} \left(A_1^\beta \rho_N \right), \quad (3.17)$$

as is clear from Eq. (3.16). In order to determine $\omega_N(\tau)$ one has to solve the same N -particle master equation (3.1) as for the density matrix $\rho_N(t)$,

$$\frac{d}{d\tau} \omega_N(\tau) = L_N(\omega_N(\tau)), \quad (3.18)$$

as follows from the definition (3.17). Eq. (3.18) has to be solved using the initial condition

$$\omega_N(0) = A_1^\beta \rho_N. \quad (3.19)$$

Thus, determining $\omega_N(\tau)$ has the same computational complexity as solving Eq. (3.1) for the state ρ_N . This is also due to the fact that $\omega_N(\tau)$ captures general two time correlation functions of the form

$$\left\langle \left(\bigotimes_{i \in \mathcal{A}} A_i^{\alpha_i} \right) (\tau) A_1^\beta \right\rangle = \text{Tr}_N \left[\omega_N(\tau) \bigotimes_{i \in \mathcal{A}} A_i^{\alpha_i} \right] \quad (3.20)$$

for all $\mathbb{A} \subseteq \{1, \dots, N\}$ involving up to N -particle correlations.

In order to arrive at an approximate description for two-time correlations involving up to some number n of particles we note first that for a given subset \mathbb{A} with $1 \in \mathbb{A}$ we have

$$\left\langle \left(\bigotimes_{i \in \mathbb{A}} A_i^{\alpha_i} \right) (\tau) A_1^\beta \right\rangle = \text{Tr}_{\mathbb{A}} \left[\omega_{\mathbb{A}}(\tau) \bigotimes_{i \in \mathbb{A}} A_i^{\alpha_i} \right]$$

where the reduced operators is

$$\omega_{\mathbb{A}}(\tau) := \text{Tr}_{\{1, \dots, N\} \setminus \mathbb{A}} \left[e^{L_N \tau} \left(A_1^\beta \rho_N \right) \right]. \quad (3.21)$$

For example, 2-particle two-time correlation functions as in (3.16) follow from

$$\left\langle A_i^\alpha(\tau) A_1^\beta \right\rangle = \text{Tr}_{\{1,2\}} \left[A_i^\alpha \omega_{\{1,2\}}(\tau) \right] \quad (3.22)$$

where

$$\omega_{\{1,2\}}(\tau) := \text{Tr}_{\{3, \dots, N\}} \left[e^{L_N \tau} \left(A_1^\beta \rho_N \right) \right]. \quad (3.23)$$

We note that $\omega_{\mathbb{A}}(\tau)$ is permutation symmetric with respect to exchange of any pair of particles $i, j \in \mathbb{A}$ for $i, j \neq 1$. In analogy to the notation for permutation symmetric reduced density matrices used in the previous section we define $\omega_n(\tau)$ as referring to the first n subsystems, e.g. $\omega_2(\tau) = \omega_{\{1,2\}}(\tau)$. Any operator $\omega_{\mathbb{A}}(\tau)$ for $|\mathbb{A}| = n$ can be constructed from $\omega_n(\tau)$ by relabeling.

Taking the derivative of (3.21) with respect to τ gives the equation of motion

$$\begin{aligned} \frac{d}{d\tau} \omega_n(\tau) &= \text{Tr}_{\{n+1, \dots, N\}} [L_N \omega_n(\tau)] \\ &= \mathcal{L}_n(\omega_{n+1}(\tau)) \end{aligned} \quad (3.24)$$

where \mathcal{L}_n is identical to the operator defined in the equation of motion (3.4) for the reduced density operator for n particles. This clearly follows from the fact that $\omega_n(\tau)$ and $\rho_N(t)$ obey the same equation of motion. Thus, as before we have to find a suitable approximation for $\omega_{n+1}(\tau)$ relating it to operators of lower order $\omega_n(\tau)$ in order to close the equation of motion (3.24).

3.4.1 Generating function of two-time correlations

The first step is to generalize the moment generating function in Eq. (3.6) to a moment generating function for two-time correlations

$$\chi \left(\tau, \{r_j^\alpha\}, \{s_l^\beta\} \right) := \text{Tr} \left[e^{\sum_{j,\alpha} r_j^\alpha A_j^\alpha} e^{L\tau} \left(e^{\sum_{l,\beta} s_l^\beta A_l^\beta} \rho_N \right) \right]$$

where $r_j^\alpha, s_l^\beta \in \mathbb{R}$. All moments of two time correlations can be derived from this generating function. For example, two-time 2-particle correlations of the type given in Eq. (3.16) are

$$\left\langle A_i^{\alpha_i}(t + \tau) A_k^{\beta_k}(t) \right\rangle = \frac{\partial^2}{\partial r_i^{\alpha_i} \partial s_k^{\beta_k}} \chi \left(\tau, \{r_j^\alpha\}, \{s_l^\beta\} \right) \Big|_{r_j^\alpha = s_k^\beta = 0}.$$

More generally, for $\mathbb{A}, \mathbb{B} \subseteq \{1, \dots, N\}$

$$\begin{aligned} & \left\langle \left(\bigotimes_{i \in \mathbb{A}} A_i^{\alpha_i} \right) (\tau) \left(\bigotimes_{k \in \mathbb{B}} A_k^{\beta_k} \right) \right\rangle \\ &= \left(\prod_{i \in \mathbb{A}} \frac{\partial}{\partial r_i^{\alpha_i}} \right) \left(\prod_{k \in \mathbb{B}} \frac{\partial}{\partial s_k^{\beta_k}} \right) \chi \left(\tau, \{r_j^\alpha\}, \{s_l^\beta\} \right) \Big|_{r_j^\alpha = s_k^\beta = 0}. \end{aligned}$$

The corresponding two time cumulants follow from their generating function in the same way as in Eq. (3.7)

$$\begin{aligned} & \left\langle \left(\bigotimes_{i \in \mathbb{A}} A_i^{\alpha_i} \right) (\tau) \left(\bigotimes_{k \in \mathbb{B}} A_k^{\beta_k} \right) \right\rangle_c \\ &= \left(\prod_{i \in \mathbb{A}} \frac{\partial}{\partial r_i^{\alpha_i}} \right) \left(\prod_{k \in \mathbb{B}} \frac{\partial}{\partial s_k^{\beta_k}} \right) \ln \chi \left(\tau, \{r_j^\alpha\}, \{s_l^\beta\} \right) \Big|_{r_j^\alpha = s_k^\beta = 0}. \end{aligned} \quad (3.25)$$

As a particular case of special importance we consider two-time 3-particle cumulants for which one finds

$$\begin{aligned} & \left\langle A_1^{\alpha_1} A_2^{\alpha_2} A_3^{\alpha_3} (\tau) A_1^\beta \right\rangle_c \\ &= \text{Tr}_{\{1,2,3\}} \left[A_1^{\alpha_1} A_2^{\alpha_2} A_3^{\alpha_3} \left\{ \omega_{\{1,2,3\}}(\tau) + 2\rho_{\{3\}} \otimes \rho_{\{2\}} \otimes \omega_{\{1\}}(\tau) \right. \right. \\ & \quad \left. \left. - \rho_{\{2,3\}} \otimes \omega_{\{1\}} - \omega_{\{1,3\}}(\tau) \otimes \rho_{\{2\}} - \omega_{\{1,2\}}(\tau) \otimes \rho_{\{3\}} \right\} \right] \end{aligned} \quad (3.26)$$

The expression in curly brackets generalizes the third order density matrix cumulant τ_3 in Eq. (3.11) to the context of two-time correlations.

3.4.2 Truncation of two-time correlations at second order

In order to evaluate 2-particle two time correlations we truncate $\omega_3(\tau)$ by setting two-time 3-particle cumulants (3.26) to zero. This is achieved by replacing $\omega_3(\tau) = \omega_{\{1,2,3\}}(\tau)$ by its truncated version

$$\begin{aligned} \omega_3^{\text{trunc}}(\tau) &:= -2\rho_{\{3\}} \otimes \rho_{\{2\}} \otimes \omega_{\{1\}} + \rho_{\{2,3\}} \otimes \omega_{\{1\}} \\ & \quad + \omega_{\{1,3\}}(\tau) \otimes \rho_{\{2\}} + \omega_{\{1,2\}}(\tau) \otimes \rho_{\{3\}} \end{aligned} \quad (3.27)$$

where $\omega_{\{1,3\}}$ follows from $\omega_2 = \omega_{\{1,2\}}$ by relabeling, and $\omega_{\{1\}} = \text{Tr}_2[\omega_{\{1,2\}}]$. It is important to note that the truncation (3.27) is linear in $\omega_2(\tau)$, in contrast to the nonlinear truncation of the density matrix in Sec. 3.3.1. Using Eq. (3.27) we can now replace $\omega_3(\tau)$ with $\omega_3^{\text{trunc}}(\tau)$ in equation system (3.24) and get a closed and linear differential equation system for 2-particle two time correlation

$$\frac{d}{d\tau} \omega_2(\tau) \approx \mathcal{L}_2 \left(\omega_3^{\text{trunc}}(\tau) \right) \quad (3.28)$$

According to Eq. (3.19) this has to be solved under the initial condition $\omega_2(0) = A_1^\beta \rho_2$ where ρ_2 solves Eq. (3.5).

We conclude this section by indicating how this result generalizes to two-time correlation functions of higher order. In the context of cavity QED the evaluation of the second order coherence function would require to determine two-time correlation functions of the form

$$\begin{aligned} \langle V_2(t)V_4(t+\tau)V_3(t+\tau)V_1(t) \rangle &= \text{Tr}_N \left[V_4 V_3 e^{L_N \tau} (V_1 \rho_N V_2) \right] \\ &= \text{Tr}_4 [V_4 V_3 \omega_4(\tau)] \end{aligned}$$

From the discussion above it will be clear that these follow from solving the four-particle master equation

$$\frac{d}{d\tau} \omega_4(\tau) = \mathcal{L}_4(\omega_5(\tau))$$

using the initial condition $\omega_4(\tau) = V_1 \rho_4 V_2$ along with a truncation of $\omega_5(\tau)$ at fourth order. Eq. (3.25) implies that the truncation will give rise to a linear equation of motion in $\omega_4(\tau)$ with inhomogeneities which depend nonlinearly on $\omega_4(\tau)$, that is, on two-time correlations of lower order (as defined in Eq. (3.21)). Analogous statements hold for two-time correlations of arbitrary order.

3.5 EXAMPLES

In this section we will provide brief illustrations of the technique developed above. In particular, we will discuss the treatment of a superradiant laser in terms of cumulant expansions up to sixth order (Sec. 3.5.1), and the time evolution of a superradiant spin ensemble under inhomogeneous dephasing as observed recently by Angerer et al. (Sec. 3.5.2).

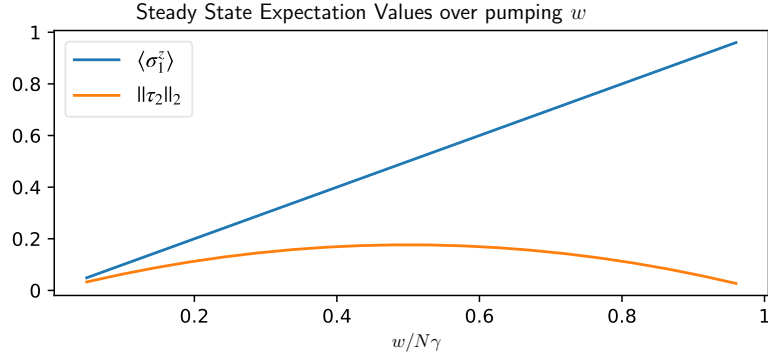


Figure 3.1: Polarization $\langle \sigma_1^z \rangle$ and norm of the two-atom density matrix cumulants $\|\tau_2\|_2$ versus the pumping rate w . The calculation was done with $n = 6$ atom correlations assuming vanishing 7th order cumulants and $N = 10^8$.

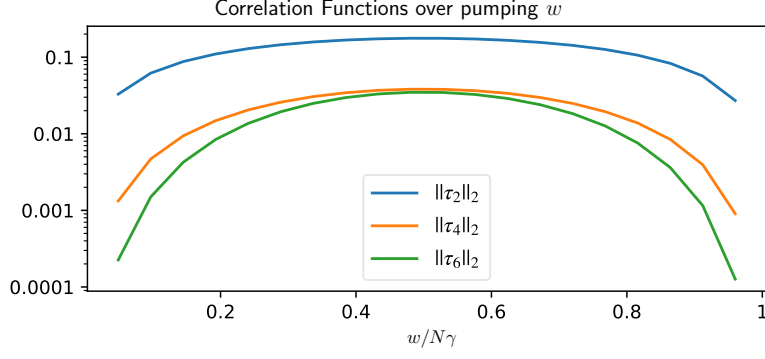


Figure 3.2: Norms of the density matrix cumulants of order 2, 4, and 6. The odd orders 3 and 5 are positive and smaller than $3 \cdot 10^{-7}$, and therefore of the same order of magnitude as the numerical precision. Truncation order and N are identical to the ones used in Fig. 3.1.

3.5.1 Steady state

We state the master equation (1.3) of the superradiant laser, introduced in Chapter 1 again

$$\dot{\rho} = w \sum_{i=1}^N \mathcal{D} [\hat{\sigma}_i^+] \rho + \gamma \mathcal{D} \left[\sum_{i=1}^N \hat{\sigma}_i^- \right] \rho. \quad (3.29)$$

Applying the density matrix cumulant method with truncation of 7-atom cumulants gives a nonlinear differential matrix equation (3.5). We integrate this equation numerically until the state is close to the steady state, meaning $\|\dot{\rho}\| \leq \epsilon/s$ with an $\epsilon \ll 1$. The polarization and atom-atom correlations, i.e., the norm of τ_2 in the steady state are plotted Fig. 3.1 confirming the analytical results plotted in Fig. 1.2 of Chapter 1.

The analytic formulas were derived by approximating that the third order cumulants vanish [19]. Due to the combined following facts approximating vanishing third-order cumulants, as done in [19], is an extremely good approximation:

- (i) $\|\tau_3\|_2$ and $\|\tau_5\|_2$ are several orders of magnitude smaller than the norms of the even order density matrix cumulants (see Fig. 3.2).
- (ii) Moments of order k couple to moments of maximum order $k + 1$, due to the fact that the collective jump operator in equation (3.1) is in essence a two-subsystem interaction term.

The norms of the odd-order density matrix cumulants must however not be small in general, where it is then crucial to take higher order density matrix cumulants into account.

3.5.2 Time evolution

Another application for the presented approximation method is to resolve the time evolution of a system with non-negligible subsystem correlations.

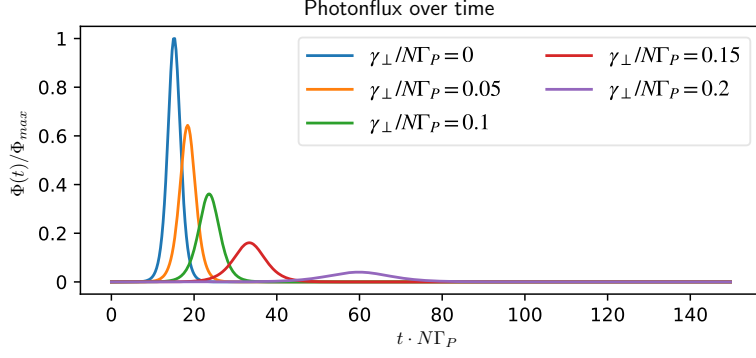


Figure 3.3: Photon flux $\Phi(t) = \kappa \langle \hat{a}^\dagger(t) \hat{a}(t) \rangle = \Gamma_P \sum_{i,j=1}^N \langle \sigma_i^+(t) \sigma_j^-(t) \rangle$ versus time t scaled to its maximum $\Phi_{\max} = \max_{t, \gamma_\perp} \Phi(t) \approx 1.24 \cdot 10^{23}$ Hz with parameters $\gamma_\perp = 2\pi \cdot 2.7$ MHz, $\Gamma_P = 4g^2/\kappa = 2\pi \cdot 7.5 \cdot 10^{-10}$ Hz $\approx 5 \cdot 10^{-9}$ Hz, $g = 2\pi \cdot 72$ mHz, $\kappa = 2\pi \cdot 13.8$ MHz. The initial state at $t = 0$ is chosen such that it is close to the fully inverted state with small correlations to shorten the delay time until a superradiant burst forms.

Angerer et al. studied a dense ensemble of approximately $N = 10^{16}$ NV-centers coupled to a fast decaying cavity [35]. Taking in account only the dominant single NV-center dephasing and collective decay we can write the evolution after eliminating the cavity mode $\hat{a} \approx \frac{2g}{\kappa} \sum_{i=1}^N \sigma_i^-$ as

$$\dot{\rho} = \gamma_\perp \sum_{i=1}^N \mathcal{D}[\sigma_i^z] \rho + \Gamma_P \mathcal{D} \left[\sum_{i=1}^N \sigma_i^- \right] \rho.$$

Similar to the superradiant laser the system has two competing terms: The dephasing term with rate γ_\perp destroying correlations between NV-centers and the collective decay term with rate Γ_P building up correlations. The correlations between NV-centers enhance the decay rate by a factor $\propto N$ resulting in a strong but quickly subsiding superradiant burst. We numerically integrate this evolution using the presented method of density matrix cumulant expansion and truncation assuming third order cumulants vanish. We plot the resulting photon flux in Fig. 3.3 and observe that the dephasing delays and reduces the intensity of the superradiant burst.

This is also visible in Fig. 3.4 showing maximal photon flux versus dephasing rate γ_\perp . The maximal photon flux decreases faster-than-exponential with increasing dephasing γ_\perp until the maximal atom-atom correlations associated with a superradiant burst would be smaller than the correlations of the initial state.

For analytical results we derive the moment system

$$\begin{aligned} \frac{d}{dt} \langle \sigma_1^z \rangle &= -\Gamma_P (1 + \langle \sigma_1^z \rangle + 2(N-1) \langle \sigma_1^+ \sigma_2^- \rangle) \\ \frac{d}{dt} \langle \sigma_1^+ \sigma_2^- \rangle &= \frac{1}{2} \Gamma_P (1 + \langle \sigma_1^z \rangle) \langle \sigma_1^z \rangle \\ &\quad + (- (4\gamma_\perp + \Gamma_P) + (N-2)\Gamma_P \langle \sigma_1^z \rangle) \langle \sigma_1^+ \sigma_2^- \rangle \end{aligned}$$

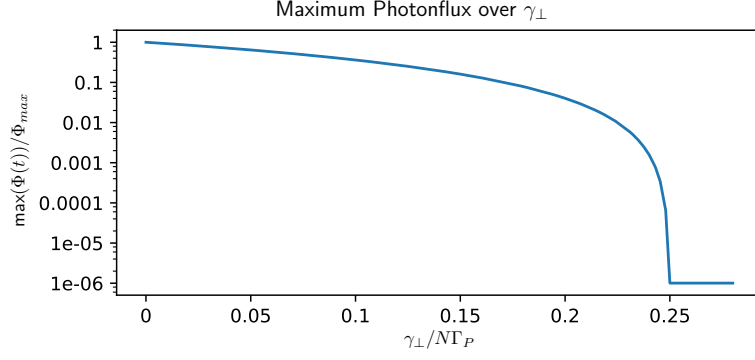


Figure 3.4: Maximal Photon flux $\Phi(t)$ versus the dephasing rate γ_{\perp} . Increasing γ_{\perp} beyond the upper bound $\gamma_c = (N-2)\Gamma_P/4$ fails to create a superradiant burst and just reduces the initial correlations, which correspond to a photon flux $\Phi(0) \approx 10^{-6}\Phi_{max}$. All parameters are chosen identical to the ones in Fig. 3.3.

where we assumed vanishing $\langle \sigma_1^z \sigma_2^z \rangle_c$ and third order cumulants, giving a closed nonlinear equation system. For $N\Gamma_P, \gamma_{\perp} \gg \Gamma_P$ we simplify the second order correlation evolution

$$\frac{d}{dt} \langle \sigma_1^+ \sigma_2^- \rangle \approx (-4\gamma_{\perp} + (N-2)\Gamma_P \langle \sigma_1^z \rangle) \langle \sigma_1^+ \sigma_2^- \rangle$$

showing that the correlations will never increase to form a superradiant burst unless

$$(N-2)\Gamma_P \langle \sigma_1^z \rangle > 4\gamma_{\perp}. \quad (3.30)$$

This gives an upper dephasing bound $\gamma_{\perp} < \gamma_c = (N-2)\Gamma_P/4$, which is clearly visible in the numerical results in Fig. 3.4.

3.6 FUNDAMENTAL PROBLEMS

Our method also allows us clearly identify certain problems and limitations of the widely used cumulant expansion approximation.

3.6.1 Estimation of approximation errors

Replacing ρ_{n+1} in (3.4) with $\rho_{n+1}^{\text{trunc}}$ in (3.5) is an approximation, based on the assumption that the density matrix cumulant τ_{n+1} does not change the dynamics significantly because it is in some sense small. This assumption can be checked systematically by increasing the truncation order as far as possible, say $1 \leq n \leq n'$ and verifying that

- (i) $\|\tau_m\|_2$ is getting smaller for increasing $1 \leq m \leq n'$.
- (ii) the expectation values converge to a certain value for increasing $1 \leq m \leq n'$. Since the density matrix is nothing but a collection of expectation values we can define the density matrix distance

$$d_m := \left\| \rho_n - \text{Tr}_{\{n+1, \dots, m\}} [\rho_m] \right\|_2 \quad (3.31)$$

which has to converge for increasing m .

Both methods are not fail-safe – one can think of the steady state ρ_N being a purely N -subsystem entangled state without any lower k -subsystem correlations. However in the presence of single subsystem jump operators O_i with a comparable rate to the collective processes we expect this problem not to occur.

3.6.2 Problems

While we introduced the formalism with density matrix cumulants and the truncation of the density matrix, they map 1:1 to cumulants and to the cumulant truncation widely used in various problems. Therefore all problems below also occur in other cumulant truncations, even when it is harder to spot them there.

INITIAL STATE DEPENDENCE Given that (3.1) has one unique steady state, it is not clear that this is also the case for (3.5), because $\rho_{n+1}^{\text{trunc}}$ depends on ρ_n nonlinearly and (3.5) is therefore a nonlinear differential equation. For specific systems one could compare the steady states of multiple integrations with varying initial states, to gain more confidence about the uniqueness of the steady state.

INTEGRATION POSITIVITY While integration of the full linear differential equation (3.1) guarantees, due to the complete positivity of the Liouvillian, that an initial density matrix will stay a density matrix, this is not the case for the approximated nonlinear differential equation (3.5). At least in the presented formalism, we have access to the density matrix ρ_n and can simply check for positivity. If one does only a cumulant expansion for a subset of operators, one cannot check positivity of the density matrix.

TRUNCATION POSITIVITY Given a symmetric density matrix ρ_{n+1} , it is not clear that $\rho_{n+1}^{\text{trunc}}$ is positive.

QUANTUM MARGINAL PROBLEM Given a symmetric density matrix ρ_n , it is not clear if there exists a symmetric ρ_N , such that $\rho_n = \text{Tr}_{\{n+1, \dots, N\}}[\rho_N]$. One counter example is ρ_2 being a symmetric maximally entangled state. This is a special case of the Quantum Marginal Problem [68], which is QMA-complete [69] (QMA is the quantum analogue of NP).

For the mean-field case, i.e. $n = 1$, the problems “Truncation positivity” and “Quantum Marginal Problem” do not occur, due to lack of any correlations.

3.7 SUMMARY

We presented how a symmetric – meaning subsystem permutation invariant – master equation with a maximum of two-subsystem interaction Hamiltonian and collective jumps of local operators can be approximately integrated for a small ensemble of n subsystems keeping up to n -order correlations. For this we decompose a density matrix into *density matrix cumulants*, see Sec. 3.3 allowing us to systematically truncate the density

matrix of $n + 1$ subsystems and closing the evolution equation for n subsystems.

Furthermore we showed in Sec. 3.4 how to derive two-time correlation functions, from which one immediately gets the spectrum via Fourier transform, using the same formalism and a generalized truncation.

The presented method works for any subsystem algebra, e.g. higher spins, and arbitrary correlation order n without any analytical effort. It only requires numerically integrating a complex nonlinear matrix differential equation, which we implemented using freely available software (python, QuTiP [50], SciPy [70], NumPy, and matplotlib [71]). We demonstrated the method for examples requiring the full time evolution in Sec. 3.5.2 and the steady state properties in Sec. 3.5.1.

COLLECTIVE EFFECTS IN ATOMIC ENSEMBLES INTERACTING WITH LIGHT

4.1 INTRODUCTION

We investigate if and how superradiance appears in an ensemble of alkali metal atoms being continuously probed by an off-resonant laser. It was demonstrated that entanglement between two atomic ensembles of alkali metal atoms in steady state can be achieved [24, 72]. These ensembles can also be used for magnetometry [73] using Faraday rotation. The work in this chapter is centered around the experiments in Eugene Polzik's lab at the Niels Bohr Institute [12, 22–24, 74, 75]. The setup contains a continuously and off-resonantly probed ensemble of Caesium atoms, each with nine relevant ground-state hyperfine levels. Orthogonal to the probe propagation direction is a magnetic field energetically splitting the hyperfine levels. A pumping laser polarizes the atoms along the axis of the magnetic field. We will break the topic down into three sections introducing different aspects of the system:

- SEC. 4.2 We define the *generalized superradiant laser*, consisting of an ensemble of two-level atoms, which additional to the collective down jumps and single-atom up jumps of the superradiant laser has collective up jumps and single-atom down jumps. Its behavior, when varying the four rates, is the key to understand the behavior of more complicated multi-level atoms.
- SEC. 4.3 Before we consider the nine-levels of the Caesium $F = 4$ ground state manifold, we introduce a simplified model with three-level $F = 1$ atoms. The jump operators between these three levels are designed such, that (1) it captures the most essential features of the Caesium atoms, e.g., the angle of linear polarization of the probe laser and ground-state Zeeman splitting, and (2) it is simple enough to understand it in terms of the generalized superradiant laser. We can numerically and approximately integrate this master equation until a steady state is reached and calculate properties like the polarization, population, and atom-atom correlations. This integration is achieved by means of the cumulant expansion method developed in Chapter 3 and its implementation in our Python program. In addition to the steady state we can also calculate the spectrum and distinguish which transition is superradiant using nonlinear level splitting.
- SEC. 4.4 In this section we start from the free-space, off-resonant atom-light interaction and derive the master equation of ground-state levels only, which include probe-induced collective and non-collective jumps. We show that the master equation contains collective jump operators of similar structure as the ones considered in Sec. 4.3 and then use the cumulant expansion method developed in Chapter

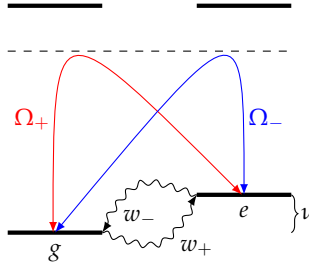


Figure 4.1: The figure shows the level scheme of an atom with a two-level ground state manifold consisting of states g and e . Off-resonant probing leads to the following coherent processes: (i) the creation of a red sideband photon with atomic transition $g \rightarrow e$ with rate Ω_+ and (2) the creation of a blue sideband photon with atomic transition $e \rightarrow g$ with rate Ω_- . Additionally, the incoherent processes are driving the population with rate w_+ to state e and with rate w_- to state g .

3 to numerically integrate the evolution. The results, e.g., polarization and atom-atom correlation, involving all nine levels, are remarkably similar to the ones in Sec. 4.3 showing that we captured the essential features in the three-level model.

4.2 GENERALIZED SUPERRADIANT LASER

We consider an ensemble of two-level systems coupling to a cavity mode \hat{a} . The two levels have an energetic difference of $\hbar\nu$ and the transitions $g - e$ and $e - g$ couple to the cavity mode with single photon Rabi frequencies $\Omega_+/2$ and $\Omega_-/2$, respectively (see Fig. 4.1). Each two-level system is also subject to incoherent jumps from $g \rightarrow e$ with rate w_+ and from $e \rightarrow g$ with rate w_- . The combined atom-cavity system can be described by the master equation

$$\begin{aligned} \dot{\rho} = & \frac{\nu}{i} [J^z, \rho] + \frac{1}{i} \left[\left(\frac{\Omega_-}{2} J^- + \frac{\Omega_+}{2} J^+ \right) \hat{a}^\dagger + \text{h.c.}, \rho \right] \\ & + w_+ \sum_{i=1}^N \mathcal{D} [\sigma_i^+] \rho + w_- \sum_{i=1}^N \mathcal{D} [\sigma_i^-] \rho + \kappa \mathcal{D} [\hat{a}] \rho \end{aligned}$$

using the collective atomic operators $J^\pm = \sum_{i=1}^N \sigma_i^\pm$ and $J^z = \frac{1}{2} \sum_{i=1}^N \sigma_i^z$. For a fast decaying cavity we can adiabatically eliminate the cavity mode \hat{a} , meaning $\hat{a} \simeq -i(\Omega_- J^- e^{-i\nu t} + \Omega_+ J^+ e^{i\nu t})/\kappa$, giving the permutation invariant master equation in the frame rotating at frequency ν

$$\begin{aligned} \dot{\rho} = & w_+ \sum_{i=1}^N \mathcal{D} [\sigma_i^+] \rho + \gamma_- \mathcal{D} \left[\sum_{i=1}^N \sigma_i^- \right] \rho \\ & + w_- \sum_{i=1}^N \mathcal{D} [\sigma_i^-] \rho + \gamma_+ \mathcal{D} \left[\sum_{i=1}^N \sigma_i^+ \right] \rho \end{aligned} \quad (4.1)$$

with the rates $\gamma_\pm = \Omega_\pm^2/\kappa$. We already applied the Rotating Wave Approximation splitting the Lindblad term and removing the fast oscillating terms with frequencies $\pm 2\nu$ compared to the coupling rate γ_\pm . The first two terms are identical to a superradiant laser [18, 19], while the third

and fourth can be regarded as a superradiant laser with interchanged levels. Switching the first and second term off, of course results in a trivial variation of the superradiant laser. However all four terms in combination give new behavior, e.g., a second Lorentz peak in the spectrum, and a more general condition for superradiance. From (4.1) we derive the evolution of the expectation values

$$\begin{aligned} \frac{d}{dt} \langle \sigma_1^z \rangle &= w_+ (1 - \langle \sigma_1^z \rangle) - w_- (1 + \langle \sigma_1^z \rangle) \\ &\quad - 2(N-1) (\gamma_- - \gamma_+) \langle \sigma_1^+ \sigma_2^- \rangle \\ \frac{d}{dt} \langle \sigma_1^+ \sigma_2^- \rangle &= ((N-2) (\gamma_- - \gamma_+) \langle \sigma_1^z \rangle - (w_+ + w_- + \gamma_- + \gamma_+)) \times \\ &\quad \times \langle \sigma_1^+ \sigma_2^- \rangle + \frac{1}{2} ((\gamma_- - \gamma_+) + (\gamma_- + \gamma_+) \langle \sigma_1^z \rangle) \langle \sigma_1^z \rangle \end{aligned} \quad (4.2)$$

where we factorized $\langle \sigma_1^z \sigma_2^z \rangle \approx \langle \sigma_1^z \rangle^2$ and $\langle \sigma_1^+ \sigma_2^- \sigma_3^z \rangle \approx \langle \sigma_1^+ \sigma_2^- \rangle \langle \sigma_1^z \rangle$ as in [19] assuming negligible cumulants $\langle \sigma_1^z \sigma_2^z \rangle_c$ and $\langle \sigma_1^+ \sigma_2^- \sigma_3^z \rangle_c$.

4.2.1 Steady State

The steady state expectation values can be obtained by setting the left hand sides of equations (4.2) to zero and solving the resulting quadratic equation. The steady state solution of $\langle \sigma_1^+ \sigma_2^- \rangle$ shows that correlations corresponding to the superradiant laser regime can only exist if the single-atom up jump rate w_+ fulfills the inequalities

$$w_- < w_+ < N (\gamma_- - \gamma_+) \frac{w_+ - w_-}{w_+ + w_-} \quad (4.3)$$

where we assumed large atom numbers $N \gg 1$, $w_+ \gg \gamma_{\pm}$ and a dominant single-atom up jump rate $w_+ > w_-$. The opposite case $w_- \gg \gamma_{\pm}$ and $w_+ < w_-$ is a trivial variation by interchanging the role of upper and lower levels, which we will not discuss further.

We show the steady state polarization $\langle \sigma_1^z \rangle$ and atom-atom correlation $\langle \sigma_1^+ \sigma_2^- \rangle$ in the contour plots in Fig. 4.2. Plots a), b), c) have no single-atom down jumps, i.e., $w_- = 0$ and plots d), e), f) have a single-atom down jump rate $w_- = N\gamma_-/60$ leading to a smaller superradiant regime.

Cuts through the contour plots at fixed γ_+ give a relatively simple behavior: the polarization is piecewise linear and the correlations have, at least for $w_- = 0$, the shape of an inverted parabola as plotted in Fig. 4.3. However cuts through the contour plot at fixed w_+ have a significantly more difficult behavior as can be seen in Fig. 4.4. These cuts are however the important ones for our discussion, as in the later sections about alkali metal atoms we show how geometrical aspects of the light-matter interactions determine the ratio of the rates Ω_{\pm} and with it the ratio of γ_{\pm} . The nonlinear behavior when varying the collective up jump rate γ_+ can also be seen for the maximal atom-atom correlations

$$\max_{w_+} \langle \sigma_1^+ \sigma_2^- \rangle = \frac{1}{8} - \frac{w_-}{N(\gamma_- - \gamma_+)}$$

at the optimal pumping strength $w_{+,opt} = -w_- + N(\gamma_- - \gamma_+)/2$.

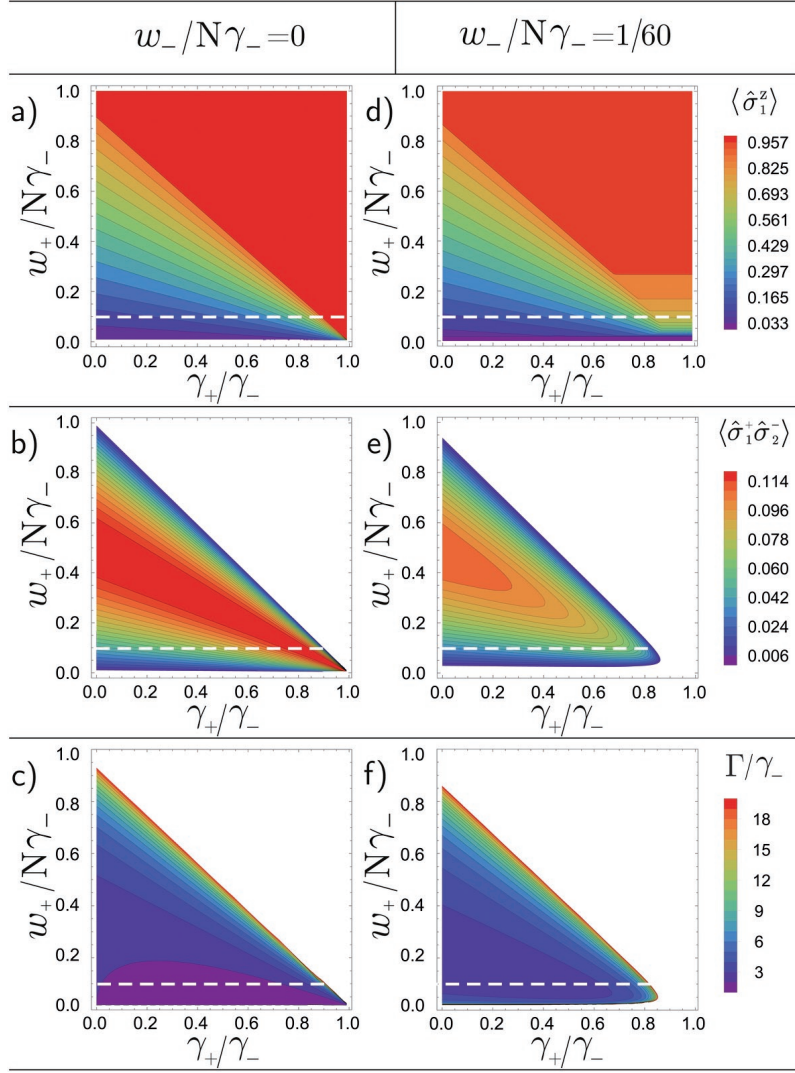


Figure 4.2: The polarization $\langle \sigma_1^z \rangle$, atom-atom correlation $\langle \sigma_1^+ \sigma_2^- \rangle$, and full-width at half maximum of the Lorentz peak Γ varied over the collective up rate γ_+ and single-atom pump rate w_+ . The single-atom down jump rate is $w_- = 0$ in a), b), c) and $w_- = N\gamma_-/60$ in d), e), f). The dashed lines are at the parameter $w_+ = N\gamma_-/10$ plotted again in Fig. 4.4.

4.2.2 Spectrum

The striking feature of the superradiant laser is its linewidth of the order of the atomic linewidth γ_- , even though the ensemble is incoherently pumped with a much stronger rate w_+ . We will now show that in the generalized superradiant laser (4.1) for $\gamma_- > \gamma_+$ we essentially get two superradiant lasers each for γ_- and γ_+ radiating at the same time, both with identical linewidth of the order of γ_- but different amplitudes.

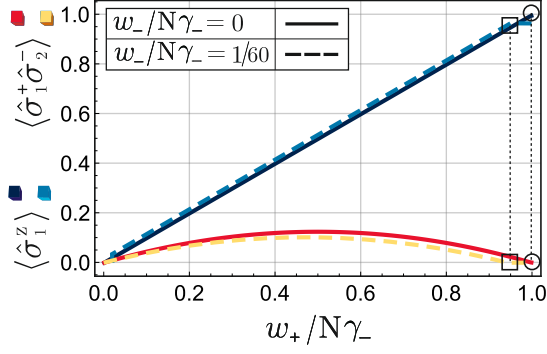


Figure 4.3: The polarization $\langle \hat{\sigma}_1^z \rangle$, and atom-atom correlation $\langle \hat{\sigma}_1^+ \hat{\sigma}_2^- \rangle$ varied over the single-atom pump rate w_+ and for vanishing collective up jump rate $\gamma_+ = 0$. The plot shows the known dependence for the single-atom down jump rate $w_- = 0$. For $w_- = N\gamma_-/60$ the plot shows a flattening of the polarization already for $\langle \hat{\sigma}_1^z \rangle < 1$ due to the reduced superradiant regime.

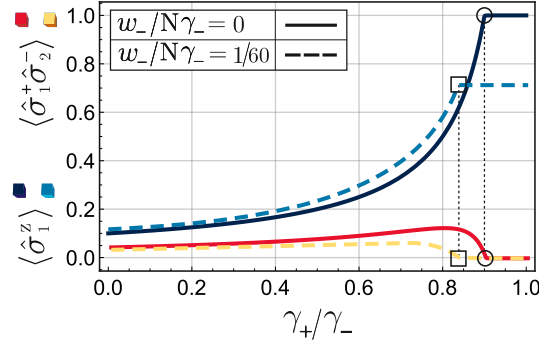


Figure 4.4: The polarization $\langle \hat{\sigma}_1^z \rangle$, and atom-atom correlation $\langle \hat{\sigma}_1^+ \hat{\sigma}_2^- \rangle$ varied over the collective up jump rate γ_+ . The single-atom up jump rate $w_+ = N\gamma_-/10$ is a special case of Fig. 4.2 (indicated by the dashed line). Varying γ_+ allows to scan through the superradiant regime. For γ_+ close below the upper threshold of the superradiant regime (4.3), the polarization and atom-atom correlation are strongly dependent on γ_+ , and therefore very sensitive to small changes.

The spectrum of the output light of the cavity is given by the Fourier transformed two-time correlation function

$$\begin{aligned}
 S(\omega) &= \mathcal{F} \left[\left\langle \hat{a}^\dagger(t) \hat{a}(0) \right\rangle \right] (\omega) \\
 &\approx \frac{\Omega^2}{\kappa^2} \mathcal{F} \left[\langle J^+(t) J^-(0) \rangle + \langle J^-(t) J^+(0) \rangle \right] (\omega)
 \end{aligned} \tag{4.4}$$

where $\mathcal{F} [f(t)] (\omega) = \frac{1}{\sqrt{2\pi}} \int_{-\infty}^{\infty} dt e^{-it\omega} f(t)$ is the Fourier transform of a function f . The terms $\langle J^\pm(t) J^\pm(0) \rangle$ are not appearing in the spectrum (4.4), because their initial value in the steady state $\langle J^\pm(0) J^\pm(0) \rangle$ vanishes due to the J^z symmetry of the master equation (4.1). Using the evolution of the expectation value

$$\frac{d}{dt} \langle J^- \rangle = - \left(i\nu + \frac{\Gamma}{2} \right) \langle J^- \rangle$$

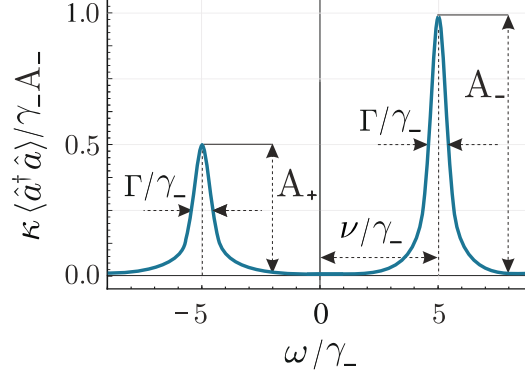


Figure 4.5: Spectrum $S(\omega)$ of the generalized superradiant laser with $w_- = 0$, $\gamma_+ = \gamma_-/2$, $\nu = 5\gamma_-$, and $w_+ = N\gamma_-/10$. We see two Lorentz peaks at $\omega/\gamma_- = \pm 5$ with identical width Γ , but different maxima A_{\pm} . The maxima ratio A_+/A_- is approximately the ratio of collective up jumps and collective down jumps γ_+/γ_- .

with the linewidth $\Gamma = \gamma_- + \gamma_+ + w_+ + w_- - (N-1)(\gamma_- - \gamma_+) \langle \sigma_1^z \rangle$ and the Quantum Regression Theorem [33], we derive the analog equation for the two-time collective atomic spin correlation functions

$$\begin{aligned} \frac{d}{dt} \langle J^-(t) J^+(0) \rangle &= \left(-i\nu - \frac{\Gamma}{2} \right) \langle J^-(t) J^+(0) \rangle \\ \frac{d}{dt} \langle J^+(t) J^-(0) \rangle &= \left(i\nu - \frac{\Gamma}{2} \right) \langle J^+(t) J^-(0) \rangle. \end{aligned} \quad (4.5)$$

These two equations can be readily solved, each giving an exponential function, such that the spectrum (4.4) is given by two Lorentz functions. While the position of the peaks is at $\pm\nu$, their width Γ is identical (see Fig. 4.5). One should note that the peak at $-\nu$ coming from the collective up jump can only exist because the collective down jump is dominant. Reducing γ_- below γ_+ will not allow any superradiance (see equation (4.1)) and both peaks will vanish.

The linewidth Γ for $w_+ > w_-$ to leading order $1/N$ is

$$\frac{\Gamma}{\gamma_-} \approx \left(\frac{1}{W_- (1 - W_+)} + \frac{W_+}{1 - W_+} - W_+ - \frac{1}{W_-} \right) \left(1 - \frac{\gamma_+}{\gamma_-} \right)$$

where we defined the dimensionless variables

$$W_{\pm} := (w_+ \pm w_-) \frac{w_+ + w_-}{N(\gamma_- - \gamma_+)(w_+ - w_-)}$$

scaling with the upper superradiant boundary (4.3). The linewidth Γ is plotted in Figs. 4.2 c), f). We see that the generalized superradiant laser preserves the remarkable feature of the superradiant laser – the linewidth of the order of the effective atomic decay rate γ_- – even for non-vanishing γ_+ . And even with additional additional single-atom down jump rate w_- the linewidth increases only slightly (see Fig. 4.2 f)).

In the spectrum of the emitted light of the cavity (see Fig. 4.5) we can see that the maximum of the peak corresponding to collective down

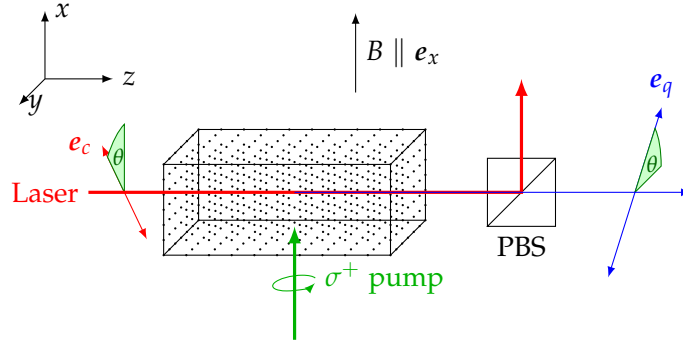


Figure 4.6: An atomic ensemble, being continuously probed by a linearly polarized laser and optically pumped by a circularly polarized laser. The probe is aligned with the z -axis and the polarization direction is tilted by the angle θ against the magnetic field B . The off-resonant two-photon transitions induced by the probe laser creates photons with orthogonal polarization, which can be extracted by a polarizing beamsplitter (PBS). The circularly polarized pump laser is parallel to the magnetic field B and polarizes the atoms orthogonal to the probe laser.

jumps at $\omega = \nu$ is significantly higher. We can calculate the Lorentz peak maxima ratio

$$\frac{A_+}{A_-} = \frac{\gamma_+}{\gamma_-} \frac{1}{1 - \frac{\langle J^z \rangle}{\langle J^+ J^- \rangle}} \approx \frac{\gamma_+}{\gamma_-} \quad (4.6)$$

for $N \gg 1$ in the superradiant regime, which is simply the ratio of collective jump rates. We want to point out that equal Lorentz peak height is not possible, because the superradiant condition (4.3) can not be fulfilled for $\gamma_+ = \gamma_-$.

4.3 THREE-LEVEL ATOM

The ensemble of two-level systems in Sec. 4.2 even including the single-atom down jump and collective up jump is in most cases an idealization, because almost all physical systems have more than two levels and in many cases more than two play a relevant part in the dynamics. One of those cases are alkali metal atoms. In Sec. 4.4 we consider e.g. the Caesium $F = 4$ ground state with nine levels combined with complicated single-atom and collective jump terms. While the two-level system in Sec. 4.2 made it possible to understand the fundamental behavior of the generalized superradiant laser, we will now progress to understand the next more complicated system: a three-level system. The advantage is that one can understand the three-level system as two stacked two-level systems, of which the behavior is known. The three-level system we are considering is the minimal idealized version of the setup in Sec. 4.4. It consists of an ensemble of alkali metal atoms being continuously probed by an off-resonant laser in z direction and being optically pumped along the x direction using a circularly polarized laser (see Fig. 4.6). The linear polarization of the probe laser is rotated compared to the quantization axis x by an angle θ . Photons created during the atom-light

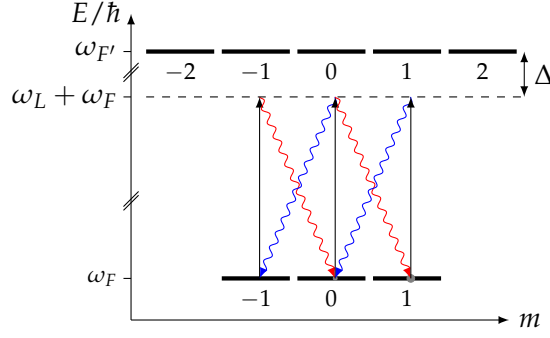


Figure 4.7: The figure shows the level scheme of the alkali metal atoms with quantization axis x parallel to the magnetic field B , creating a Zeeman splitting (not visible in figure). The transitions are two-photon Raman transitions due to the off-resonant laser: A laser photon with frequency ω_L (black) with vertical polarization is absorbed, indicated by the virtual level (dashed). Then there are two possible transitions: (1) emission of a horizontal polarized blue-detuned photon to a $m - 1$ level, (2) emission of a horizontal polarized red-detuned photon to a $m + 1$ level.

interaction with orthogonal linear polarization to the probe laser, which are associated with a change of magnetic quantum number m , can be extracted via a polarizing beamsplitter. Each atom has three levels in the ground state manifold and five in the excited state manifold (see Fig. 4.7). The probe laser frequency ω_L is far detuned from the resonance frequency $\omega_{F'} - \omega_F$, inducing two-photon butterfly-transitions. The levels of the ground state manifold are non-degenerate due to a magnetic field B in x direction, leading to distinct red and blue sidebands around the laser frequency, associated with distinguishable atomic up and down jumps, respectively. The simplified version of the dynamics of the ground state density matrix is

$$\begin{aligned} \dot{\rho} = & \frac{1}{i} \sum_{i=1}^N \left[\sum_{m=-1}^1 \omega_m |m\rangle \langle m|_i, \rho \right] \\ & + w_+ \sum_{i=1}^N \mathcal{D} [F_i^+] \rho + \gamma \mathcal{D} [V^-(\theta)] \rho \\ & + w_- \sum_{i=1}^N \mathcal{D} [F_i^-] \rho + \gamma \mathcal{D} [V^+(\theta)] \rho \end{aligned} \quad (4.7)$$

where $F_i^\pm := (\mp F_i^z + iF_i^y)/\sqrt{2}$ and $F_i^0 := F_i^x$ are the angular momentum operators in the spherical basis with quantization axis x of atom i . The angular momentum vector $\mathbf{F}_i = (F_i^x \ F_i^y \ F_i^z)^t$ in Cartesian basis fulfills $\mathbf{F}_i \times \mathbf{F}_i := i\mathbf{F}_i$. We choose a simplified version of the collective jump operators $V^\pm(\theta) := \sum_{i=1}^N V_i^\pm(\theta)$ and the single-atom jump operators

$$V_i^\pm(\theta) = \left(1 + \epsilon \cos(2\theta) \left(\mp F_i^0 + 1/2 \right) \right) F_i^\pm \quad (4.8)$$

depending on the linear polarization angle $\theta \in [0, 2\pi)$ for the small parameter $0 \leq \epsilon < 1$. The dynamics of master equation (4.7) can also be

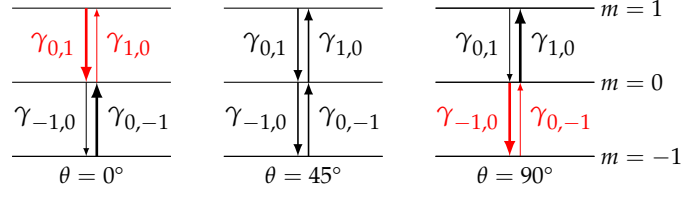


Figure 4.8: Transition rates $\gamma_{m,n}$ between the different ground state levels m of the alkali metal atom for angles $\theta = 0^\circ, 45^\circ, 90^\circ$. The thickness of the line represents a measure for the transition strength. Transition with superradiant lasing are shown in red.

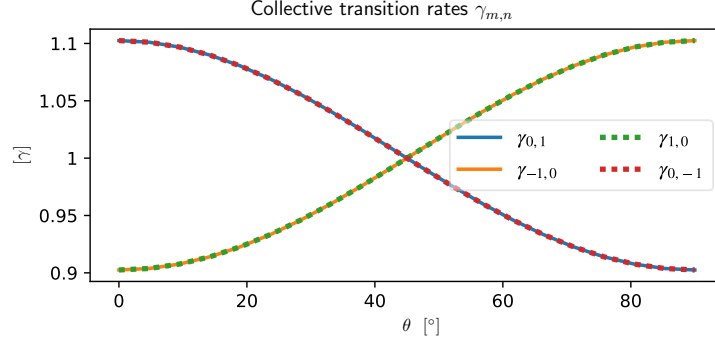


Figure 4.9: Transition rates $\gamma_{m,n}$ over the angle θ , for $\epsilon = 0.1$. One can see that the rates of opposite direction and involving different levels are identical, i.e., $\gamma_{0,1} = \gamma_{0,-1}$ and $\gamma_{-1,0} = \gamma_{1,0}$.

analyzed for higher spins, but for simplicity we restrict (4.7) to spin-1 atoms ($F = 1$) with three angular momentum levels $m \in \{-1, 0, 1\}$, i.e., $(F_i)^2 |1, m\rangle_i = F(F+1) |1, m\rangle_i = 2 |1, m\rangle_i$. As in the case of the generalized superradiant laser in Sec. 4.2 we restrict the analysis to $w_+ > w_-$, because $w_+ < w_-$ corresponds to a trivial interchange of the upper and lower levels.

The collective jump operators $V^\pm(\theta)$ capture the most essential feature of the much more complicated jump operators in Sec. 4.4, meaning the angle θ tunes the imbalance of the collective up and down rates

$$\begin{aligned} \gamma_{m,n} &:= \gamma |\langle 1, m | V_i^{m-n}(\theta) | 1, n \rangle|^2 \\ &= \gamma (1 + \epsilon \cos(2\theta) (\mp m + 1/2))^2 \end{aligned} \quad (4.9)$$

of the jump operator $V_i^\pm(\theta)$ where $m - n = \pm 1$ and $m, n \in \{-1, 0, 1\}$. Their schematic θ and level dependence is shown in the level scheme in Fig. 4.8, and their exact θ dependence in Fig. 4.9. This imbalance is additionally level dependent, such that the imbalance $\gamma_{0,1}/\gamma_{1,0}$ of the upper transition is exactly the inverse of the imbalance $\gamma_{-1,0}/\gamma_{0,-1}$ of the lower transition.

4.3.1 Steady state expectation values

Using the numerical approximation method developed in Chapter 3 we can integrate the dynamics (4.7) and extract both the reduced density

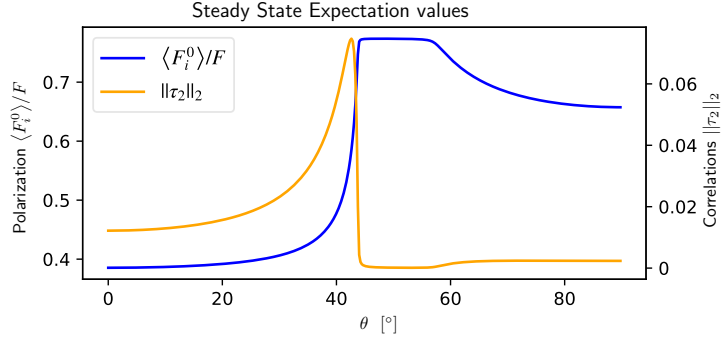


Figure 4.10: Polarization $\langle F_i^0 \rangle / F$, and norm of second order density matrix cumulant $\|\tau_2\|_2$ over the angle θ . The parameters are chosen the following way: For a fixed $N\gamma_-$ we need a small single-atom down jump rate $w_- = N\gamma/1000$ to be in a regime of significant collective effects. The single-atom up jump rate follows as $w_+ = 5w_-$ to create a significant population inversion.

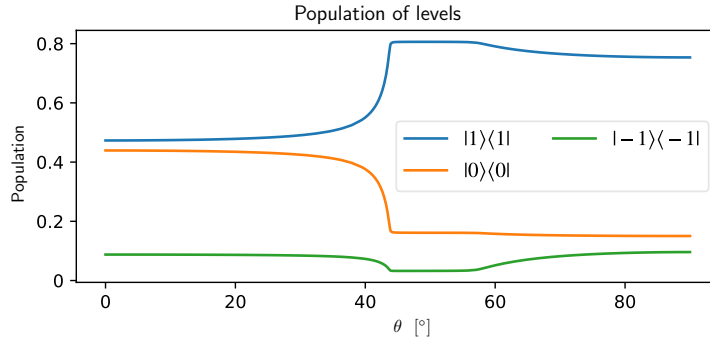


Figure 4.11: The population of the levels $|m\rangle\langle m|$ indicates which transition is lasing because it shifts the population compared to the non-lasing behavior at $\theta = 45^\circ$. The parameters are the same as in Fig. 4.10

matrix for two atoms and the two-time correlation functions in the steady state. From the steady state reduced density matrix we can calculate expectation values such as the polarization $\langle F_i^0 \rangle / F$ (see Fig. 4.10) and the population of different levels $|m\rangle\langle m|$ (see Fig. 4.11) depending on the angle θ . The polarization $\langle F_i^0 \rangle / F$ strongly depends on the parameter θ caused by the collective jump operators $V_i^\pm(\theta)$. We can understand this behavior by considering each transition in Fig. 4.8 involving only two levels and comparing it with the superradiant condition (4.3) of the generalized superradiant laser. For the upper transition $m = 1 \leftrightarrow m = 0$ and $\theta = 0$ the collective down jump is dominant, due to $\gamma_{0,1}/\gamma_{1,0} = ((2 + \epsilon)/(2 - \epsilon))^2 > 1$, while the single-atom up jumps are dominant, i.e., $w_+ > w_-$. This allows superradiance, meaning correlations between atoms build up and the atoms emit collectively such that the emitted intensity scales with N^2 . For $\theta \geq 45^\circ$ the collective up jumps are dominant, due to $\gamma_{0,1}/\gamma_{1,0} \leq 1$, meaning the superradiant condition (4.3) cannot be fulfilled. Tuning θ between 0° and 45° gives a polarization curve

in Fig. 4.10 similar to Fig. 4.4. This similarity is even more impressive, because in Fig. 4.10 *both* rates $\gamma_{0,1}$, $\gamma_{1,0}$ are *nonlinearly* dependent on θ , while in Fig. 4.4 only $\gamma_{1,0}$ is changed linearly.

The lower transition can fulfill the superradiant condition (4.3) only for $\theta > 45^\circ$, with a maximum dominant collective down rate $\gamma_{-1,0}$ for $\theta = 90^\circ$, resulting in polarization curve similar to Fig. 4.4 with inverted x -Axis.

Superradiance implies an enhanced collective jump rate proportional to N , necessarily decreasing the polarization $\langle F_i^0 \rangle / F$.

- The superradiant transition for $\theta < 45^\circ$ shifts much of the population from $|1\rangle \langle 1|$ to $|0\rangle \langle 0|$ (see Fig. 4.11). The small change in population of $|-1\rangle \langle -1|$ is a result of the single-atom down jumps with rate w_- shifting the population of $|0\rangle \langle 0|$ downwards.
- The superradiant transition for $\theta > 45^\circ$ shifts the population from $|0\rangle \langle 0|$ to $|-1\rangle \langle -1|$. The change in population of $|1\rangle \langle 1|$ is a result of the single-atom down jumps with rate w_- shifting the population of $|1\rangle \langle 1|$ downwards.

The two dips in polarization in Fig. 4.10 have different depth due to the difference in available population of the involved levels (see Fig. 4.11). For example, the collective jumps for $\theta = 90^\circ$ involve fewer atoms than for $\theta = 0^\circ$, because there are fewer atoms in the state $|0\rangle \langle 0|$ than in $|1\rangle \langle 1|$, due to the dominant single-atom up jump rate w_+ . One can estimate that due to the ratio of level population $\langle 0 | \rho_i | 0 \rangle / \langle 1 | \rho_i | 1 \rangle \approx 0.2$ of atom i in the uncorrelated steady state ($\theta = 45^\circ$) the intensity ratio of the two peaks should be approximately $(0.2)^2 = 0.04$, due to the quadratic intensity dependence on available atoms N in the superradiant regime. This fits well with the approximate ratio 0.03 of the maximum of the Lorentz peaks of the spectrum (see the color legends of Fig. 4.12).

4.3.2 Spectrum

We consider equation (4.7) as the dynamics of atoms identically coupling to a fast decaying cavity, where the cavity mode was adiabatically eliminated (compare with Sec. 4.2). The spectrum of the light leaving the cavity in the steady state can be calculated via the Fourier transition of atomic two-time correlation functions

$$\begin{aligned} & \sum_{i,j=1}^N \langle V_i(t+\tau) V_j(t) \rangle \\ &= N(N-1) \langle V_2(t+\tau) V_1(t) \rangle + N \langle V_1(t+\tau) V_1(t) \rangle. \end{aligned}$$

where we defined $V_i := V_i^+(\theta) + V_i^-(\theta)$. These correlation functions allow calculating the spectrum $S(\omega) \propto \sum_{i,j=1}^N \mathcal{F} [\langle V_i(\tau) V_j(0) \rangle]$ (ω) where $t = 0$ refers to the steady state and are accessible using the numerical approximation method introduced in Chapter 3 and.

To be able to distinguish upper and lower transitions in the spectrum we assume a nonlinear splitting Zeeman states and set

$$\omega_{-1} = 0, \quad \omega_0 = 10\gamma, \quad \omega_1 = 30\gamma$$

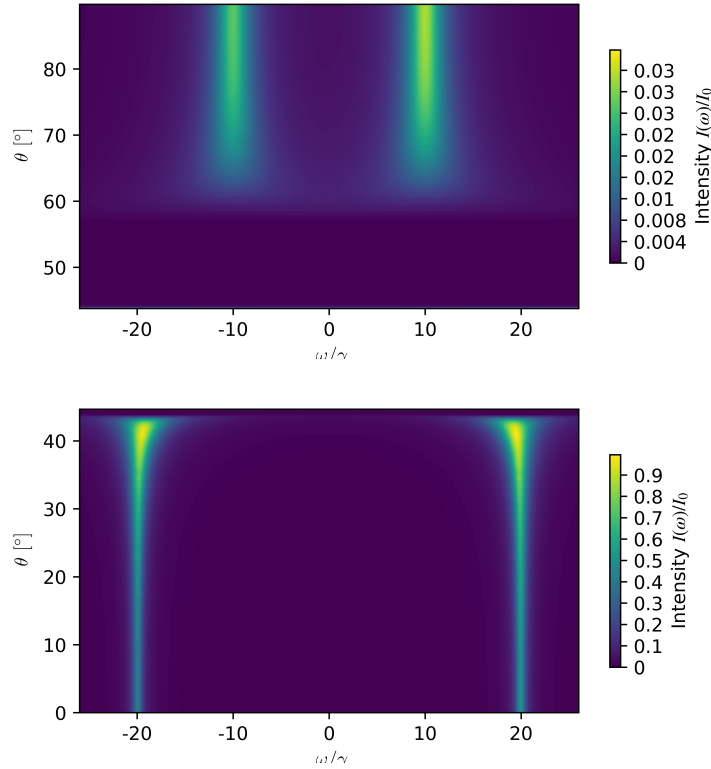


Figure 4.12: The Spectrum $S(\omega)$ plotted as color over the frequency ω on the x-axis and angle θ on the y-axis (separated in two plots due to different color scales). The lower plot shows the two Lorentz peaks at $\omega = \pm 20\gamma$ associated with a superradiant transition on the upper levels, while the upper plot has the Lorentz peaks at $\omega = \pm 10\gamma$ associated with a superradiant transition of the lower levels. One also can see the left and right Lorentz peaks at $\omega = \pm 20\gamma$ and $\omega = \pm 10\gamma$ are imbalanced, having an approximate ratio of maxima identical to the collective up and down ratios as in the generalized superradiant laser (see equation (4.6)). The maximum intensity of the upper plot reaches only about $0.03S_0$ of the maximum intensity $S_0 = \max_{\omega} S(\omega)$ in the lower plot. The parameters are identical to Fig. 4.10.

such that the lower transition $m = 0 \leftrightarrow m = -1$ has the difference $\omega_0 - \omega_{-1} = 10\gamma$ and the upper transition $m = 1 \leftrightarrow m = 0$ has the difference $\omega_1 - \omega_0 = 20\gamma$. The spectrum in Fig. 4.12 reveals clearly that for $0^\circ \leq \theta < 45^\circ$ only the upper transition is superradiant and for $45^\circ \leq \theta \leq 90^\circ$ only the lower transition as expected from the superradiant condition (4.3).

Additionally we can extract the full-width at half maximum Γ of the dominant Lorentz peak and plot it in Fig. 4.13. The width Γ is in the superradiant regions on the left and right of 45° of the same order of magnitude as the collective jump rate γ , while in the non-superradiant regime around 45° the linewidth increases three orders of magnitude.

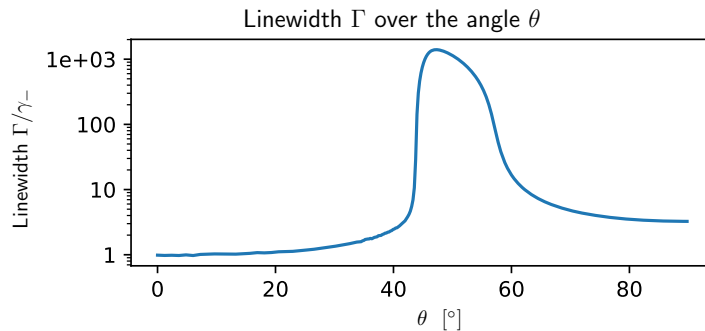


Figure 4.13: Full-width at half maximum – also called linewidth – Γ plotted versus the angle θ . The superradiant regimes for $\theta \lesssim 45^\circ$ and $\theta \gtrsim 50^\circ$ have a linewidth of the order of the collective jump rate γ , while in the uncorrelated regime in between the linewidth increases three orders of magnitude. The parameters are identical to Fig. 4.10.

4.4 ALKALI METAL ATOMS WITH OFF-RESONANT PROBE BEAM

4.4.1 Introduction and definitions

This section contains the derivation of the dynamics of the Caesium atoms being probed and optically pumped continuously and in orthogonal directions. The addressed transition involves nine non-degenerate hyperfine levels in ground-state manifold and multiple excited-state manifolds. There has been previous work about this kind of off-resonant probing focusing on different aspects, e.g., the polarizability tensor [76], pulsed schemes [75, 77], and two ground-state levels [72]. We derive the ground-state only master equation

- for arbitrary spins of the ground state manifold of alkali-metal atoms with the example of Caesium (spin four)
- for large hyperfine splitting in the ground state manifold
- including probe induced single atom-decay
- arbitrary angle of linear polarization of the probe laser

4.4.1.1 Atomic ensemble

We consider an ensemble of N alkali metal atoms in a box see Fig. 4.6. The atoms are continuously probed by an off-resonant laser of wavelength λ_c propagating in z direction. Its linear polarization is rotated by an angle θ relative to the x -axis. The atoms have an optical transition with central wavelength $\lambda_a = 2\pi c/(\omega_{F'} - \omega_F)$ between the excited state manifolds with average energy $\hbar\omega_{F'}$ and the ground state manifold with energy $\hbar\omega_F$ (see Fig. 4.14). The magnetic field B in x direction leads to a Zeeman splitting Ω_Z of the hyperfine levels of the atoms. At the same time the atoms are being continuously optically pumped by a circularly polarized pump laser in the x direction. If the collective atomic spin would be aligned with the laser propagation direction we would expect a Faraday

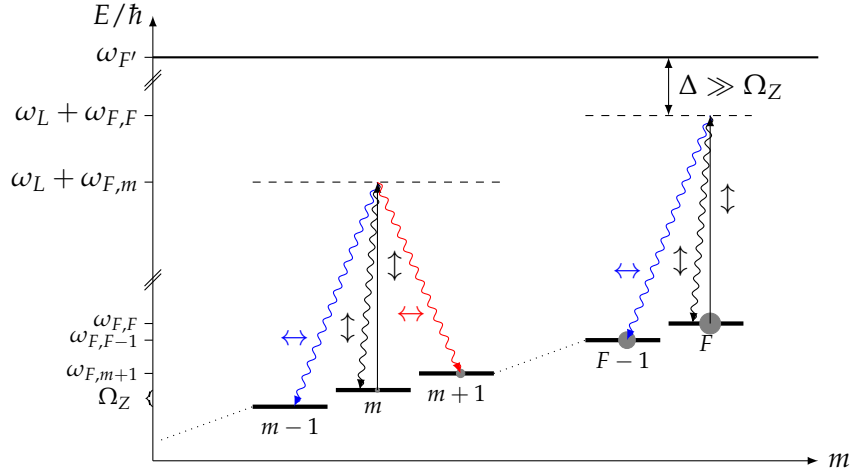


Figure 4.14: The figure shows the level scheme with quantization axis x parallel to the magnetic field B . The levels in the ground state manifold are different angular momentum states $|F, m\rangle$, in the x -quantization axis, splitted by the Zeeman frequency Ω_Z . The transitions are two-photon Raman transitions due to the off-resonant laser: A laser photon with vertical polarization is (virtually) absorbed, indicated by the virtual level (dashed). Then there are three possible transitions: (1) emission of a vertical polarized photon back to the same level, (2) emission of a blue-detuned horizontal polarized photon to a $m - 1$ level, (3) emission of a red-detuned horizontal polarized photon to a $m + 1$ level. The strength of the transitions is given by the Clebsch-Gordon coefficients, and the rate depends additionally on the mean populations of the different levels. The single-atom up jump rate w_+ shifts the population (indicated by gray spheres) up to $m = F$, increasing the intensity of the blue-detuned Lorentz peak.

rotation of the light polarization – which corresponds to a transfer of angular momentum of the atoms to the light mode. Here, however, the collective spin is polarized in x direction orthogonal to the light propagating in z direction, meaning the Faraday rotation is due to the fluctuations of the collective atomic spin in the z direction. The fluctuations in the z direction result in simultaneous clockwise and anti-clockwise Faraday rotation with vanishing average. Both rotations can be resolved not only due to orthogonal polarization compared to the probe laser, but also due to the Zeeman splitting of the hyperfine levels, leading to clearly distinguishable sidebands around the laser frequency ω_L .

Another picture to explain the behavior is to set the quantization axis of the atomic hyperfine levels in the x direction along the magnetic field B (see Fig. 4.14). Here we can interpret the interaction of atom i with the probe laser as up and down jumps between total angular momentum states $|F, m\rangle_i$. The linear polarization of the emitted photons when $\Delta m = \pm 1$ is orthogonal to the quantization direction x , and parallel when $\Delta m = 0$.

Even though the atoms are thermal in the setup [22] they can emit collectively into the forward scattered mode, but dominantly non-collectively in all other directions, due to motional averaging [78]. We will not go into the details of this but merely mention that a two-photon process

with emission in any but the forward direction – the probe laser direction z – contains a phase based on the quickly changing position of the atoms. This position dependence leads to a dominantly non-collective decay into all but the forward direction where the interaction is position independent. Additionally one could enhance the direction of collective emission by shaping the optical density of the atomic ensemble in the forward direction.

4.4.1.2 Relevant transitions

The relevant optical transition (see Fig. 4.14) is due to a change of orbital angular momentum of the single electron in the outer-most shell of the alkali metal atom. In the single-electron model of all alkali metal atoms we have three angular momentum operators coupling together resulting in the hyperfine structure [79]: the electron spin S , the orbital angular momentum L of the electron, and the total nuclear angular momentum I . While the electron spin $S = 1/2$ and the core spin $I = 7/2$ for Caesium are fixed, The angular momentum quantum number changes between the ground state $L = 0$ and the excited state $L = 1$ resulting in an energy splitting with optical frequency. Considering the atom as one object, the three angular momenta couple together to the total angular momentum $F = S + L + I$. To understand the states involved we couple first the spin and orbital angular momentum $J = S + L$ giving the ground state $J = 1/2$, also called $6^2S_{1/2}$. For the excited state we can have $J = 1/2$ and $J = 3/2$, also called $6^2P_{1/2}$ and $6^2P_{3/2}$ respectively. From both excited states there are two optical transitions to the ground state, also called $D_1 : 6^2P_{1/2} \rightarrow 6^2S_{1/2}$ and $D_2 : 6^2P_{3/2} \rightarrow 6^2S_{1/2}$ line, of which only the D_2 line is addressed by the probe laser. One can further couple the total nuclear angular momentum I to the spin-orbit angular momentum J , giving the total angular momentum $F = J + I$. For the ground state one gets $F \in \{3, 4\}$, of which only $F = 4$ is relevant for our discussion (in reality one needs to repump $F = 3$ to $F = 4$). For the excited state involved in the D_2 transition, i.e., $J = 3/2$, we get $F' \in \mathbb{F}' := \{2, 3, 4, 5\}$, which we denote with a prime to indicate the excited state. In Fig. 4.14 are the ground state levels depicted, while we only indicate the excited state manifolds F' by their average frequency $\omega_{F'}$.

4.4.1.3 Angular momentum operators

We already mentioned that the vectors F, S, L, I , each composed of three linear operators, e.g., $F = (F_x \ F_y \ F_z)^t$ in the Cartesian basis, are angular momentum operators [80, Sec. 18.1], meaning they fulfill the angular momentum algebra

$$[F_m, F_n] = i \sum_k \epsilon_{mnk} F_k \quad (4.10)$$

for $m, n, k \in \{x, y, z\}$. Using the Casimir operator F^2 and choosing the quantization axis $F_0 = F_x$ we can define the eigenbasis $|F, m_F\rangle_x$ fulfilling the eigenvalue equations

$$F^2 |F, m_F\rangle_x = F(F+1) |F, m_F\rangle_x, \quad (4.11)$$

$$F_0 |F, m_F\rangle_x = m_F |F, m_F\rangle_x \quad (4.12)$$

corresponding to the *angular momentum quantum number* F and the *magnetic quantum number* $m_F \in \{-F, -F+1, \dots, F\}$. Unless otherwise stated we always use the quantization axis x and just write $|F, m_F\rangle$ or even shorter $|F, m\rangle$. The Hilbert space \mathcal{H}_i of atom i can be spanned by the eigenbasis $|F, m_F\rangle$ associated with angular momentum operator $F_i \in \mathbb{O}_i^3$ where $\mathbb{O}_i := \mathcal{B}(\mathcal{H}_i)$ is the space of linear operators on the single atom Hilbert space.

4.4.1.4 Dipole operator

To write the atom-light interaction in the master equation we require the *dipole operator* \mathbf{d}_i of the D_2 transition of atom i (see [79, 81]). We can split up the dipole operator $\mathbf{d}_i = \mathbf{d}_{i,F'F}^+ + \mathbf{d}_{i,F'F}^-$ into an up jump and down jump

$$\mathbf{d}_{i,F'F}^+ := \pi_i^{F'} \mathbf{d}_i \pi_i^F, \quad \mathbf{d}_{i,F'F}^- := \left(\mathbf{d}_{i,F'F}^+ \right)^\dagger, \quad (4.13)$$

respectively using the projection $\pi_i^F := \sum_{m_F=-F}^F |F, m_F\rangle \langle F, m_F|_{i,x}$. We also define dimensionless transition operators

$$\sigma_{i,F'F}^+ := \frac{\mathbf{d}_{i,F'F}^+}{d_{F'}}, \quad \sigma_{i,F'F}^- := \left(\sigma_{i,F'F}^+ \right)^\dagger \quad (4.14)$$

using the Reduced Matrix Element $d_{F'} := \langle F' || \mathbf{d}_i^+ || F \rangle$ in the convention of Brink et al. [82].

4.4.1.5 Notation

A vector operator, such as the angular momentum operator, $\mathbf{O} \in \mathbb{O}_i^3$ has an outer three-dimensional vector structure and an inner operator structure. We need to clarify that the transposition of the inner operator structure of an operator $O \in \mathbb{O}_i$ is denoted with a capital T, such that the transposition and conjugation can be written as $O^\dagger = (O^*)^T$. The transposition of the outer vector structure $\mathbf{O}^t \equiv (O^x \ O^y \ O^z)$ is denoted by a small t. For a matrix of operators $M \in \mathbb{O}_i^{3 \times 3}$ we define the symbol +h.c. by an outer transposition t , an operator transposition T , and a complex conjugation $*$, i.e., $M + \text{h.c.} := M + (M^t)^\dagger$, which allows us to write

$$\mathbf{v}^t M \mathbf{v}^\dagger + \text{h.c.} = \mathbf{v}^t (M + \text{h.c.}) \mathbf{v}^\dagger \in \mathbb{O}_i$$

for $\mathbf{v} \in \mathbb{O}_i^3$. Furthermore we define a simplified summation notation $\sum_{m_F} := \sum_{m_F=-F}^F$ for a sum over the entire manifold F , analog for F' , and denote by $\sum_i := \sum_{i=1}^N$ a sum over all atoms i .

4.4.2 Full atom-light interaction

As mentioned, the atoms couple only to the forward scattered light mode collectively such that we can split the wave vectors \mathbf{k} into a forward set $b = \{\mathbf{k} : (1 - \mathbf{k}^t \mathbf{k}_c / k_c^2) < \vartheta\}$ and its complement \bar{b} . In total we consider three electrical fields at the positions \mathbf{r}_i of atom i :

- The probe laser $\mathcal{E} = \mathcal{E}^- + \text{h.c.}$ as a classical field with wave vector \mathbf{k}_c and linear polarization vector $\mathbf{e}_c = (\cos \theta \quad \sin \theta \quad 0)^t$ being tilted by θ with respect to the x axis. We define

$$\mathcal{E}^-(\mathbf{r}_i, t) = \rho_c \sqrt{\frac{N_{ph}}{T}} u(\mathbf{r}_i) e^{-i(\mathbf{k}_c^t \mathbf{r}_i - \omega_L t)} \mathbf{e}_c \quad (4.15)$$

where A is the beam cross section, N_{ph}/T the photonflux, $\rho_c = \sqrt{\frac{\hbar \omega_L}{2\epsilon_0 c A}}$ the electrical field per photon, ω_L the angular frequency, and $u(\mathbf{r}_i) = 1$ inside the area A perpendicular to the propagation direction and vanishes otherwise.

- The forward scattered electrical field $\mathbf{E}_{\text{fwd}} = \mathbf{E}_{\text{fwd}}^- + \text{h.c.}$ we model as a quantum field, containing only the forward scattered wave vectors $\mathbf{k} \in b$ with

$$\mathbf{E}_{\text{fwd}}^-(\mathbf{r}_i) = \sum_{\lambda} \int_b d\mathbf{k} \rho_{\omega} \hat{a}_{\mathbf{k},\lambda}^{\dagger} e^{-i\mathbf{k}^t \mathbf{r}_i} \mathbf{e}_{\mathbf{k},\lambda} \quad (4.16)$$

where λ labels the polarization direction, $\rho_{\omega} = \sqrt{\frac{\hbar \omega}{2\epsilon_0 (2\pi)^3}}$, and $[\hat{a}_{\mathbf{k},\lambda}, \hat{a}_{\mathbf{k}',\lambda'}^{\dagger}] = \delta(\mathbf{k} - \mathbf{k}') \delta_{\lambda,\lambda'}$.

- The electrical field $\mathbf{E}_{\text{se}} = \mathbf{E}_{\text{se}}^- + \text{h.c.}$ in all other directions $\mathbf{k} \in \bar{b}$, resulting from spontaneous emission of the atoms with

$$\mathbf{E}_{\text{se}}^-(\mathbf{r}_i) = \sum_{\lambda} \int_{\bar{b}} d\mathbf{k} \rho_{\omega} \hat{a}_{\mathbf{k},\lambda}^{\dagger} e^{-i\mathbf{k}^t \mathbf{r}_i} \mathbf{e}_{\mathbf{k},\lambda}. \quad (4.17)$$

We write down the master equation for the light-atom interaction in the dipole approximation (See [39, (10.10-1) to (10.10-4)], and [81, (4.4.15), (4.8.30)])

$$\begin{aligned} \dot{\rho} &= \frac{1}{i\hbar} [H_A + H_{\hat{a}} + H_{A\hat{a}}, \rho] \quad (4.18) \\ H_A &= \hbar \sum_{i=1}^N \left\{ \sum_{\substack{F' \in \mathbb{F}' \\ m_{F'}}} \omega'_{F',m_{F'}} |F', m_{F'}\rangle \langle F', m_{F'}|_i \right. \\ &\quad \left. + \sum_{m_F} \omega_{F,m_F} |F, m_F\rangle \langle F, m_F|_i \right\} \\ H_{\hat{a}} &= \hbar \sum_{\lambda} \int d\mathbf{k} \omega_{\mathbf{k}} \hat{a}_{\mathbf{k},\lambda}^{\dagger} \hat{a}_{\mathbf{k},\lambda} \\ H_{A\hat{a}} &= \sum_{i=1}^N (\mathcal{E}^-(\mathbf{r}_i, t) + \mathbf{E}_{\text{fwd}}^-(\mathbf{r}_i) + \mathbf{E}_{\text{se}}^-(\mathbf{r}_i))^t \sum_{F' \in \mathbb{F}'} \mathbf{d}_{i,FF'}^- + \text{h.c.}, \end{aligned}$$

define the detuning of the laser frequency ω_L to the atom transition frequency $\omega'_{F',m_{F'}} - \omega_{F,m_F}$ as

$$\Delta_{F',m_{F'},m_F} := \omega'_{F',m_{F'}} - \omega_{F,m_F} - \omega_L, \quad (4.19)$$

and the detuning between the maximal levels (see Fig. 4.14) as $\Delta := \Delta_{5,5,4}$.

In the following subsections we will reduce the complexity of this master equation step by step using adiabatic eliminations of

- the incoherently scattered light in Sec. 4.4.3,
- the excited atomic states in Sec. 4.4.5,
- and the forward scattered light field in Sec. 4.4.6.

4.4.2.1 Rotating frame

The optical frequency of the electric fields and the atomic transition frequencies are many orders of magnitude larger than other frequencies in the master equation (4.18), e.g., Δ and Ω_Z . It is therefore convenient to transform the master equation into the interaction picture – also called rotating frame – with respect to the Hamiltonian

$$H_0 := \hbar\omega_L \sum_{i=1}^N \sum_{\substack{F' \in \mathbb{F}' \\ m_{F'}}} |F', m_{F'}\rangle \langle F', m_{F'}|_i. \quad (4.20)$$

This results in the transformed Hamiltonians

$$\begin{aligned} H_A &= \hbar \sum_{i=1}^N \left\{ \sum_{\substack{F' \in \mathbb{F}' \\ m_{F'}}} (\omega'_{F', m_{F'}} - \omega_L) |F', m_{F'}\rangle \langle F', m_{F'}|_i \right. \\ &\quad \left. + \sum_{m_F} \omega_{F, m_F} |F, m_F\rangle \langle F, m_F|_i \right\} \\ H_{A\hat{a}} &= \sum_{i=1}^N \left(\tilde{\mathcal{E}}^-(\mathbf{r}_i, t) + \tilde{\mathbf{E}}_{\text{fwd}}^-(\mathbf{r}_i, t) + \tilde{\mathbf{E}}_{\text{se}}^-(\mathbf{r}_i, t) \right)^t \sum_{F' \in \mathbb{F}'} \mathbf{d}_{i, FF'}^- + \text{h.c.} \end{aligned} \quad (4.21)$$

containing no optical frequencies but only the slowly varying probe field $\tilde{\mathcal{E}}^-(\mathbf{r}_i, t) := \mathcal{E}^- e^{-i\omega_L t}$, forward scattered mode $\tilde{\mathbf{E}}_{\text{fwd}}^- := \mathbf{E}_{\text{fwd}}^- e^{-i\omega_L t}$, and spontaneous emission mode $\tilde{\mathbf{E}}_{\text{se}}^- := \mathbf{E}_{\text{se}}^- e^{-i\omega_L t}$.

4.4.3 Elimination of the spontaneous emission modes

We now adiabatically eliminate the spontaneous emission field $\tilde{\mathbf{E}}_{\text{se}}$ leading to non-collective atomic jumps analogous to the derivation in [75]. The evolution of the light modes with wave vector $\mathbf{k} \in \bar{b}$ is given by the Heisenberg equation of motion

$$\begin{aligned} \frac{d}{dt} \hat{a}_{\mathbf{k}, \lambda}(t) &= \frac{i}{\hbar} [H_{\hat{a}} + H_{A\hat{a}}, \hat{a}_{\mathbf{k}, \lambda}] \\ &= -i\omega_{\mathbf{k}} \hat{a}_{\mathbf{k}, \lambda} - \frac{i}{\hbar} \rho_{\omega} \sum_{i=1}^N e^{-i(\mathbf{k}^t \mathbf{r}_i + \omega_L t)} \mathbf{e}_{\mathbf{k}, \lambda}^t \sum_{F' \in \mathbb{F}'} \mathbf{d}_{i, FF'}^-(t) \end{aligned}$$

with the formal solution for $t_0 = 0$:

$$\begin{aligned} \hat{a}_{\mathbf{k}, \lambda}(t) &= e^{-i\omega_{\mathbf{k}} t} \hat{a}_{\mathbf{k}, \lambda}(0) \\ &\quad - \sum_{i=1}^N e^{-i(\mathbf{k}^t \mathbf{r}_i + \omega_{\mathbf{k}} t)} \frac{i}{\hbar} \rho_{\omega} \int_0^t d\tau e^{i(\omega_{\mathbf{k}} - \omega_L)\tau} \mathbf{e}_{\mathbf{k}, \lambda}^t \sum_{F' \in \mathbb{F}'} \mathbf{d}_{i, FF'}^-(\tau). \end{aligned} \quad (4.22)$$

We can insert this formal solution into the spontaneous emission mode $\tilde{E}_{se}^-(\mathbf{r}_j, t)$ evaluated for atom j , apply a standard Markov approximation (see appendix C.1) and we get the approximate evolution of the spontaneous emission mode

$$\tilde{E}_{se}^-(\mathbf{r}_j, t) = \tilde{E}_{se,free}^-(\mathbf{r}_j, t) + i\hbar\gamma' \sum_{F' \in \mathbb{F}'} \mathbf{d}_{j,F'F}^+(t)$$

where we used the definitions $\gamma' := \frac{\omega_L^3}{6\pi\hbar\epsilon_0 c^3}$ and the freely evolving vacuum field

$$\tilde{E}_{se,free}^-(\mathbf{r}_j, t) := \sum_{\lambda} \int_{\bar{b}} d\mathbf{k} \rho_{\omega} e^{-i(\mathbf{k}^t \mathbf{r}_j + (\omega_L - \omega_k)t)} \mathbf{e}_{\mathbf{k},\lambda} \hat{a}_{\mathbf{k},\lambda}^{\dagger}(0)$$

at atom position \mathbf{r}_j with vanishing mean $\langle \tilde{E}_{se,free}^-(\mathbf{r}_j, t) \rangle = 0$.

4.4.3.1 Evolution of the atomic operators

The expectation value of an arbitrary atomic operator A_j of atom j related to the interaction with the spontaneous emission mode \tilde{E}_{se} is given by:

$$\begin{aligned} & \text{Tr} [A_j \dot{\rho}] \\ &= \frac{i}{\hbar} \sum_{F' \in \mathbb{F}'} \left\langle \tilde{E}_{se}^-(\mathbf{r}_j, t)^t \left[\mathbf{d}_{j,FF'}^-, A_j \right] \right\rangle + \text{h.c.} \\ &= - \sum_{F', G' \in \mathbb{F}'} \gamma' \left\langle \left(\mathbf{d}_{j,G'F}^+(t) \right)^t \left[\mathbf{d}_{j,FF'}^-, A_j \right] \right\rangle + \text{h.c.} \\ &= \text{Tr} \left[A_j \sum_{k=1}^3 \mathcal{D} [L_{A,j,k}] \rho \right] \end{aligned}$$

with the jump operators

$$L_{A,j,k} := \sqrt{\gamma'} \sum_{F' \in \mathbb{F}'} \left(\mathbf{d}_{j,FF'}^- \right)_k$$

for $k \in \{x, y, z\}$ and element wise evaluated commutator. Since this equation holds for arbitrary operators A_j of atom j we get the operator identity for the evolution of the density matrix $\dot{\rho} = \sum_{k=1}^3 \mathcal{D} [L_{A,j,k}] \rho$. Repeating this procedure for every atom j gives the Lindblad term

$$[\dot{\rho}]_{se} = \sum_{i=1}^N \sum_{k=1}^3 \mathcal{D} [L_{A,i,k}] \rho \quad (4.23)$$

in the master equation.

4.4.4 Replacing free space by a single mode cavity

Keeping in mind that we later have to adiabatically eliminate the excited levels and the forward scattered light mode, we want to first simplify the forward scattered mode as much as possible. For this purpose we replace the free multimode field with a fast decaying cavity mode \hat{a} [81, (5.1.1)] with frequency $\omega_{\hat{a}}$. Of the forward scattered light mode only

the linear polarization vector $\mathbf{e}_q = (-\sin\theta \ \cos\theta \ 0)^t$ orthogonal to the probe laser $\mathbf{e}_q \perp \mathbf{e}_c$ is of interest for us, because (i) this polarization can be extracted via a polarizing beamsplitter from the probe laser and (ii) all two-photon transitions involving the probe-laser polarization vector twice are dominated by the probe laser, which is included in our description. We can therefore define the forward scattered light mode as

$$\tilde{\mathbf{E}}_{\text{fwd}}^-(z, t) = \rho_{\text{fwd}} \hat{a}^\dagger e^{-i(k_{\omega_{\hat{a}}}z + \omega_{\hat{a}}t)} \mathbf{e}_q \quad (4.24)$$

where we normalized the electric field per cavity photon $\rho_{\text{fwd}} = \sqrt{\kappa} \rho_c / 2$ such that the decaying cavity emits into the free space modes, just as if the atoms would interact directly with the free space modes (we derive this in appendix C.2). Additional terms in the master equation are the Hamiltonian

$$H_{\hat{a}} = \hbar \omega_{\hat{a}} \hat{a}^\dagger \hat{a}$$

and the cavity decay Lindblad term

$$[\dot{\rho}]_{\hat{a}} = \kappa \mathcal{D}[\hat{a}] \rho \quad (4.25)$$

where we chose the cavity decay rate κ much larger than any other rate in the master equation (the exact value is irrelevant and will cancel in all results). From now on we restrict the atom positions and also the probe field to the z axis $\tilde{\mathcal{E}}^-(\mathbf{r}, t) = \tilde{\mathcal{E}}^-(z, t)$.

4.4.5 Elimination of the excited atom levels

We assume the probe laser is far detuned from any resonance between the F and $F' \in \mathbb{F}'$ manifolds. More precisely we assume

$$\Delta \gg \Omega, \quad (4.26)$$

meaning the detuning Δ is large compared to Rabi frequency $\Omega = d_{F'=5} \|\mathcal{E}\| / \hbar$ where the Rabi frequency is a measure for the atom-light interaction strength. This assumption means that the excited manifolds are weakly coupled to the ground manifold. We can therefore adiabatically eliminate the excited state manifolds using the powerful and elegant method for an off-resonant drive developed in [83, Sec. IV. A.]. The method allows for non-perturbative ground-state coupling, such as significant ground-state splitting in H_A and incoherent jump operators associated with the spontaneous emission (4.23). To apply the method directly we define single-atom Hamiltonians

$$\begin{aligned} H_{Ag,i} &:= \hbar \sum_{m_F} \omega_{F,m_F} |F, m_F\rangle \langle F, m_F|_i \\ H_{Ae,i} &:= \hbar \sum_{\substack{F' \in \mathbb{F}' \\ m_{F'}}} \left(\omega'_{F',m_{F'}} - \omega_L \right) |F', m_{F'}\rangle \langle F', m_{F'}|_i \end{aligned}$$

and jump operators

$$\begin{aligned} V_i^- &:= \left(\tilde{\mathcal{E}}^-(z) + \tilde{\mathbf{E}}_{\text{fwd}}^-(z, t) \right)^t \sum_{F' \in \mathbb{F}'} \mathbf{d}_{i,FF'}^- \\ V_i^+ &:= (V_i^-)^\dagger \end{aligned}$$

resulting in the rewritten master equation

$$\dot{\rho} = \frac{1}{i\hbar} \left[\sum_{i=1}^N (H_{Ag,i} + H_{Ae,i} + V_i^- + V_i^+) + H_{\hat{a}}, \rho \right] + \sum_{i=1}^N \sum_{k=1}^3 \mathcal{D} [L_{A,i,k}] \rho + \kappa \mathcal{D} [\hat{a}] \rho.$$

The effective ground-state evolution [83, Eq. (63)] after the adiabatic elimination is:

$$\dot{\rho} = \frac{1}{i\hbar} \left[\sum_{i=1}^N H_{Ag,i}^{\text{eff,tot}} + H_{\hat{a}}, \rho \right] + \sum_{i=1}^N \sum_{k=1}^3 \mathcal{D} [L_{A,i,k}^{\text{eff}}] \rho + \kappa \mathcal{D} [\hat{a}] \rho \quad (4.27)$$

$$H_{Ag,i}^{\text{eff,tot}} := H_{Ag,i} - \frac{1}{2} \left(V_i^- \sum_{m_F} \left(H_{\text{NH},i}^{m_F} \right)^{-1} V_i^+ |F, m_F\rangle \langle F, m_F|_i + \text{h.c.} \right)$$

$$H_{\text{NH},i}^{m_F} := H_{Ae,i} - \frac{i}{2} \sum_{k=1}^3 L_{A,i,k}^\dagger L_{A,i,k} - \hbar \omega_{F,m_F} \mathbb{1}$$

$$L_{A,i,k}^{\text{eff}} := L_{A,i,k} \sum_{m_F} \left(H_{\text{NH},i}^{m_F} \right)^{-1} V_i^+ |F, m_F\rangle \langle F, m_F|_i$$

While this is of course a quite complicated formula, we can see the same structure in the Hamiltonian $H_{Ag,i}^{\text{eff,tot}}$ and also the jump operators $L_{A,i,k}^{\text{eff}}$:

- (i) The input state is spanned by the eigenstates $|F, m_F\rangle_i$ of $H_{Ag,i}$.
- (ii) The jump operator V_i^+ excites the eigenstate $|F, m_F\rangle_i$ to the upper manifold
- (iii) The state evolves according to $\left(H_{\text{NH},i}^{m_F} \right)^{-1}$, which includes the Hamiltonian of the upper manifolds $H_{Ae,i}$

After this evolution the state is either deexcited with V_i^- or $L_{A,i,k}$ corresponding to the coherent or incoherent evolution, respectively.

The non-hermitian Hamiltonian $H_{\text{NH},i}^{m_F}$ contains also the term $L_{A,i,k}^\dagger L_{A,i,k}$ describing a jump to the lower manifold and up again. The rate of this term depends on the population in the excited manifold. We can estimate the population difference between ground and excited state manifolds by considering a two-level system. The optical Bloch equations show that the population difference between ground and excited state $w_{ss} = (\rho_{gg} - \rho_{ee}) / 2 = S / 2(S + 1)$ is close to $1/2$ for small saturation $S = \Omega^2 / \Delta^2 \ll 1$, due to large detuning Δ . The low population in the excited state means that the coherences of the excited state manifold $\|\gamma' \left(\mathbf{d}_{i,F'F}^+ \right)^\dagger \mathbf{d}_{i,F'F}^-\|$ is negligible compared to the frequency differences $\Delta_{F',m_{F'},m_F}$ due to the ground state splitting. This assumption is equivalent to assumption (4.34), which we will introduce in Sec. 4.4.6. This approximation allows us to write the non-hermitian Hamiltonian

$$H_{\text{NH},i}^{m_F} = H_{Ae,i} - \frac{i}{2} \sum_{F' \in \mathbb{F}'} \gamma' \left(\mathbf{d}_{i,F'F}^+ \right)^\dagger \mathbf{d}_{i,F'F}^- - \hbar \omega_{F,m_F} \mathbb{1}$$

$$\approx \sum_{\substack{F' \in \mathbb{F}' \\ m_{F'}}} \left(\hbar \Delta_{F',m_{F'},m_F} \right) |F', m_{F'}\rangle \langle F', m_{F'}|_i \quad (4.28)$$

in diagonal form, important for its analytic inverse. The effective ground state evolution $H_{Ag,i}^{\text{eff,tot}}$ contains both the electrical fields and atomic operators. We restructure this Hamiltonian by grouping the atomic operators into the polarizability tensor

$$\begin{aligned}
\overleftrightarrow{\alpha}_i &:= \sum_{F' \in \mathbb{F}'} |d_{F'}|^2 \sigma_{i,FF'}^- \sum_{\substack{m_F \\ m_{F'}}} \left(\hbar \Delta_{F',m_{F'},m_F} \right)^{-1} \times \\
&\quad \times |F', m_{F'}\rangle \langle F', m_{F'}|_i \left(\sigma_{i,F'F}^+ \right)^t |F, m_F\rangle \langle F, m_F|_i \\
&\stackrel{(i)}{\approx} \sum_{F' \in \mathbb{F}'} |d_{F'}|^2 \sigma_{i,FF'}^- \left(\sigma_{i,F'F}^+ \right)^t \sum_{m_F} \frac{|F, m_F\rangle \langle F, m_F|_i}{\hbar \Delta_{F',F',m_F}} \\
&\stackrel{(ii)}{\approx} \sum_{F' \in \mathbb{F}'} \frac{|d_{F'}|^2}{\hbar \Delta_{F',F',F}} \sigma_{i,FF'}^- \left(\sigma_{i,F'F}^+ \right)^t. \tag{4.29}
\end{aligned}$$

Both approximation steps (i) $|\omega'_{F',m_{F'}} - \omega'_{F',F'}| \ll \Delta$ and (ii) $|\omega_{F,m_F} - \omega_{F,F}| \ll \Delta$ are based on the fact that the detuning of the probe laser to the excited state manifold is large compared to hyperfine splittings. To separate the units out we also define the dimensionless polarizability tensor

$$\mathcal{T}_i := \frac{\hbar \Delta}{|d_5|^2} \overleftrightarrow{\alpha}_i. \tag{4.30}$$

The polarizability tensor allows for a compact expression of the effective ground state evolution

$$H_{Ag,i}^{\text{eff,tot}} \approx - \left((\tilde{\mathbf{E}}_{\text{fwd}}^-)^t \overleftrightarrow{\alpha}_i \tilde{\mathbf{E}}^+ + \text{h.c.} \right) + H_{\text{stark},i} + H_{Ag,i}$$

where we used $(\overleftrightarrow{\alpha}_i)^{\dagger t} = \overleftrightarrow{\alpha}_i$, defined the Hamiltonian $H_{\text{stark},i} = -(\tilde{\mathbf{E}}^-)^t \overleftrightarrow{\alpha}_i \tilde{\mathbf{E}}^+$ creating the Stark shift, and neglected the terms describing an emission and reabsorption of a photon, due to the dominance of the probe laser compared to the emitted light. The effective spontaneous emission jump operators (also neglecting forward scattered light) can similarly be described with the polarizability tensor as

$$\begin{aligned}
L_{A,i,k}^{\text{eff}} &= \sqrt{\gamma'} \left(\overleftrightarrow{\alpha}_i \left(\tilde{\mathbf{E}}^+ + \tilde{\mathbf{E}}_{\text{fwd}}^+ \right) \right)_k \\
&\approx \sqrt{\gamma'} \left(\overleftrightarrow{\alpha}_i \tilde{\mathbf{E}}^+ \right)_k.
\end{aligned}$$

4.4.5.1 Rotation of the effective spontaneous emission operators

The effective spontaneous emission operators $L_{A,i,k}^{\text{eff}}$ are indexed by $k \in \{x, y, z\}$ denoting a direction in the Cartesian coordinate system. The effective Hamiltonian $H_{Ag,i}^{\text{eff,tot}}$ contains however terms relative to the fields $\tilde{\mathbf{E}}_{\text{fwd}}^-$ and $\tilde{\mathbf{E}}^-$, which are in the rotated coordinate system with basis vectors e_q , and e_c respectively. It is therefore helpful to apply a rotation matrix

$$R = \begin{pmatrix} \cos \theta & -\sin \theta & 0 \\ \sin \theta & \cos \theta & 0 \\ 0 & 0 & 1 \end{pmatrix}$$

to the three effective spontaneous emission operators of atom i

$$L_{A,i,k}^{\text{eff}} \rightarrow \sum_{k'} R_{kk'}^t L_{A,i,k'}^{\text{eff}}$$

leaving the sum of Lindblad operators invariant

$$\begin{aligned} \sum_{k=1}^3 \mathcal{D} [L_{A,i,k}^{\text{eff}}] \rho &= \sum_{k=1}^3 \mathcal{D} \left[\sum_{k'} R_{kk'}^t L_{A,i,k'}^{\text{eff}} \right] \rho \\ &= \gamma' \sum_{k=1}^3 \mathcal{D} \left[\sum_{k'} R_{kk'}^t e_{k'}^t \vec{\alpha}'_i \tilde{\mathcal{E}}^+(z) \right] \rho \\ &= \gamma_{\text{eff}} \sum_{k \in \{c,q,z\}} \mathcal{D} [V_i^k] \rho \end{aligned}$$

where we used the effective spontaneous emission rate

$$\gamma_{\text{eff}} := \gamma' \frac{N_{ph}}{T} \left(\frac{|d_5|^2}{\hbar \Delta} \rho_c \right)^2$$

and the dimensionless jump operators

$$V_i^k := e_k^t \mathcal{T}_i e_c \quad (4.31)$$

for the rotated coordinates $k \in \{c, q, z\}$. The Hamiltonian terms can also be simplified using the dimensionless jump operators. Additionally we go into rotating frame with respect to the Hamiltonian $H_{\hat{a}}$ and set cavity frequency $\omega_{\hat{a}}$ to be identical to the coherent laser drive ω_L and obtain the master equation

$$\begin{aligned} \dot{\rho} &= \frac{1}{i\hbar} \sum_{i=1}^N \left[H_{\hat{a},A,i}^{\text{eff}} + H_{Ag,i}^{\text{eff}} \right] \rho + \gamma_{\text{eff}} \sum_{i=1}^N \sum_{k \in \{c,q,z\}} \mathcal{D} [V_i^k] \rho \\ &\quad + \kappa \mathcal{D} [\hat{a}] \rho \quad (4.32) \\ H_{\hat{a},A,i}^{\text{eff}} &\approx \hbar \Omega_{\text{eff}} \hat{a}^\dagger V_i^q + \text{h.c.} \\ H_{Ag,i}^{\text{eff}} &= \hbar \sum_{m_F} \omega_{F,m_F} |F, m_F\rangle \langle F, m_F|_i + \hbar \Omega_{\text{stark}} V_i^c \end{aligned}$$

with the effective coherent ground state coupling and Stark rates:

$$\Omega_{\text{eff}} := -\rho_{\text{fwd}} \rho_c \sqrt{\frac{N_{ph}}{T} \frac{|d_5|^2}{\hbar^2 \Delta}}, \quad \Omega_{\text{stark}} := -\rho_c^2 \frac{N_{ph}}{T} \frac{|d_5|^2}{\hbar^2 \Delta}.$$

The structure of the master equation becomes now very simple: Coherent and incoherent atom-light interaction all involve the atomic jump operators V_i^k , which are nothing else than different components of the polarizability tensor.

4.4.6 Elimination of the cavity mode

The decay rate κ of the “virtual” cavity mode \hat{a} is much larger than any other rate in our master equation, which allows us to adiabatically eliminate it too. To apply the adiabatic elimination formula (1.2) to

master equation (4.32) we first restructure it into system A (the atoms) and system B (the cavity mode) giving

$$\begin{aligned} L_A \rho &= \frac{1}{i\hbar} \left[H_{A_g}^{\text{eff}}, \rho \right] + \gamma_{\text{eff}} \sum_{i=1}^N \sum_{k \in \{c,q,z\}} \mathcal{D} \left[V_i^k \right] \rho \\ L_B \rho &= \kappa \mathcal{D} [\hat{a}] \rho \\ L_{AB} \rho &= \frac{1}{i} \Omega_{\text{eff}} \left[\hat{a}^\dagger V^q + \text{h.c.}, \rho \right] \\ \dot{\rho} &= L_A \rho + L_B \rho + L_{AB} \rho \end{aligned}$$

where we defined $V^q := \sum_i V_i^q$ and $H_{A_g}^{\text{eff}} = \sum_i H_{A_g,i}^{\text{eff}}$. The incoherent dynamics of system A does not contribute, due to the fast cavity decay, leaving a unitary evolution

$$e^{\mp L_A \tau} \rho(t) \approx e^{\pm \frac{i}{\hbar} H_{A_g}^{\text{eff}} \tau} \rho(t) e^{\mp \frac{i}{\hbar} H_{A_g}^{\text{eff}} \tau}$$

of system A . Plugging this into the adiabatic elimination formula (1.2) and suppressing the time-dependence of the density matrix gives

$$\begin{aligned} \dot{\rho}_A - L_A \rho_A &= \frac{\Omega_{\text{eff}}}{i} \text{Tr}_B \left[L_{AB} \int_0^\infty d\tau e^{L_B \tau} \left(e^{-\frac{i}{\hbar} H_{A_g}^{\text{eff}} \tau} V^q e^{\frac{i}{\hbar} H_{A_g}^{\text{eff}} \tau} \rho_A \otimes \hat{a}^\dagger \rho_B^{\text{ss}} - \text{h.c.} \right) \right] \\ &= \frac{\Omega_{\text{eff}}}{i} \text{Tr}_B \left[L_{AB} \int_0^\infty d\tau \left(e^{-\frac{i}{\hbar} H_{A_g}^{\text{eff}} \tau} V^q e^{\frac{i}{\hbar} H_{A_g}^{\text{eff}} \tau} \rho_A \otimes e^{L_B \tau} \hat{a}^\dagger \rho_B^{\text{ss}} - \text{h.c.} \right) \right] \\ &= -\Omega_{\text{eff}}^2 \int_0^\infty d\tau \left[e^{-\frac{\kappa}{2} \tau} (V^q)^\dagger, e^{-\frac{i}{\hbar} H_{A_g}^{\text{eff}} \tau} V^q e^{\frac{i}{\hbar} H_{A_g}^{\text{eff}} \tau} \rho_A \right] + \text{h.c.} \quad (4.33) \end{aligned}$$

We are interested in the case where the free evolution Hamiltonian

$$H_{A_g,i}^{\text{eff}} = \sum_{E \in \mathbb{E}} E |E\rangle \langle E|_i$$

with eigenstates $|E\rangle_i$ and eigenvalues E , has eigenenergy differences that are large compared to the effective spontaneous emission rate and the effective coupling rate, i.e.,

$$\begin{aligned} \min_{E \neq E'} (E - E') &\gg \hbar \gamma_{\text{eff}}, \\ \min_{E \neq E'} (E - E') &\gg \hbar \frac{\Omega_{\text{eff}}^2}{\kappa}. \end{aligned} \quad (4.34)$$

Physically this means that the emitted photons allow distinguishing atomic jumps, implying that the transitions with different energies effectively couple to different baths. This treatment is consistent with the non-perturbative treatment of the ground-state manifold in the adiabatic elimination of the excited levels (see Sec. 4.4.5). One way to realize the condition (4.34) is the Zeeman effect splitting the eigenenergies large enough to fulfill both conditions

$$\begin{aligned} \min_{m_F \neq m'_F} \left| \omega_{F,m_F} - \omega_{F,m'_F} \right| &\gg \gamma_{\text{eff}}, \\ \min_{m_F \neq m'_F} \left| \omega_{F,m_F} - \omega_{F,m'_F} \right| &\gg \hbar \frac{\Omega_{\text{eff}}^2}{\kappa}, \end{aligned} \quad (4.35)$$

such that the Stark shift can be neglected. Independent of how the energy splitting is realized we define the components

$$V_i^k(\omega) = \sum_{E-E'=\hbar\omega} |E\rangle \langle E| V_i^k |E'\rangle \langle E'| \quad (4.36)$$

of jump operator $V_i^k = \sum_{\omega} V_i^k(\omega)$ of atom i for $k \in \{c, q, z\}$ associated with the energy difference $\hbar\omega$. They are eigenoperators of $H_{Ag,i}^{\text{eff}}$ meaning they fulfill $[H_{Ag,i}^{\text{eff}}, V_i^k(\omega)] = \hbar\omega V_i^k(\omega)$. The components

$$V^k(\omega) = \sum_i V_i^k(\omega)$$

of the collective jump operators $V^k = \sum_{\omega} V^k(\omega)$ associated with the energy difference $\hbar\omega$ are eigenoperators of the summed up Hamiltonian $H_{Ag}^{\text{eff}} = \sum_i H_{Ag,i}^{\text{eff}}$ allowing us to express the unitary evolution of the components as:

$$e^{-\frac{i}{\hbar} H_{Ag}^{\text{eff}} \tau} V^q(\omega) e^{\frac{i}{\hbar} H_{Ag}^{\text{eff}} \tau} = e^{-i\omega\tau} V^q(\omega).$$

We plug this expression into (4.33) giving

$$\begin{aligned} \dot{\rho}_A(t) &= \frac{1}{i\hbar} [H_{Ag}^{\text{eff}}, \rho] + \gamma_{\text{eff}} \sum_{i=1}^N \sum_{k \in \{c, q, z\}} \mathcal{D} [V_i^k] \rho - \Omega_{\text{eff}}^2 \int_0^{\infty} d\tau \times \\ &\quad \times \sum_{\omega, \omega'} \left(\left[e^{-\frac{\kappa}{2}\tau} (V^q)^\dagger(\omega'), e^{-i\omega\tau} V^q(\omega) \rho_A(t) \right] + \text{h.c.} \right) \\ &= \sum_{\omega, \omega'} e^{i(\omega' - \omega)t} \left\{ -\frac{\gamma_{\text{eff}}}{2} \sum_{i=1}^N \sum_{k \in \{c, q, z\}} \left[(V_i^k)^\dagger(\omega'), V_i^k(\omega) \rho \right] \right. \\ &\quad \left. - \frac{\Omega_{\text{eff}}^2}{\kappa} \left[\frac{\kappa}{2} + i\omega \right] (V^q)^\dagger(\omega'), V^q(\omega) \rho_A(t) \right\} + \text{h.c.} \quad (4.37) \end{aligned}$$

where we evaluated the integral and transformed into rotating frame according to Hamiltonian H_{Ag}^{eff} in the last step. Due to the assumption (4.34) of large ground state splitting compared to the evolution rate $\Omega_{\text{eff}}^2/\kappa$ and the effective decay rate γ_{eff} , vanish the fast oscillating terms with $\omega' - \omega \neq 0$ leaving only the equal frequency terms

$$\begin{aligned} \dot{\rho}_A(t) &\approx \sum_{\omega} \left\{ -\frac{\gamma_{\text{eff}}}{2} \sum_{i=1}^N \sum_{k \in \{c, q, z\}} \left[(V_i^k)^\dagger(\omega), V_i^k(\omega) \rho \right] \right. \\ &\quad \left. - \Omega_{\text{eff}}^2 \frac{1}{\frac{\kappa}{2} + i\omega} \left[(V^q)^\dagger(\omega), V^q(\omega) \rho_A(t) \right] \right\} + \text{h.c.} \end{aligned}$$

Removing the fast oscillating terms is also called Rotating Wave Approximation (for the second term this is a necessary procedure to ensure a completely positive map [34, p. 132]).

Going back into non-rotating frame with respect to H_{Ag}^{eff} and adding incoherent optical pumping term $\sum_{i=1}^N \mathcal{D} [F_i^+] \rho$ with rate w using the

angular momentum ladder operators $F_i^\pm := (\mp F_i^z + iF_i^y)/\sqrt{2}$ gives the master equation

$$\begin{aligned} \dot{\rho} = & w \sum_{i=1}^N \mathcal{D}[F_i^+] \rho + \frac{1}{i\hbar} [H_{Ag'}^{\text{eff}}, \rho] \\ & + \sum_{\omega} \left\{ \gamma_{\text{eff}} \sum_{i=1}^N \sum_{k \in \{c,q,z\}} \mathcal{D}[V_i^k(\omega)] \rho \right. \\ & \left. + \frac{\gamma_{\text{Im},\omega}}{i} [V^q(\omega)^\dagger V^q(\omega), \rho] + \gamma_{\text{Re},\omega} \mathcal{D}[V^q(\omega)] \rho \right\} \end{aligned} \quad (4.38)$$

where we defined the rates

$$\gamma_{\text{Im},\omega} := \Omega_{\text{eff}}^2 \text{Im} \left[\frac{1}{\frac{\kappa}{2} + i\omega} \right], \quad \gamma_{\text{Re},\omega} := \Omega_{\text{eff}}^2 \frac{\kappa}{|\frac{\kappa}{2} + i\omega|^2}, \quad (4.39)$$

governing the two-atom interaction Hamiltonian and collective jumps respectively.

4.4.7 Analysis

Master equation (4.38) is the end result of the long derivation, which started in Sec. 4.4. It is important to recognize the structure of the master equation: (i) it is permutation invariant, (ii) it has up to two-atom interaction Hamiltonians, and (iii) it has single-atom and collective jump operators. It therefore belongs to the class of master equations (3.1) and can be approximately integrated using the cumulant expansion developed in Chapter 3.

We additionally want to point out that the spontaneous emission jump operators, the two-atom interaction Hamiltonian, and the collective jump operators are composed out of operators $V_i^k(\omega)$, where $k = q$ for the two-atom interaction Hamiltonian and the collective jump operators and $k \in \{c, q, z\}$ for the spontaneous emission jump operators. The operators $V_i^k(\omega)$ are all dependent on the angle of linear polarization of the probe laser θ (see equation (4.31)) and in the following discussion we will mostly discuss how this θ dependence influences the collective effects dominantly created by the collective jump operators. However depending on the parameter regime the single-atom jump operators can be the dominant contribution to an observed θ dependence.

In the following we discuss more properties of this master equation and also how it relates to the three-level atom model of Sec. 4.3 before we will show numerical results in Sec. 4.4.8.

4.4.7.1 Symmetries

We assume the ground-state Hamiltonian $H_{Ag,i}^{\text{eff}}$ is, that the Stark shift can be neglected compared to the ground state splittings ω_{F,m_F} , leaving only the bare detunings of the ground state levels

$$H_{Ag,i}^{\text{eff}} \approx \hbar \sum_{m_F} \omega_{F,m_F} |F, m_F\rangle \langle F, m_F|_i \quad (4.40)$$

In this case the optical pumping jump operator F_i^+ is also an eigenoperator of the ground-state Hamiltonian $H_{Ag,i}^{\text{eff}}$ fulfilling

$$[H_{Ag,i}, F_i^+] = \hbar\Omega_Z [F_i^0, F_i^+] = \hbar\Omega_Z F_i^+, \quad (4.41)$$

meaning the entire master equation (4.38) consists of eigenoperators of H_{Ag}^{eff} . This allows to easily go into a rotating frame with regard to H_{Ag}^{eff} giving the master equation

$$\begin{aligned} \dot{\rho} = & w \sum_{i=1}^N \mathcal{D} [F_i^+] \rho + \sum_{\omega} \left\{ \gamma_{\text{eff}} \sum_{i=1}^N \sum_{k \in \{c,q,z\}} \mathcal{D} [V_i^k(\omega)] \rho \right. \\ & \left. + \frac{\gamma_{\text{Im},\omega}}{i} [V^q(\omega)^\dagger V^q(\omega), \rho] + \gamma_{\text{Re},\omega} \mathcal{D} [V^q(\omega)] \rho \right\}. \end{aligned} \quad (4.42)$$

4.4.7.2 Steady state properties

Another consequence of the master equation (4.42) being entirely composed of eigenoperators of H_{Ag}^{eff} is that $U = \exp(i\frac{\tau}{\hbar} H_{Ag}^{\text{eff}})$ is a symmetry, meaning $L(U\rho U^\dagger) = UL(\rho)U^\dagger$ for the superoperator L summarizing the right hand side of (4.42). It follows for the steady state that the expectation values $\langle V_i^k(\omega) \rangle = 0$ vanish for all $\omega \neq 0$, because the steady state ρ_{ss} must also fulfill $L\rho_{\text{ss}} = 0$ for L summarizing also the right hand side of (4.38) (see [84, 85]). This implies, that any collective effects beyond the possibly non-vanishing mean field $\langle V_i^k(0) \rangle$ are encoded in second or higher order correlation functions such as $\langle V_i^k(\omega) V_j^{k'}(\omega') \rangle$.

4.4.7.3 Tensor decomposition

The dimensionless polarizability tensor defined in (4.30) needs in principle no further explanation. However it is instructive to split the dyadic product $\sigma_{i,F'F}^- (\sigma_{i,F'F}^+)^\dagger$ into Irreducible Tensors Operators $\hat{T}_i^{(k)}$ of the angular momentum vector F_i . As was shown in [76, 86] (see also [80, 82]) we get the decomposition

$$\mathcal{T}_i = \sum_{k=0}^2 s_k \hat{T}_i^{(k)} \quad (4.43)$$

where we defined

$$\begin{aligned} s_k &:= \sum_{F' \in \mathbb{F}'} \frac{\Delta}{\Delta_{F',F',F}} \frac{|d_{F'}|^2}{|d_5|^2} a_k^{F'}, \\ a_k^{F'} &:= \frac{(2F'+1) \sqrt{2k+1} (-)^{-F'-F-3k}}{\sqrt{2F+1} \langle F || \hat{T}_i^{(k)} || F \rangle} \begin{Bmatrix} F & k & F \\ 1 & F' & 1 \end{Bmatrix}_6 \end{aligned}$$

and used the Reduced Matrix Element $\langle F || \hat{T}_i^{(k)} || F \rangle$ in the convention of [82, (4.15)]. We can express the Irreducible Tensors Operators in a basis independent form

$$\begin{aligned}\hat{T}_i^{(0)} &= -\frac{1}{\sqrt{3}}\mathbb{1}_i \\ \hat{T}_i^{(1)} &= \frac{i}{\sqrt{2}}\mathbf{F}_i \times . \\ \hat{T}_i^{(2)} &= \frac{1}{-2} \left(-2\mathbf{F}_i \otimes \mathbf{F}_i - i\mathbf{F}_i \times . + \frac{2}{3} (\mathbf{F}_i)^2 \right)\end{aligned}$$

and clearly see that the Irreducible Tensors Operators are associated with the number of occurring angular momentum vectors \mathbf{F}_i . We call $\hat{T}_i^{(1)}$ the *vector component* and $\hat{T}_i^{(2)}$ the *tensor component*. The relative strength of the vector to tensor component varies with the quotients $\Delta/\Delta_{F',F',F}$ for $F' \in \mathbb{F}'$, that is the laser detuning to the $F' = 5$ manifold as compared to the laser detuning to the other F' manifolds. For the detuning regime considered in the Caesium experiment [22] the tensor component prefactor s_2 is approximately one order of magnitude smaller than s_1 of the vector component. In the limit of infinite detuning compared to the splitting of the upper manifolds $\Delta/\max_{F',G' \in \mathbb{F}'} |\Delta_{F',F',F} - \Delta_{G',G',F}| \rightarrow \infty$ the tensor component prefactor s_2 vanishes [75]. Even though the tensor component prefactor s_2 is an order of magnitude smaller than s_1 is cannot be neglected and is crucial in the superradiant effects we will show in the following sections.

4.4.7.4 Representation of the Irreducible Tensors Operators

While the basis independent representations of the Irreducible Tensors Operators are very elegant and compact, to use them one first needs to derive the representations of the identity $\mathbb{1}_i$, the vector product \times and the tensor product \otimes in the desired basis. We will now express the Irreducible Tensors Operators in terms of the often used Cartesian and spherical basis.

Let us first consider a real vector \mathbf{A} , given in Cartesian coordinate representation $\mathbf{A} = \sum_{k \in \{x,y,z\}} e_k A_k$ with coefficients $A_k \in \mathbb{R}$. It can also be represented in the spherical basis representation $\mathbf{A} = \sum_{q \in \{-1,0,1\}} e_q^* A_q$ with coefficients $A_q \in \mathbb{C}$. The unitary transformation U , defined by

$$\begin{pmatrix} A_- \\ A_0 \\ A_+ \end{pmatrix}_{\text{sph}} = \underbrace{\begin{pmatrix} 0 & \frac{i}{\sqrt{2}} & \frac{1}{\sqrt{2}} \\ 1 & 0 & 0 \\ 0 & \frac{i}{\sqrt{2}} & -\frac{1}{\sqrt{2}} \end{pmatrix}}_{=U} \begin{pmatrix} A_x \\ A_y \\ A_z \end{pmatrix}_{\text{Cart}}$$

maps the Cartesian coefficients A_k to the spherical coefficients A_q for quantization axis x . While we can represent any vector through linear combinations of the basis vectors e_q^* , we can also represent any tensor A through the decomposition $A = \sum_{k=0}^{\infty} \sum_{q=-k}^k T_q^{(k)} A_q^k$ into the Irreducible Tensors Operator $T_q^{(k)}$ – we call this the kq basis – with coefficients A_q^k .

There does not seem to be a widely used convention of the Irreducible Tensors Operator $T_q^{(k)}$, leading us to the recursive definition of Irreducible Tensors Operator

$$T_q^{(k)} = \sum_{q_1, q_2} T_{q_1}^{(1)} T_{q_2}^{(k-1)} \langle 1 q_1, k-1 q_2 | k q \rangle,$$

for all orders k using the angular momentum coupling and the initial definitions $\hat{T}^{(0)} = -\mathbb{1}/\sqrt{3}$ and $\hat{T}^{(1)} = i/\sqrt{2}\mathbf{F} \times ..$ In this definition we used the Clebsch-Gordon coefficients $\langle 1 q_1, k-1 q_2 | k q \rangle$ [82] and sums without limits denote the sum over all values with non-vanishing Clebsch-Gordon coefficient. We also state the spherical basis and Cartesian (shown as a matrix) representations of the first three Irreducible Tensors Operators

$$\begin{aligned} \hat{T}^{(0)} &= \sum_{q, q'} \langle 1 q, 1 q' | 0 0 \rangle \mathbf{e}_q^* \mathbf{e}_{q'}^{*t} = -\frac{1}{\sqrt{3}} \begin{pmatrix} 1 & 0 & 0 \\ 0 & 1 & 0 \\ 0 & 0 & 1 \end{pmatrix} \\ \hat{T}^{(1)} &= \sum_{q, q', Q} \langle 1 q, 1 q' | 1 Q \rangle F^Q \mathbf{e}_q^* \mathbf{e}_{q'}^{*t} = \frac{i}{\sqrt{2}} \begin{pmatrix} 0 & -F^z & F^y \\ F^z & 0 & -F^x \\ -F^y & F^x & 0 \end{pmatrix} \\ \hat{T}^{(2)} &= \sum_{q, q', Q} \langle 1 q, 1 q' | 2 Q \rangle \sum_{q_1, q_2} F^{q_1} F^{q_2} \langle 1 q_1, 1 q_2 | 2 Q \rangle \mathbf{e}_q^* \mathbf{e}_{q'}^{*t} \\ &= \frac{1}{2} \begin{pmatrix} 2(F^x)^2 - \frac{2}{3}(\mathbf{F})^2 & 2F^x F^y - iF^z & 2F^x F^z + iF^y \\ 2F^y F^x + iF^z & 2(F^y)^2 - \frac{2}{3}(\mathbf{F})^2 & 2F^y F^z - iF^x \\ 2F^z F^x - iF^y & 2F^z F^y + iF^x & 2(F^z)^2 - \frac{2}{3}(\mathbf{F})^2 \end{pmatrix}. \end{aligned}$$

4.4.7.5 Comparison to three levels system

Using the dimensionless polarizability tensor in (4.30), its decomposition into Irreducible Tensors Operators in (4.43), and the Cartesian representations in the previous subsection we can calculate the exact form of the jump operators in (4.31) for the linear probe polarization vector

$$\begin{aligned} V_i^q &= \mathbf{e}_q^t \mathcal{T}_i \mathbf{e}_c \\ &= \mathbf{e}_q^t \sum_k s_k \hat{T}_i^{(k)} \mathbf{e}_c \\ &= i \frac{s_1}{2} (F_i^- - F_i^+) - s_2 \left(\frac{i \cos(2\theta)}{\sqrt{2}} W_1 + \frac{\sin(2\theta)}{4} W_2 \right), \end{aligned} \quad (4.44)$$

where we defined the operators

$$\begin{aligned} W_1 &:= \left(F_i^0 + \frac{1}{2} \right) F_i^- + \left(F_i^0 - \frac{1}{2} \right) F_i^+, \\ W_2 &:= 3 \left(F_i^0 \right)^2 - (F_i)^2 + (F_i^-)^2 + (F_i^+)^2, \end{aligned}$$

grouping the number of up or down jumps induced by the ladder operators F_i^\pm . The operator W_1 contains terms with one up or down jump, and W_2 contains zero or two up or down jumps. The jump operators in (4.8) of the system containing three-level atoms in Sec. 4.3 have identical

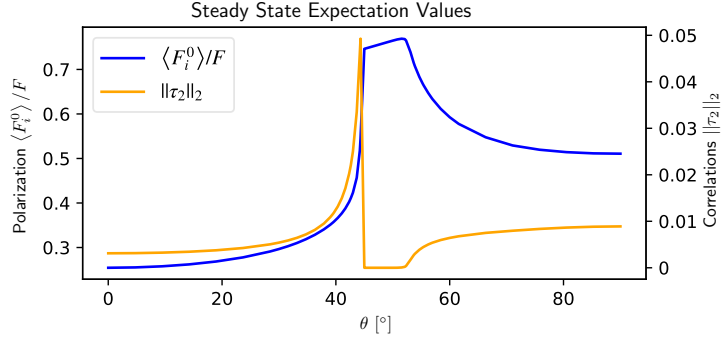


Figure 4.15: Polarization $\langle F_i^0 \rangle / F$, and norm of second order density matrix cumulant $\|\tau_2\|_2$ versus the angle θ for $F = 4$, i.e., a nine-level ground state manifold. The parameters are $N = 10^9$ atoms, the collective jump rate $\gamma_{re}/\gamma_{\text{eff}} \approx 1.9 \cdot 10^{-6}$, a pump rate $w/\gamma_{\text{eff}} \approx 5.8 \cdot 10^{-3}$, and a vanishing collective Hamiltonian $\gamma_{im} = 0$. These rates correspond to a laser power $\hbar\omega_L N_{ph}/T = 6$ mW, probe beam area $A = (300 \mu\text{m})^2$, laser wavelength $\lambda_L = 852$ nm, a detuning $\Delta = 2\pi \cdot 3$ GHz, and pump rate $w = 1$ kHz.

structure to V_i^q capturing all single up or down jumps, after removing the higher terms W_2 and defining $\epsilon = \sqrt{2}s_2/s_1$. The θ -dependence in the term proportional to s_2 is the effect of the tensor component $\hat{T}^{(2)}$ in the polarizability tensor.

4.4.8 Results

The master equation (4.42) can be integrated using the numerical approximation method developed in Chapter 3 for Caesium with $F = 4$, meaning 9 hyperfine levels. The resulting reduced steady state density matrix of two atoms gives access to expectation values, e.g., polarization and atom-atom correlations, measurable by the norm of the second-order density matrix cumulant. One can immediately see that the behavior in the Caesium system with 9 levels shown in Fig. 4.15 is very similar to Fig. 4.10 the three level model in Sec. 4.3. The main reason for the good agreement is of course the choice of the simplified jump operators (4.8), which capture the dominant θ dependence of the full jump operators (4.44). The simplified three level system model in Sec. 4.3 lacks the following properties of the full master equation (4.42) resulting in the small differences:

- (i) The effective spontaneous emission rate $\gamma_{\text{eff}} \sum_{\omega} \sum_{i=1}^N \mathcal{D} [V_i^z(\omega)] \rho$ is θ dependent, because the jump operators $V_i^z(\omega)$ are θ dependent. Since the norm of $V_i^z(-\Omega_Z)$ is decreasing for increasing θ from 0° to 90° , the polarization will increase, as one can see in the range of non-correlated atoms for the approximate range of 45° to 50° in Fig. 4.15.
- (ii) The jump operators $V_i^z(\omega)$ contain in general non-zero elements for all $\omega/\Omega_Z \in \{-2, -1, 0, 1, 2\}$. However the jumps $\omega/\Omega_Z = \pm 1$ are dominant because of the small prefactor of the tensor polarizability

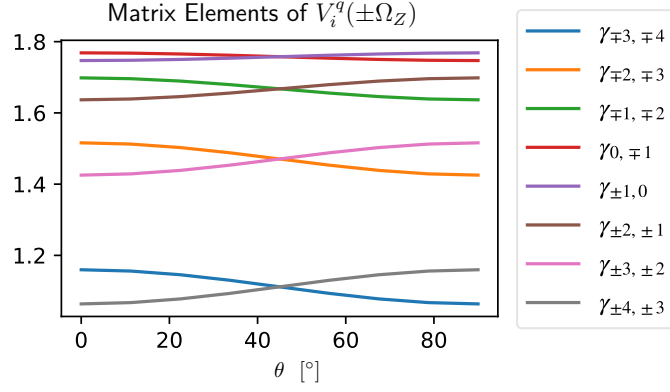


Figure 4.16: Transition rates $\gamma_{n\pm 1,n} = \langle n \pm 1 | V_i^q(\pm\Omega_Z) | n \rangle$ versus the angle θ for $F = 4$ with the parameters given in Fig. 4.15. The rates show a similar θ dependence as in the simplified three level model in Fig. 4.9, but their absolute value is also dependent on the hyperfine level m .

(see Sec. 4.4.7.3) and explain the good agreement with the three level system model in Sec. 4.3.

- (iii) The jump operators $V_i^q(\mp\Omega_Z)$ induce transitions between neighboring hyperfine levels and have θ dependent transition strengths $\gamma_{m,n} = \langle m | V_i^q(\pm\Omega_Z) | n \rangle$, see Fig. 4.16. Each neighboring level pair $n - 1, n$ has a structurally identical θ dependence as in the simplified model, see Fig. 4.8. However the transition rates for different transitions $\gamma_{n-1,n}$, $\gamma_{n,n+1}$ and even the up-down ratios $\gamma_{n-1,n}/\gamma_{n,n-1}$, $\gamma_{n,n+1}/\gamma_{n+1,n}$ are not equal. Because they all have a similar θ dependence, multiple transitions can fulfill the superradiant condition (4.3) and we expect multiple transitions contribute to the superradiance at the same time. An independent indication of which transitions are involved in the superradiance is the population distribution over the different hyperfine levels plotted in Fig. 4.17. For uncorrelated atoms around $\theta \approx 45^\circ$ the single-atom up jumps dominate, due to the pumping rate w , giving an exponential population distribution. For $\theta = 0^\circ$ Fig. 4.17 shows the approximately flat distribution for $m \geq 0$, indicating that all upper transitions have net collective down jumps balancing the single-atom up jumps dominantly created by the pumping rate w . This implies that all transitions between levels $m \geq 0$ are radiating collectively enhanced, i.e., are superradiant. For $\theta = 90^\circ$ one has an inverted behavior: The population of the upper levels is almost exponential, while the lower levels $m \leq 0$ show a flat distribution. In the lower levels the collective down jumps are balancing the single-atom up jumps, meaning the transitions between the levels $m \leq 0$ are radiating superradiantly.

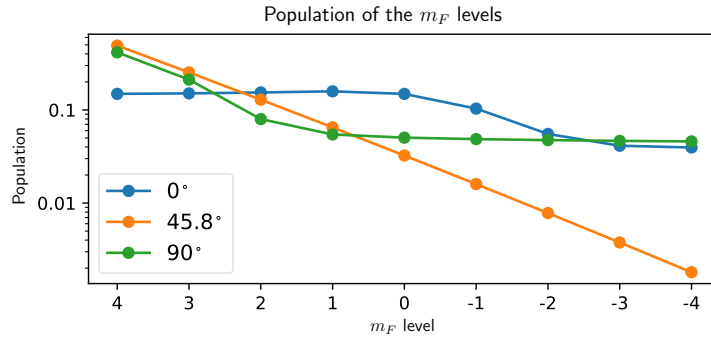


Figure 4.17: Population distribution for different angles $\theta = 0^\circ, 45.8^\circ, 90^\circ$ versus the hyperfine levels m with the parameters given in Fig. 4.15. The lines connecting the dots are meant as a guide for the eye. The uncorrelated atoms at $\theta = 45.8^\circ$ show an exponential distribution of the levels, consistent with up and down rates independent on the level m . For $\theta = 0^\circ$ the upper transitions become superradiant, meaning also the collective down jump rate shifts the population to lower levels canceling the single-atom up jumps and resulting in an almost flat population distribution for $m \geq 0$. For $\theta = 90^\circ$ the lower transitions are superradiant competing with the single-atom up jumps, giving an almost flat distribution for $m \leq 0$.

4.5 SUMMARY

Our goal was to understand collective effects – namely superradiance – in an ensemble of alkali metal atoms being probed and pumped continuously and orthogonally. While it was clear from [18, 41] how to theoretically build a superradiant laser, it does not show how superradiance, wanted or unwanted, changes the behavior of ensembles of atoms with more than two levels. To understand the behavior of commonly used atoms – alkali metal atoms – we introduced the generalized superradiant laser in Sec. 4.2, and the idealized alkali metal atom with three levels and simplified dynamics in Sec. 4.3.

The generalized superradiant laser in Sec. 4.2 gives a condition for the superradiant regime (4.2) and makes it clear, that there are two Lorentz peaks with identical linewidth in the spectrum (see Fig. 4.5) while their amplitude depends on the rate ratio of collective down and up jumps. It also allowed us to vary the collective up jump rate giving a polarization and correlation dependence in Fig. 4.4, which agrees qualitatively well with the numerical results between 0° and 45° of the Caesium ensemble in Fig. 4.15.

A more complete picture gives the idealized alkali metal atom with three levels in Sec. 4.3. It captures the most important parts of master equation (4.42) and made it clear that the angle θ of the linear polarization of the probe laser tunes the collective jump operators, such that the superradiant condition is only satisfiable on the upper transition for $0^\circ \leq 45^\circ$, and only for the lower transition for $45^\circ \leq 90^\circ$. The angle θ therefore allows to control which transition is superradiant. The numerical results

of polarization and atom-atom correlation in Fig. 4.10 agree very well with the ones of the Caesium ensemble in Fig. 4.15.

To analyze the behavior of the Caesium ensemble we derived master equation (4.42) involving several adiabatic eliminations. We could numerically integrate the resulting symmetric atom-only master equation including low order atom-atom correlations using the cumulant expansion method derived in Chapter 3. The population of the different levels in Fig. 4.17 show that, due to the abundance of levels with similar rates, multiple transitions are contributing to the superradiant emission at the same time.

In Chapter 2 we studied the synchronization behavior of the superradiant laser in different configurations. We have learned that synchronization of superradiant lasers can be achieved also unidirectionally and is fundamentally a classical effect. Both will be very relevant for a future network of active atomic clocks — being nothing else than superradiant lasers — with the capability of surpassing traditional atomic clocks based on a reference laser probing atoms with the Ramsey protocol. The obvious step to generalize our findings is to consider not only two frequency detuned ensembles, but atomic ensembles with Gaussian distributions of frequencies. So far unclear but very relevant is amplitude damping loss between two active atomic clocks. In a network with closed cycles delay times and stability in time are difficult but necessary to take into account.

In Chapter 4 we discussed how superradiance plays an important role in off-resonantly probed atomic ensembles in steady state. This included the full level-scheme of alkali metal atoms and atom-atom correlations responsible for the observed collective effects. Contrary to previous work in the field of off-resonantly probed atomic ensembles creating entanglement [72], which could be used in repeaters, we treat collective effects in a self-consistent manner having an effect on the emitted light *and* the atomic state. This is especially relevant if the collective effects are strong, as one desires for entanglement creation. Based on the findings in this part of the thesis one could extend the discussion to a repeater setup with, e.g., two atomic ensembles with energetically inverted hyperfine levels or a hybrid setup consisting of an atomic ensemble and a mechanical oscillator.

The intermediate Chapter 3 is doubtlessly the one which could significantly ease future theoretical analysis of collective effects in a wide variety of systems. We cast the known cumulant expansion and approximation method into a new formalism — a basis independent form — which allows deriving an approximate evolution equation and two-time correlation functions for a whole class of master equations. The discussed class of symmetric master equations with up to two-subsystem Hamiltonians, and local and collective jump operators encompasses many relevant systems, which were explored only to very low atom numbers due to the polynomially increasing dimensionality of the total Hilbert space, and the complicated basis-dependent cumulant expansion and approximation. There are so many exciting possibilities to extend our discussion, it is difficult to judge which of the following ones are most important.

- If the truncation order needs to be $\gtrsim 10$ the presented formalism requires a density matrix of dimension d^{20} , which is challenging for a common desktop PC even for two-level systems, where $d = 2$. If higher correlations are needed even computer clusters will quickly become insufficient due to the exponential scaling of the reduced density matrix dimension with the cutoff order. However the re-

duced density matrix contains only the information of a symmetric system and can therefore be reduced to parameters scaling polynomially in cutoff order. A scheme combining efficient polynomial scaling and the basis-independent cumulant approximation would significantly improve the power of the presented method.

- In our discussion we explicitly derived two-time correlation functions and only outlined how to get arbitrary multi-time correlation functions. This generalization can be done in a straightforward manner, but requires some combinatorial effort to express the hierarchy of evolution equations of objects ρ_n^{trunc} , $\omega_n^{\text{trunc}}(\tau)$ and higher orders involving multiple times in a unified framework.
- The expansion of density matrices into density matrix cumulants works for all density matrices regardless of symmetry and even for non-identical subsystems. We applied this expansion to symmetric systems, which allowed us to approximate the density matrix of $n + 1$ subsystems by the density matrix of n subsystems. One could apply the expansion also to another important class of master equations: translation invariant master equations.
- One can extend the formalism for symmetric systems to treat an even larger class of symmetric master equations. One way to relax the requirements is to allow $2k$ subsystem interaction Hamiltonians and allow quasi-local collective jump operators $\sum_{p \in S(N)} \otimes_{i=1}^k V_{p(i)}$ involving clusters of k atoms. We restricted our discussion to $k = 1$.
- The presented formalism could be generalized to encompass composite systems, each with their own symmetry, e.g., the composite system of two symmetric systems or the composite of one symmetric system and one system with no symmetry. This would allow to apply the method to the important case of repeater-type setups, e.g., [72].

Atomic ensembles interacting with light are a powerful tool for future technology, such as quantum repeaters, active atomic clocks, and magnetometers. Using not only the single-atom but the collective properties of the ensemble in the steady state can lead to fascinating new possibilities, as was demonstrated for the superradiant laser. This thesis contributes to the understanding of synchronization of superradiant lasers, to superradiance in ensembles of multi-level atoms, and especially to the theoretical description of correlations by introducing the basis-independent density matrix cumulants and their application to approximate the evolution of symmetric systems.

Part I

APPENDIX

A.1 THE PROJECTOR METHOD

The projector method [33, 5.1.2] is such a crucial method used throughout this thesis that we will go through its derivation step by step. We start from a master equation of the form

$$\dot{\rho}_{AB}(t) = (L_A + L_B + L_{AB}) \rho_{AB}(t)$$

where L_A , L_B , and L_{AB} are time-independent superoperators acting on systems A , B , and both, respectively. Our goal is to derive an evolution equation for the reduced density matrix

$$\rho_A(t) = \text{Tr}_B [\rho_{AB}(t)]$$

of system A . We assume

- (i) there exists a unique state ρ_B^{ss} fulfilling $L_B \rho_B^{ss} = 0$.
- (ii) the interaction term is such that $PL_{AB}P = 0$ holds.

The crucial assumption throughout this method is that the evolution of L_{AB} is much slower than the evolution L_B , which is also called weak coupling assumption. We can now define the projector

$$P := \lim_{t \rightarrow \infty} e^{L_B t}$$

projecting any state ρ_{AB} such, that system B is in the steady state. In the following discussion we will not consider infinite long times, but times t long compared to the evolution of L_B allowing us to approximate

$$P \approx e^{L_B t}.$$

In the case of a tensor structure between systems A and B the action of the projector can be written as

$$v(t) := P \rho_{AB}(t) = \text{Tr}_B [\rho_{AB}(t)] \otimes \rho_B^{ss}.$$

We also define the complement projection $Q := \mathbb{1} - P$ with $w(t) := Q \rho_{AB}(t)$, which allows to write the complete density matrix of systems A and B as

$$\rho_{AB}(t) = v(t) + w(t).$$

The following properties (some of them trivial) are handy in the following calculation:

- (i) $[P, L_A] = 0$
- (ii) $[Q, L_A] = [\mathbb{1} - P, L_A] = [P, L_A] = 0$
- (iii) $PL_B = L_B P = 0$
- (iv) $QL_B = L_B Q = L_B$, that means also $[Q, L_B] = 0$
- (v) $PQ = QP = 0$
- (vi) $P^2 = P$ and $Q^2 = Q$

A.1.0.1 *Integration*

The evolution equations for v and w are

$$\begin{aligned}\dot{v}(t) &= P(L_A + L_B + L_{AB})(P + Q)\rho_{AB}(t) \\ &= L_A v(t) + PL_{AB}w(t)\end{aligned}\quad (\text{A.1})$$

$$\begin{aligned}\dot{w}(t) &= Q(L_A + L_B + L_{AB})(P + Q)\rho_{AB}(t) \\ &= QL_{AB}v(t) + (L_A + L_B + QL_{AB})w(t).\end{aligned}\quad (\text{A.2})$$

We formally solve the second equation

$$\begin{aligned}w(t) &= e^{(L_A + L_B + QL_{AB})t} \left(w(0) + \int_0^t d\tau e^{-(L_A + L_B + QL_{AB})\tau} QL_{AB}v(\tau) \right) \\ &\approx e^{(L_A + L_B + QL_{AB})t} \int_0^t d\tau e^{-(L_A + L_B + QL_{AB})\tau} QL_{AB}v(\tau) \\ &= \int_0^t d\tau e^{(L_A + L_B + QL_{AB})(t-\tau)} QL_{AB}v(\tau) \\ &= \int_0^t dt' e^{(L_A + L_B + QL_{AB})t'} QL_{AB}v(t-t')\end{aligned}\quad (\text{A.3})$$

where we approximated

$$\begin{aligned}e^{(L_A + QL_{AB} + L_B)t} w(0) &\approx e^{(L_A + L_B)t} w(0) \\ &= e^{L_A t} e^{L_B t} w(0) \\ &\approx e^{L_A t} P w(0) \\ &= 0,\end{aligned}$$

due to the fast evolution of L_B compared to L_{AB} . We plug (A.3) into (A.1) giving

$$\dot{v}(t) = L_A v(t) + PL_{AB} \int_0^t dt' e^{(L_A + L_B + QL_{AB})t'} QL_{AB}v(t-t'). \quad (\text{A.4})$$

A.1.0.2 *Weak coupling Approximation*

We assumed that the system B is weakly coupled to A meaning the superoperators L_{AB} contains a parameter $\epsilon \ll 1$, such that for $\epsilon \rightarrow 0$ the coupling of both systems vanishes. To demonstrate the following approximation we replace L_{AB} by ϵL_{AB} and keep only the leading order ϵ^2 significantly simplifying (A.4)

$$\begin{aligned}\dot{v}(t) &= L_A v(t) + \epsilon^2 PL_{AB} \int_0^t dt' e^{(L_A + L_B + \epsilon QL_{AB})t'} QL_{AB}v(t-t') \\ &\approx L_A v(t) + \epsilon^2 PL_{AB} \int_0^t dt' e^{(L_A + L_B)t'} QL_{AB}v(t-t')\end{aligned}\quad (\text{A.5})$$

A.1.0.3 Extending the integral limit

The damping rate κ in L_B exponentially suppresses any contribution of the integrand for times $t > 1/\kappa$, such that we can extend the integral limit to infinity

$$\dot{v}(t) = L_A v(t) + PL_{AB} \int_0^\infty dt' e^{(L_A+L_B)t'} QL_{AB}(t-t')v(t-t') \quad (\text{A.6})$$

where we absorbed ϵ again in L_{AB} .

A.1.0.4 Markov approximation

We can integrate (A.6) in lowest order, meaning no coupling,

$$v(t-t') = e^{-t'L_A}v(t')$$

which removes the dependence of $\dot{v}(t)$ on previous times when plugged back into (A.6)

$$\dot{v}(t) = L_A v(t) + PL_{AB} \int_0^\infty dt' e^{(L_A+L_B)t'} QL_{AB}e^{-L_A t'} v(t').$$

We can consider this removal of the ‘‘memory’’ as a Markov approximation, which is in this case derived from the weak coupling approximation.

A.1.0.5 Final equation

We can now trace out system B and get a compact evolution equation of system A .

$$\dot{\rho}_A(t) = L_A \rho_A(t) + \text{Tr}_B \left[L_{AB} \int_0^\infty d\tau e^{(L_A+L_B)\tau} QL_{AB}e^{-L_A\tau} \rho_A(t) \otimes \rho_B^{ss} \right] \quad (\text{A.7})$$

A subtle but important point is that this equation in general does not give a physical evolution of system A . For non-vanishing L_A one has to be able to apply the Rotating Wave Approximation to guarantee (A.7) is a master equation [34, p. 132,133].

SYNCHRONIZATION OF SUPERRADIANT LASERS

B.1 COMPLETE DERIVATION FOR THE BIDIRECTIONAL SYNCHRONIZATION USING A CLASSICAL CHANNEL

In this section we give a complete derivation of the results presented in Section 2.3.2. The system (see Fig. 2.9) is comprised out of two one-sided cavities, with decay rate $\tilde{\kappa}$ and are measured with ideal heterodyne measurements. The measurement results are then used by ideal lasers to recreate the measured coherent state with a certain gain. This can then be injected through the fully reflecting mirror by considering the limit of vanishing transmission and infinitely large laser gain resulting in a constant amplitude of the injected signal. Since measurement and feedback are symmetric, they realize a symmetric classical coupling channel between both cavities. To describe the system we use the unconditional feedback master equation (2.15) twice. Once with the measurement operator $\hat{s}_{\hat{a}} = \sqrt{\tilde{\kappa}}\hat{a}$ with cavity decay rate $\tilde{\kappa}$ and feedback operators $\hat{F}_{\pm}^{\hat{b}} = g_{\pm}\hat{b} + g_{\pm}^*\hat{b}^{\dagger}$, and then with the measurement operator $\hat{s}_{\hat{b}} = \sqrt{\tilde{\kappa}}\hat{b}$ and feedback operator $\hat{F}_{\pm}^{\hat{a}} = g_{\pm}\hat{a} + g_{\pm}^*\hat{a}^{\dagger}$, where $g_{+} := g_{-}/i$. Without loss of generality we can define the feedback strength as $g_{-} := -\zeta\sqrt{\tilde{\kappa}}$ with $\zeta \in [0, \infty)$ giving the master equation in a rotating frame:

$$\begin{aligned} \dot{\rho} = & -i \left[\frac{\Omega}{2} (J_A^+ \hat{a} + J_B^+ \hat{b} + h.c.) + \frac{\delta}{2} (J_A^z - J_B^z), \rho \right] \\ & + w \sum_{\substack{T \in \{A, B\} \\ i \in \{1..N\}}} \mathcal{D} [\hat{\sigma}_{T,i}^+] \rho + \tilde{\kappa} \mathcal{D} [\hat{a} + \zeta \hat{b}] \rho + \zeta^2 \tilde{\kappa} \mathcal{D} [\hat{b}^{\dagger}] \rho \\ & + \tilde{\kappa} \mathcal{D} [\hat{b} + \zeta \hat{a}] \rho + \zeta^2 \tilde{\kappa} \mathcal{D} [\hat{a}^{\dagger}] \rho. \end{aligned}$$

B.1.0.1 Stability

First it is important to recognize the stability regime of this feedback for the parameters $\tilde{\kappa}$ and ζ . One might think of the case where the feedback is effectively larger than the measurement result, giving in a net amplification and diverging amplitudes of the cavity fields. The dynamics of the expectation values

$$\frac{d}{dt} \begin{pmatrix} \langle \hat{a} \rangle \\ \langle \hat{b} \rangle \end{pmatrix} = -\frac{\tilde{\kappa}}{2} \begin{pmatrix} 1 & \zeta \\ \zeta & 1 \end{pmatrix} \begin{pmatrix} \langle \hat{a} \rangle \\ \langle \hat{b} \rangle \end{pmatrix} \quad (\text{B.1})$$

including only the fields is a stable system, if and only if all eigenvalues $-\frac{1}{2}\tilde{\kappa}(1 \pm \zeta)$ are negative. This gives the stability condition $\zeta < 1$. Furthermore (B.1) shows that for $\zeta = 0$ the fields \hat{a}, \hat{b} are completely decoupled, while for $\zeta \lesssim 1$ the fields couple strongly.

B.1.0.2 *Adiabatic elimination*

Using the reparameterization $\hat{c}_+ := (\hat{b} - \hat{a})/\sqrt{2}$ and $\hat{c}_- := (\hat{b} + \hat{a})/\sqrt{2}$ the Lindblad operators decouple and drive the fields \hat{c}_\pm into a thermal product state. Following the adiabatic elimination in this reparameterization we get the master equation for the atoms only

$$\begin{aligned} \dot{\rho} = & \frac{\delta}{2i} [J_A^z - J_B^z, \rho] + \sum_{\substack{T \in \{A, B\} \\ i \in \{1..N\}}} w \mathcal{D} \left[\hat{\sigma}_{T,i}^+ \right] \rho + \sum_{s=\pm} \frac{\Omega^2}{2\kappa_s} \times \\ & \times \left((1 + \bar{n}_s) \mathcal{D} [J_A^- - sJ_B^-] + \bar{n}_s \mathcal{D} [J_A^+ - sJ_B^+] \right) \rho, \end{aligned} \quad (\text{B.2})$$

where $\kappa_\pm := \tilde{\kappa} (1 \pm \zeta)$ and $\bar{n}_\pm := \zeta^2 / (4(1 \pm \zeta))$.

B.1.0.3 *Coupling parameterization*

Two free parameters $\tilde{\kappa}$ and ζ remain in (B.2). We would like however to have one free parameter tuning between decoupled cavities and strongly coupled cavities simulating the setup in section 2.2.1. We can fix the remaining free parameter $\tilde{\kappa}$ using the dynamics of the expectation value

$$\begin{aligned} \frac{d}{dt} \langle \hat{\sigma}_A^+ \rangle = & \langle \hat{\sigma}_A^+ \rangle \sum_{s=\pm} \frac{\Omega^2}{4\kappa_s} ((N-1) \langle \hat{\sigma}^z \rangle - 1 - 2\bar{n}_s) \\ & + \langle \hat{\sigma}_A^+ \rangle \frac{i\delta - w}{2} - \langle \hat{\sigma}_B^+ \rangle \langle \hat{\sigma}^z \rangle N \sum_{s=\pm} \frac{s\Omega^2}{4\kappa_s}, \end{aligned} \quad (\text{B.3})$$

where we factorized the mean field $\langle \hat{\sigma}^z \rangle$, and compare it to the dynamics for uncoupled cavities and strongly coupled cavities as in Section 2.2.1.

UNCOUPLED, $\zeta = 0$ (B.3) simplifies to:

$$\frac{d}{dt} \langle \hat{\sigma}_A^+ \rangle = \langle \hat{\sigma}_A^+ \rangle \left(\frac{\Omega^2}{\tilde{\kappa}} ((N-1) \langle \hat{\sigma}_A^z \rangle - 1) - w + i\delta \right) / 2$$

This can be compared to the top left matrix element of (2.11) in Sec. 2.2.2, since (2.11) is was derived using the quantum regression theorem and holds identically also for the dynamics of $(\langle \hat{\sigma}_A^+ \rangle, \langle \hat{\sigma}_B^+ \rangle)^T$. Considering a shifted frequency detuning $\pm\delta/2$ restricts $\tilde{\kappa}(\zeta = 0) = \kappa$.

STRONGLY COUPLED, $\zeta \rightarrow 1$ The coefficients in (B.3) should be identical to the top left matrix element of (2.5) in Sec. 2.2.1 for all variables scaling with the system size N . This gives the restriction for $\zeta \rightarrow 1$:

$$\tilde{\kappa}(\zeta) = \frac{\kappa}{2(1 - \zeta)}.$$

For ζ very close to unity the term not scaling with system size,

$$\langle \hat{\sigma}_A^+ \rangle \sum_{s=\pm} \frac{\Omega^2}{4\kappa_s} (-1 - 2\bar{n}_s),$$

diverges and becomes dominant. This noise term grows $\propto (1 - \zeta)^{-1}$ when ζ approaches the stability border and is negligible for completely decoupled systems and large N .

MEDIUM COUPLING Satisfying both extreme cases discussed before we can choose in between:

$$\tilde{\kappa}(\xi) := \frac{\kappa}{(1-\xi)(1+\xi)}. \quad (\text{B.4})$$

B.1.0.4 Steady state

From master equation (B.2) with the parameterization (B.4) we can calculate the dynamics of the expectation values of $\langle \hat{\sigma}^z \rangle, \langle \hat{\sigma}_1^+ \hat{\sigma}_2^- \rangle, \langle \hat{\sigma}_A^+ \hat{\sigma}_B^- \rangle$

$$\begin{aligned} \partial_t \langle \hat{\sigma}^z \rangle &= w(1 - \langle \hat{\sigma}^z \rangle) - \gamma - \langle \hat{\sigma}^z \rangle \gamma \zeta \\ &\quad - 2\gamma (\langle \hat{\sigma}_1^+ \hat{\sigma}_2^- \rangle (N-1) + \xi N \text{Re} [\langle \hat{\sigma}_A^+ \hat{\sigma}_B^- \rangle]) \\ \partial_t \langle \hat{\sigma}_1^+ \hat{\sigma}_2^- \rangle &= \langle \hat{\sigma}_1^+ \hat{\sigma}_2^- \rangle (-w + \gamma(N-2) \langle \hat{\sigma}^z \rangle - \gamma \zeta) \\ &\quad + \frac{\gamma}{2} \langle \hat{\sigma}^z \rangle (1 + \zeta \langle \hat{\sigma}^z \rangle + 2N\xi \text{Re} [\langle \hat{\sigma}_A^+ \hat{\sigma}_B^- \rangle]) \\ \partial_t \langle \hat{\sigma}_A^+ \hat{\sigma}_B^- \rangle &= \langle \hat{\sigma}_A^+ \hat{\sigma}_B^- \rangle (\gamma(N-1) \langle \hat{\sigma}^z \rangle - \gamma \zeta - w + i\delta) \\ &\quad + \frac{\gamma}{2} \zeta \langle \hat{\sigma}^z \rangle \left(2 \langle \hat{\sigma}^z \rangle \zeta (\xi^4 - \xi^2 + 2)^{-1} + 1 \right) \\ &\quad + \gamma \zeta \langle \hat{\sigma}^z \rangle \langle \hat{\sigma}_1^+ \hat{\sigma}_2^- \rangle (N-1) \end{aligned} \quad (\text{B.5})$$

with $\zeta := (\xi^4 - \xi^2 + 2) / (2(1 - \xi^2))$ and factorized $\langle \hat{\sigma}^z \rangle$ from all occurring correlation functions, giving a closed system of equations. The steady state can now simply be calculated setting all time-derivatives equal to zero. These algebraic equations can be solved numerically or analytically, while filtering out the stable solution. One might try the limit $\xi \rightarrow 1$ to approach the coupling in Section 2.2.1, only to discover that the term ζ , playing the role of a noise term, diverges. One recovers the equations of [19], when disregarding the relation between ζ and ξ and setting $\zeta = \xi = 1$, which shows that the quantum coupling has no inherent coupling noise.

B.1.0.5 Analysis and comparison of the Lorentz peak width

Analog to Section 2.2.1 we can extract the information of the Lorentz peaks from the two-time correlation functions. They can be obtained by using (B.3) and the quantum regression theorem giving a differential equation system similar to (2.5), which can be easily solved. The two-time correlation functions consist out of linear combinations of exponential functions $\exp\left(-\frac{1}{2}(\Gamma_1 \pm x_1)\tau\right)$ with $x_1 = \sqrt{(\gamma N \xi \langle \hat{\sigma}^z \rangle)^2 - \delta^2}$ and $\Gamma_1 = w - \gamma(N-1) \langle \hat{\sigma}^z \rangle + \gamma \zeta$. The width of the Lorentz curve is nothing else but the real part $\Gamma = \text{Re}[\Gamma_1 \pm x_1]$. To analyze the linewidth Γ we solve the system (B.5) up to leading order in $1/N$ giving:

$$\langle \hat{\sigma}^z \rangle = \begin{cases} \text{Min}\left(1, \frac{w - \sqrt{w^2 \xi^2 - \delta^2 (1 - \xi^2)}}{N \gamma (1 - \xi^2)}\right), & 0 \leq \delta < w \xi \\ \text{Min}\left(1, \frac{w}{N \gamma}\right), & \delta \geq w \xi \end{cases}. \quad (\text{B.6})$$

Plugging (B.6) back into $\Gamma = \text{Re}[\Gamma_1 \pm x_1]$ gives

$$\Gamma / \gamma = \zeta + \begin{cases} \frac{w - \sqrt{w^2 \xi^2 - \delta^2 (1 - \xi^2)}}{N \gamma (1 - \xi^2)}, & 0 \leq \delta < w \xi \\ \frac{w}{N \gamma}, & \delta \geq w \xi \end{cases},$$

which is valid in the superradiant regime, i.e. upper bounded by $\langle \hat{\sigma}^z \rangle < 1$ using (B.6).

For the plots of the relevant functions and their analysis we refer to Section 2.3.2.

COLLECTIVE EFFECTS IN ATOMIC ENSEMBLES
INTERACTING WITH LIGHT

C.1 SCATTERING ELIMINATION RELATIONS

In the calculation of Sec. 4.4.3 we insert the formal solution of $\hat{a}_{k,\lambda}(t)$ (4.22) into the spontaneous emission mode $\tilde{\mathbf{E}}_{se}^-(\mathbf{r}_j, t)$ (4.17) and apply the Markov approximation, which is based on the atomic operators varying slowly compared to optical frequencies. This gives

$$\begin{aligned}
& \tilde{\mathbf{E}}_{se}^-(\mathbf{r}_j, t) - \tilde{\mathbf{E}}_{se,free}^-(\mathbf{r}_j, t) \\
&= \frac{i}{\hbar} \sum_{\lambda} \int_{\bar{b}} d\mathbf{k} \rho_{\omega}^2 \mathbf{e}_{k,\lambda} \sum_{i=1}^N e^{i\mathbf{k}(\mathbf{r}_i - \mathbf{r}_j)} \times \\
&\quad \times \int_0^t d\tau e^{i(\omega_k - \omega_L)(t-\tau)} \mathbf{e}_{k,\lambda}^{\dagger} \sum_{F' \in \mathbb{F}'} \mathbf{d}_{i,F'F}^+(\tau) \\
&\stackrel{(i)}{\approx} \frac{i}{\hbar} \sum_{\lambda} \int_{\bar{b}} d\mathbf{k} \rho_{\omega} \mathbf{e}_{k,\lambda} \mathbf{e}_{k,\lambda}^{\dagger} \rho_{\omega} \int_0^t d\tau e^{i(\omega_k - \omega_L)(t-\tau)} \sum_{F' \in \mathbb{F}'} \mathbf{d}_{j,F'F}^+(\tau) \\
&\stackrel{(ii)}{\approx} \frac{i\rho_{\omega_L}^2 \omega_L^2}{\hbar c^3} \sum_{\lambda} \int_{\bar{b}} d\Omega \mathbf{e}_{k_L,\lambda} \mathbf{e}_{k_L,\lambda}^{\dagger} \times \\
&\quad \times \int_0^t d\tau \int_0^{\infty} d\omega e^{i(\omega - \omega_L)(t-\tau)} \sum_{F' \in \mathbb{F}'} \mathbf{d}_{j,F'F}^+(\tau) \\
&\stackrel{(iii)}{\approx} \frac{i\rho_{\omega_L}^2 \omega_L^2}{\hbar c^3} \frac{8\pi^2}{3} \sum_{F' \in \mathbb{F}'} \mathbf{d}_{j,F'F}^+(t) \\
&= i\hbar\gamma' \sum_{F' \in \mathbb{F}'} \mathbf{d}_{j,F'F}^+(t)
\end{aligned}$$

where we used in step (i) that the phases $e^{i\mathbf{k}(\mathbf{r}_i - \mathbf{r}_j)}$ are rapidly oscillating and vanish on average due the low density of atoms, i.e., $n\lambda_a^3 \ll 1$. In step (ii) we assumed that the emitted frequency ω is close to the probe laser frequency $\omega \approx \omega_L$ with a frequency-independent coupling. In step (iii) we used the relations

$$\sum_{\lambda} \int_{\bar{b}} d\Omega \mathbf{e}_{k_L,\lambda} \mathbf{e}_{k_L,\lambda}^{\dagger} \approx \frac{8\pi}{3} \mathbb{1}, \tag{C.1}$$

for cutout cone with infinitesimal opening angle $\vartheta \ll 1$, and

$$\begin{aligned}
& \int_0^t d\tau \int_0^\infty d\omega e^{i(\omega-\omega_L)(t-\tau)} \sum_{F' \in \mathbb{F}'} \mathbf{d}_{j,F'F}^+(\tau) \\
& \approx 2\pi \int_0^t d\tau \delta(t-\tau) \sum_{F' \in \mathbb{F}'} \mathbf{d}_{j,F'F}^+(\tau) \\
& = \pi \sum_{F' \in \mathbb{F}'} \mathbf{d}_{j,F'F}^+(t)
\end{aligned} \tag{C.2}$$

where we assumed $\mathbf{d}_{j,F'F}^+(\tau)$ varies slowly on the optical timescale $1/\omega_L$.

C.2 GAUGING THE ELECTRIC FIELD OF THE CAVITY

In Sec. 4.4.4 we replaced the forward scattering mode $\tilde{\mathbf{E}}_{\text{fwd}}^-(\mathbf{r}_i, t)$ composed of the continuum of free space modes $\hat{a}_{\mathbf{k},\lambda}^+$ with wave vectors \mathbf{k} included in the cone-like set b with a fast decaying cavity mode \hat{a} . To be an equivalent description we have to gauge the electric field per cavity photon ρ_{fwd} (see (4.24)) such that the atom-bath coupling strength is identical to the previous free-space case (see (4.21)). For this we will proceed with the following steps:

SEC. C.2.1 Derive the formal solution for the free space modes.

SEC. C.2.2 Derive the formal solution for the bath modes to which the cavity couples.

SEC. C.2.3 Compare both solutions fixing the electrical field per cavity photon ρ_{fwd} .

Having eliminated the spontaneous emission modes in Sec. 4.4.3 we start from the master equation

$$\begin{aligned}
\dot{\rho} &= \frac{1}{i\hbar} [H_A + H_{\hat{a}} + H_{A\hat{a}}, \rho] + \sum_{k=1}^3 \mathcal{D}[L_{A,i,k}] \rho \\
H_{A\hat{a}} &= \sum_{i=1}^N \left(\tilde{\mathcal{E}}^-(\mathbf{r}_i, t) + \tilde{\mathbf{E}}_{\text{fwd}}^-(\mathbf{r}_i, t) \right)^t \sum_{F' \in \mathbb{F}'} \mathbf{d}_{i,F'F}^- + h.c.
\end{aligned} \tag{C.3}$$

C.2.1 Free space

In the following thesis we will only consider identical atom-light coupling such that it is sufficient to formally place all atoms at $\mathbf{r} = 0$ and describe the forward scattered light mode

$$\begin{aligned}
\tilde{\mathbf{E}}_{\text{fwd}}^-(z=0, t) &= \int_b d\omega \sqrt{\frac{\hbar\omega}{4\pi\epsilon_0 c A}} \hat{a}_\omega^+ e^{-i\omega t} \mathbf{e}_q \\
&\approx \rho_{1d} \mathbf{e}_q \int_b d\omega \hat{a}_\omega^+ e^{-i\omega t}
\end{aligned}$$

with a one-dimensional continuum of modes \hat{a}_ω^+ , where $[\hat{a}_\omega, \hat{a}_{\omega'}^+] = \delta(\omega - \omega')$ [33, (5.3.2)], and we approximated $\omega \approx \omega_L$ due to the integration

over the narrow frequency band b around ω_L , and the flat coupling $\sqrt{\frac{\hbar\omega}{4\pi\epsilon_0 c A}} \approx \frac{\rho_c}{\sqrt{2\pi}} =: \rho_{1d}$. According to master equation (C.3) the free space mode with annihilation operators \hat{a}_ω evolves as

$$\begin{aligned} \frac{d}{dt}\hat{a}_\omega &= \frac{i}{\hbar} [H_{\hat{a}} + H_{A\hat{a}}, \hat{a}_\omega] \\ &= -i\omega\hat{a}_\omega - \frac{i}{\hbar} \sum_{i=1}^N \rho_{1d} e^{-i\omega_L t} \mathbf{e}_q^t \sum_{F' \in \mathbb{F}'} \mathbf{d}_{i,FF'}^-(t) \end{aligned}$$

with the formal solution

$$\hat{a}_\omega(t) = e^{-i\omega t} \hat{a}_\omega(0) - e^{-i\omega t} \frac{i}{\hbar} \rho_{1d} \int_0^t d\tau e^{i(\omega - \omega_L)\tau} \mathbf{e}_q^t \sum_i \sum_{F' \in \mathbb{F}'} \mathbf{d}_{i,FF'}^-(\tau). \quad (\text{C.4})$$

The second term contains the coupling strength given by ρ_{1d} .

C.2.2 Cavity

To describe the evolution of the free space bath modes \hat{b}_ω we start from a coherent cavity bath coupling [33, p. 5.3.1]

$$\begin{aligned} \dot{\rho} &= \frac{1}{i\hbar} [H_A + H_{\text{sys}}^{\text{temp}} + H_{\text{bath}}^{\text{temp}} + H_{\text{int}}^{\text{temp}}, \rho] + \sum_{k=1}^3 \mathcal{D}[L_{A,i,k}] \rho \\ &+ \kappa \mathcal{D}[\hat{a}] \rho \end{aligned} \quad (\text{C.5})$$

with

$$\begin{aligned} H_{\text{sys}}^{\text{temp}} &= \hbar\omega_{\hat{a}} \hat{a}^\dagger \hat{a} + H_{A\hat{a}} \\ H_{\text{bath}}^{\text{temp}} &= \hbar \int d\omega \omega \hat{b}_\omega^\dagger \hat{b}_\omega \\ H_{\text{int}}^{\text{temp}} &= i\hbar \int d\omega \kappa(\omega) (\hat{b}_\omega^\dagger \hat{a} - \hat{b}_\omega \hat{a}^\dagger) \\ \tilde{\mathbf{E}}_{\text{fwd}}^-(z=0, t) &= \rho_{\text{fwd}} \hat{a}^\dagger e^{-i\omega_{\hat{a}} t} \mathbf{e}_q, \end{aligned}$$

where $[\hat{b}(\omega), \hat{b}^\dagger(\omega')] = \delta(\omega - \omega')$ and we approximate a frequency independent coupling $\kappa(\omega) \approx \sqrt{\frac{\kappa}{2\pi}}$. The cavity mode decays much faster than the evolution of the atomic dipole operator $\mathbf{d}_{i,FF'}^-$. The relevant timescale is however the atomic evolution such that we consider only times t fulfilling

$$t\kappa \gg 1. \quad (\text{C.6})$$

We formally solve for the bath modes

$$\hat{b}_\omega(t) = e^{-i\omega t} \hat{b}_\omega(0) + \kappa(\omega) \int_0^t d\tau e^{-i\omega(t-\tau)} \hat{a}(\tau) \quad (\text{C.7})$$

which, plugged into the evolution of the cavity mode \hat{a} , give the quantum Langevin equation [33, (5.3.26)]

$$\begin{aligned} \frac{d}{dt}\hat{a}(t) &= -\frac{\kappa}{2}\hat{a}(t) + \frac{i}{\hbar} \left[H_{sys}^{temp}, \hat{a}(t) \right] - \sqrt{\kappa}\hat{b}_{in}(t) \\ &= -\left(\frac{\kappa}{2} + i\omega_{\hat{a}}\right)\hat{a}(t) - \sqrt{\kappa}\hat{b}_{in}(t) \\ &\quad - \frac{i}{\hbar}\rho_{fwd}e^{-i\omega_{\hat{a}}t} \sum_i \sum_{F' \in \mathbb{F}'} e_q^{\dagger} \mathbf{d}_{i,FF'}^{-}(t) \end{aligned}$$

where $\hat{b}_{in}(t) = \frac{1}{\sqrt{2\pi}} \int d\omega e^{-i\omega t} \hat{b}_{\omega}(0)$ and $[\hat{b}_{in}(t), \hat{b}_{in}^{\dagger}(t')] = \delta(t-t')$. We can integrate this differential equation

$$\begin{aligned} \hat{a}(t) &= e^{-(\frac{\kappa}{2} + i\omega_{\hat{a}})t} \hat{a}(0) - \int_0^t ds \left\{ \sqrt{\kappa} e^{-(\frac{\kappa}{2} + i\omega_{\hat{a}})s} \hat{b}_{in}(t-s) \right. \\ &\quad \left. + e^{-\frac{\kappa}{2}s - i\omega_{\hat{a}}t} \frac{i}{\hbar} \rho_{fwd} \sum_i \sum_{F' \in \mathbb{F}'} e_q^{\dagger} \mathbf{d}_{i,FF'}^{-}(t-s) \right\} \\ &\stackrel{(i)}{\approx} - \left(\sqrt{\kappa} \hat{b}_{in}(t) + e^{-i\omega_{\hat{a}}t} \frac{i}{\hbar} \rho_{fwd} \sum_i \sum_{F' \in \mathbb{F}'} e_q^{\dagger} \mathbf{d}_{i,FF'}^{-}(t) \right) \int_0^t ds e^{-\frac{\kappa}{2}s} \\ &\stackrel{(ii)}{\approx} -\frac{2}{\kappa} \left(\sqrt{\kappa} \hat{b}_{in}(t) + e^{-i\omega_{\hat{a}}t} \rho_{fwd} \frac{i}{\hbar} \sum_i \sum_{F' \in \mathbb{F}'} e_q^{\dagger} \mathbf{d}_{i,FF'}^{-}(t) \right) \quad (C.8) \end{aligned}$$

where we used assumption (C.6) repeatedly. In (i) we neglected the initial state $\hat{a}(0)$ because of the exponential decay $\exp(-\frac{\kappa}{2}t)$ and approximated the atomic evolution to be constant $\mathbf{d}_{i,FF'}^{-}(t-s) = \mathbf{d}_{i,FF'}^{-}(t)$ in the kernel of the integral. This is valid because only times s fulfilling $s \lesssim 1/\kappa$ can contribute significantly to the integral, because the exponential decay suppresses the rest. The same argument holds for the slow evolution of the input signal \hat{b}_{in} which we approximated as $\hat{b}_{in}(t-s) \approx \hat{b}_{in}(t)$. In (ii) we evaluated the integral $\int_0^t ds \exp(-\frac{\kappa}{2}s) \approx -\frac{2}{\kappa}$ also using assumption (C.6).

We can now plug the cavity evolution (C.8) into the formal solution of the bath modes (C.7) giving us the solution of the bath modes coupling directly to the atoms

$$\begin{aligned} \hat{b}_{\omega}(t) &= e^{-i\omega t} \hat{b}_{\omega}(0) - \kappa(\omega) \int_0^t d\tau e^{-i\omega(t-\tau)} \frac{2}{\kappa} \times \\ &\quad \times \left(e^{-i\omega_{\hat{a}}\tau} \rho_{fwd} \frac{i}{\hbar} \sum_i \sum_{F' \in \mathbb{F}'} e_q^{\dagger} \mathbf{d}_{i,FF'}^{-}(\tau) + \sqrt{\kappa} \hat{b}_{in}(\tau) \right) \\ &= -e^{-i\omega t} \hat{b}_{\omega}(0) - \sqrt{\frac{2}{\kappa\pi}} e^{-i\omega t} \rho_{fwd} \frac{i}{\hbar} \times \\ &\quad \times \int_0^t d\tau e^{i(\omega - \omega_{\hat{a}})\tau} \sum_i \sum_{F' \in \mathbb{F}'} e_q^{\dagger} \mathbf{d}_{i,FF'}^{-}(\tau) \quad (C.9) \end{aligned}$$

c.2.3 Comparison

We compare the coupling strength of (C.4) and (C.9), which fixes ρ_{fwd} to

$$\rho_{fwd} = \sqrt{\frac{\kappa\pi}{2}}\rho_{1d} = \frac{\sqrt{\kappa}}{2}\rho_c. \quad (\text{C.10})$$

BIBLIOGRAPHY

- [1] P. Shor. "Polynomial-Time Algorithms for Prime Factorization and Discrete Logarithms on a Quantum Computer." In: *SIAM Review* 41.2 (Jan. 1, 1999), pp. 303–332. DOI: 10.1137/S0036144598347011.
- [2] G. Wendin. "Quantum information processing with superconducting circuits: a review." In: *Reports on Progress in Physics* 80.10 (2017), p. 106001. DOI: 10.1088/1361-6633/aa7e1a.
- [3] Jay M. Gambetta, Jerry M. Chow, and Matthias Steffen. "Building logical qubits in a superconducting quantum computing system." In: *npj Quantum Information* 3.1 (Jan. 13, 2017), p. 2. DOI: 10.1038/s41534-016-0004-0.
- [4] Philipp Schindler et al. "A quantum information processor with trapped ions." In: *New Journal of Physics* 15.12 (2013), p. 123012. DOI: 10.1088/1367-2630/15/12/123012.
- [5] H. Häffner, C. F. Roos, and R. Blatt. "Quantum computing with trapped ions." In: *Physics Reports* 469.4 (Dec. 1, 2008), pp. 155–203. DOI: 10.1016/j.physrep.2008.09.003.
- [6] Mario Krenn, Mehul Malik, Thomas Scheidl, Rupert Ursin, and Anton Zeilinger. "Quantum Communication with Photons." In: *Optics in Our Time*. 2016, pp. 455–482. DOI: 10.1007/978-3-319-31903-2_18.
- [7] H. J. Kimble. *The quantum internet*. Nature. June 18, 2008. URL: <https://www.nature.com/articles/nature07127>.
- [8] Sreraman Muralidharan, Linshu Li, Jungsang Kim, Norbert Lütkenhaus, Mikhail D. Lukin, and Liang Jiang. "Optimal architectures for long distance quantum communication." In: *Scientific Reports* 6 (Feb. 15, 2016), p. 20463. DOI: 10.1038/srep20463.
- [9] Ye Wang, Mark Um, Junhua Zhang, Shuoming An, Ming Lyu, Jing-Ning Zhang, L.-M. Duan, Dahyun Yum, and Kihwan Kim. "Single-qubit quantum memory exceeding ten-minute coherence time." In: *Nature Photonics* 11.10 (Oct. 2017), pp. 646–650. DOI: 10.1038/s41566-017-0007-1.
- [10] Holger P. Specht, Christian Nölleke, Andreas Reiserer, Manuel Uphoff, Eden Figueroa, Stephan Ritter, and Gerhard Rempe. "A single-atom quantum memory." In: *Nature* 473.7346 (May 2011), pp. 190–193. DOI: 10.1038/nature09997.
- [11] Nicolas Sangouard, Christoph Simon, Hugues de Riedmatten, and Nicolas Gisin. "Quantum repeaters based on atomic ensembles and linear optics." In: *Reviews of Modern Physics* 83.1 (Mar. 21, 2011), pp. 33–80. DOI: 10.1103/RevModPhys.83.33.
- [12] Lu-Ming Duan, J. I. Cirac, P. Zoller, and E. S. Polzik. "Quantum Communication between Atomic Ensembles Using Coherent Light." In: *Physical Review Letters* 85.26 (Dec. 25, 2000), pp. 5643–5646. DOI: 10.1103/PhysRevLett.85.5643.

- [13] W. Tittel, M. Afzelius, T. Chanelière, R. L. Cone, S. Kröll, S. A. Moiseev, and M. Sellars. “Photon-echo quantum memory in solid state systems.” In: *Laser & Photonics Reviews* 4.2 (Feb. 17, 2010), pp. 244–267. DOI: 10.1002/lpor.200810056.
- [14] Klemens Hammerer, Anders S. Sørensen, and Eugene S. Polzik. “Quantum interface between light and atomic ensembles.” In: *Reviews of Modern Physics* 82.2 (Apr. 5, 2010), pp. 1041–1093. DOI: 10.1103/RevModPhys.82.1041.
- [15] Frank Verstraete, Michael M. Wolf, and J. Ignacio Cirac. “Quantum computation and quantum-state engineering driven by dissipation.” In: *Nature Physics* 5.9 (Sept. 2009), pp. 633–636. DOI: 10.1038/nphys1342.
- [16] R. H. Dicke. “Coherence in Spontaneous Radiation Processes.” In: *Physical Review* 93.1 (Jan. 1, 1954), pp. 99–110. DOI: 10.1103/PhysRev.93.99.
- [17] M. Gross and S. Haroche. “Superradiance: An essay on the theory of collective spontaneous emission.” In: *Physics Reports* 93.5 (Dec. 1982), pp. 301–396. DOI: 10.1016/0370-1573(82)90102-8.
- [18] D. Meiser, Jun Ye, D. R. Carlson, and M. J. Holland. “Prospects for a Millihertz-Linewidth Laser.” In: *Physical Review Letters* 102.16 (Apr. 20, 2009), p. 163601. DOI: 10.1103/PhysRevLett.102.163601.
- [19] Minghui Xu, D. A. Tieri, E. C. Fine, James K. Thompson, and M. J. Holland. “Synchronization of Two Ensembles of Atoms.” In: *Physical Review Letters* 113.15 (Oct. 6, 2014), p. 154101. DOI: 10.1103/PhysRevLett.113.154101.
- [20] Alexander Roth and Klemens Hammerer. “Synchronization of active atomic clocks via quantum and classical channels.” In: *Physical Review A* 94.4 (Oct. 21, 2016), p. 043841. DOI: 10.1103/PhysRevA.94.043841.
- [21] Alexander Roth and Klemens Hammerer. “ n -th order correlations in symmetric systems.” In: *to be published* (2018).
- [22] Christoffer B. Møller, Rodrigo A. Thomas, Georgios Vasilakis, Emil Zeuthen, Yeghishe Tsaturyan, Mikhail Balabas, Kasper Jensen, Albert Schliesser, Klemens Hammerer, and Eugene S. Polzik. “Quantum back-action-evading measurement of motion in a negative mass reference frame.” In: *Nature* 547.7662 (July 12, 2017), pp. 191–195. DOI: 10.1038/nature22980.
- [23] D. V. Kupriyanov, O. S. Mishina, I. M. Sokolov, B. Julsgaard, and E. S. Polzik. “Multimode entanglement of light and atomic ensembles via off-resonant coherent forward scattering.” In: *Physical Review A* 71.3 (Mar. 29, 2005), p. 032348. DOI: 10.1103/PhysRevA.71.032348.
- [24] Hanna Krauter, Christine A. Muschik, Kasper Jensen, Wojciech Wasilewski, Jonas M. Petersen, J. Ignacio Cirac, and Eugene S. Polzik. “Entanglement Generated by Dissipation and Steady State Entanglement of Two Macroscopic Objects.” In: *Physical Review Letters* 107.8 (Aug. 17, 2011), p. 080503. DOI: 10.1103/PhysRevLett.107.080503.

- [25] Alexander Roth, Kirill Tikhonov, Rodrigo A. Thomas, Eugene S. Polzik, and Klemens Hammerer. "Collective Effects in atomic ensembles interacting with light." In: *to be published* (2018).
- [26] T. L. Nicholson et al. "Systematic evaluation of an atomic clock at 2×10^{-18} total uncertainty." In: *Nature Communications* 6 (Apr. 21, 2015), p. 6896. DOI: 10.1038/ncomms7896.
- [27] Andrew D. Ludlow, Martin M. Boyd, Jun Ye, E. Peik, and P. O. Schmidt. "Optical atomic clocks." In: *Reviews of Modern Physics* 87.2 (June 26, 2015), pp. 637–701. DOI: 10.1103/RevModPhys.87.637.
- [28] Ali Al-Masoudi, Sören Dörscher, Sebastian Häfner, Uwe Sterr, and Christian Lisdat. "Noise and instability of an optical lattice clock." In: *Physical Review A* 92.6 (Dec. 8, 2015), p. 063814. DOI: 10.1103/PhysRevA.92.063814.
- [29] D. Meiser and M. J. Holland. "Intensity fluctuations in steady-state superradiance." In: *Physical Review A* 81.6 (June 25, 2010), p. 063827. DOI: 10.1103/PhysRevA.81.063827.
- [30] Justin G. Bohnet, Zilong Chen, Joshua M. Weiner, Dominic Meiser, Murray J. Holland, and James K. Thompson. "A steady-state superradiant laser with less than one intracavity photon." In: *Nature* 484.7392 (Apr. 5, 2012), pp. 78–81. DOI: 10.1038/nature10920.
- [31] Justin G. Bohnet, Zilong Chen, Joshua M. Weiner, Kevin C. Cox, and James K. Thompson. "Active and passive sensing of collective atomic coherence in a superradiant laser." In: *Physical Review A* 88.1 (July 17, 2013), p. 013826. DOI: 10.1103/PhysRevA.88.013826.
- [32] Matthew A. Norcia, Matthew N. Winchester, Julia R. K. Cline, and James K. Thompson. "Superradiance on the milliHertz linewidth strontium clock transition." In: *arXiv:1603.05671 [physics, physics:quant-ph]* (Mar. 17, 2016).
- [33] C. W Gardiner and P Zoller. *Quantum noise: a handbook of Markovian and non-Markovian quantum stochastic methods with applications to quantum optics*. Berlin; New York, 2004.
- [34] Heinz-Peter Breuer and Francesco Petruccione. *The Theory of Open Quantum Systems*. Oxford, Mar. 29, 2007.
- [35] Andreas Angerer, Kirill Streltsov, Thomas Astner, Stefan Putz, Hitoshi Sumiya, Shinobu Onoda, William J. Munro, Kae Nemoto, Jörg Schmiedmayer, and Johannes Majer. "Superradiant Hybrid Quantum Devices." In: *arXiv:1802.07100 [cond-mat, physics:physics, physics:quant-ph]* (Feb. 20, 2018).
- [36] Dave Bacon, Isaac L. Chuang, and Aram W. Harrow. "Efficient Quantum Circuits for Schur and Clebsch-Gordan Transforms." In: *Physical Review Letters* 97.17 (Oct. 27, 2006), p. 170502. DOI: 10.1103/PhysRevLett.97.170502.
- [37] A. Young. "On Quantitative Substitutional Analysis." In: *Proceedings of the London Mathematical Society* s1-33.1 (Nov. 1900), pp. 97–145. DOI: 10.1112/plms/s1-33.1.97.

- [38] Michael Gegg and Marten Richter. "Efficient and exact numerical approach for many multi-level systems in open system CQED." In: *New Journal of Physics* 18.4 (2016), p. 043037. DOI: 10.1088/1367-2630/18/4/043037.
- [39] Leonard Mandel and Emil Wolf. *Optical coherence and quantum optics*. Cambridge, 1995.
- [40] Howard J. Carmichael. *An Open Systems Approach to Quantum Optics: Lectures Presented at the Université Libre De Bruxelles, October 28 to November 4, 1991*. Berlin ; New York, May 1993.
- [41] D. Meiser and M. J. Holland. "Steady-state superradiance with alkaline-earth-metal atoms." In: *Physical Review A* 81.3 (Mar. 29, 2010), p. 033847. DOI: 10.1103/PhysRevA.81.033847.
- [42] Joshua M. Weiner, Kevin C. Cox, Justin G. Bohnet, and James K. Thompson. "Phase Synchronization between Two Superradiant Lasers." In: *arXiv:1503.06464* (Mar. 22, 2015).
- [43] P. Kómár, E. M. Kessler, M. Bishof, L. Jiang, A. S. Sørensen, J. Ye, and M. D. Lukin. "A quantum network of clocks." In: *Nature Physics* 10.8 (Aug. 2014), pp. 582–587. DOI: 10.1038/nphys3000.
- [44] O. V. Zhirov and D. L. Shepelyansky. "Quantum synchronization and entanglement of two qubits coupled to a driven dissipative resonator." In: *Physical Review B* 80.1 (July 24, 2009), p. 014519. DOI: 10.1103/PhysRevB.80.014519.
- [45] Tony E. Lee and H. R. Sadeghpour. "Quantum Synchronization of Quantum van der Pol Oscillators with Trapped Ions." In: *Physical Review Letters* 111.23 (Dec. 4, 2013), p. 234101. DOI: 10.1103/PhysRevLett.111.234101.
- [46] A. Mari, A. Farace, N. Didier, V. Giovannetti, and R. Fazio. "Measures of Quantum Synchronization in Continuous Variable Systems." In: *Physical Review Letters* 111.10 (Sept. 6, 2013), p. 103605. DOI: 10.1103/PhysRevLett.111.103605.
- [47] Stefan Walter, Andreas Nunnenkamp, and Christoph Bruder. "Quantum Synchronization of a Driven Self-Sustained Oscillator." In: *Physical Review Letters* 112.9 (Mar. 6, 2014), p. 094102. DOI: 10.1103/PhysRevLett.112.094102.
- [48] Tony E. Lee, Ching-Kit Chan, and Shenshen Wang. "Entanglement tongue and quantum synchronization of disordered oscillators." In: *Physical Review E* 89.2 (Feb. 12, 2014), p. 022913. DOI: 10.1103/PhysRevE.89.022913.
- [49] Bihui Zhu, Johannes Schachenmayer, Minghui Xu, F. Herrera, Juan G. Restrepo, Murray J. Holland, and Ana Maria Rey. "Synchronization of Interacting Quantum Dipoles." In: *New Journal of Physics* 17.8 (Sept. 1, 2015), p. 083063. DOI: 10.1088/1367-2630/17/8/083063.
- [50] J. R. Johansson, P. D. Nation, and Franco Nori. "QuTiP 2: A Python framework for the dynamics of open quantum systems." In: *Computer Physics Communications* 184.4 (Apr. 2013), pp. 1234–1240. DOI: 10.1016/j.cpc.2012.11.019.

- [51] Sebastian G. Hofer, Denis V. Vasilyev, Markus Aspelmeyer, and Klemens Hammerer. "Time-Continuous Bell Measurements." In: *Physical Review Letters* 111.17 (Oct. 22, 2013), p. 170404. DOI: 10.1103/PhysRevLett.111.170404.
- [52] H. M. Wiseman and G. J. Milburn. "Quantum theory of optical feedback via homodyne detection." In: *Physical Review Letters* 70.5 (Feb. 1, 1993), pp. 548–551. DOI: 10.1103/PhysRevLett.70.548.
- [53] H. D. Ursell. "The evaluation of Gibbs' phase-integral for imperfect gases." In: *Mathematical Proceedings of the Cambridge Philosophical Society* 23.6 (Apr. 1927), pp. 685–697. DOI: 10.1017/S0305004100011191.
- [54] Ryogo Kubo. "Generalized Cumulant Expansion Method." In: *Journal of the Physical Society of Japan* 17.7 (July 15, 1962), pp. 1100–1120. DOI: 10.1143/JPSJ.17.1100.
- [55] K. Kladko and P. Fulde. "Geometrical Properties of Cumulant Expansions." In: *arXiv:cond-mat/9709044* (Sept. 3, 1997).
- [56] Heinrich A. M. Leymann, Alexander Foerster, and Jan Wiersig. "Expectation value based cluster expansion." In: *physica status solidi (c)* 10.9 (Sept. 1, 2013), pp. 1242–1245. DOI: 10.1002/pssc.201200711.
- [57] H. A. M. Leymann, A. Foerster, and J. Wiersig. "Expectation value based equation-of-motion approach for open quantum systems: A general formalism." In: *Physical Review B* 89.8 (Feb. 19, 2014), p. 085308. DOI: 10.1103/PhysRevB.89.085308.
- [58] Ryoichi Kikuchi. "A Theory of Cooperative Phenomena." In: *Physical Review* 81.6 (Mar. 15, 1951), pp. 988–1003. DOI: 10.1103/PhysRev.81.988.
- [59] J. M. Sanchez, F. Ducastelle, and D. Gratias. "Generalized cluster description of multicomponent systems." In: *Physica A: Statistical Mechanics and its Applications* 128.1 (Nov. 1, 1984), pp. 334–350. DOI: 10.1016/0378-4371(84)90096-7.
- [60] Mackillo Kira and Stephan W. Koch. *Semiconductor Quantum Optics*. 1 edition. Cambridge ; New York, Apr. 30, 2012.
- [61] Lorenzo Pucci, Analabha Roy, and Michael Kastner. "Simulation of quantum spin dynamics by phase space sampling of Bogoliubov-Born-Green-Kirkwood-Yvon trajectories." In: *Physical Review B* 93.17 (May 4, 2016), p. 174302. DOI: 10.1103/PhysRevB.93.174302.
- [62] G. A. Prataviera and S. S. Mizrahi. "Many-particle Sudarshan-Lindblad equation: mean-field approximation, nonlinearity and dissipation in a spin system." In: *arXiv:1408.4764 [cond-mat, physics:quant-ph]* (Aug. 16, 2014).
- [63] Sebastian Krämer and Helmut Ritsch. "Generalized mean-field approach to simulate the dynamics of large open spin ensembles with long range interactions." In: *The European Physical Journal D* 69.12 (Dec. 1, 2015), p. 282. DOI: 10.1140/epjd/e2015-60266-5.
- [64] T. P. Speed. "Cumulants and Partition Lattices¹." In: *Australian Journal of Statistics* 25.2 (Feb. 1, 1983), pp. 378–388. DOI: 10.1111/j.1467-842X.1983.tb00391.x.

- [65] Peter McCullagh. "Cumulants and Partition Lattices." In: *Selected Works of Terry Speed*. Selected Works in Probability and Statistics. 2012, pp. 277–293. DOI: 10.1007/978-1-4614-1347-9_6.
- [66] Claude A. Pruneau. *Data analysis techniques for physical scientists*. Cambridge, 2017.
- [67] P. McCullagh. *Tensor methods in statistics*. Monographs on statistics and applied probability. London ; New York, 1987.
- [68] Christian Schilling. "The Quantum Marginal Problem." In: *arXiv:1404.1085 [math-ph, physics:quant-ph]* (Apr. 3, 2014).
- [69] Yi-Kai Liu. "Consistency of Local Density Matrices Is QMA-Complete." In: *Approximation, Randomization, and Combinatorial Optimization. Algorithms and Techniques*. Ed. by Josep Díaz, Klaus Jansen, José D. P. Rolim, and Uri Zwick. Berlin, Heidelberg, 2006, pp. 438–449.
- [70] Jones Eric, Travis Oliphant, Pearu Peterson, et al. *SciPy*. 2001.
- [71] John D. Hunter. "Matplotlib: A 2D Graphics Environment." In: *Computing in Science & Engineering* 9.3 (2007), pp. 90–95. DOI: 10.1109/MCSE.2007.55.
- [72] Christine A. Muschik, Eugene S. Polzik, and J. Ignacio Cirac. "Dissipatively driven entanglement of two macroscopic atomic ensembles." In: *Physical Review A* 83.5 (May 17, 2011), p. 052312. DOI: 10.1103/PhysRevA.83.052312.
- [73] Florian Wolfgramm, Alessandro Cerè, Federica A. Beduini, Ana Predojević, Marco Koschorreck, and Morgan W. Mitchell. "Squeezed-Light Optical Magnetometry." In: *Physical Review Letters* 105.5 (July 29, 2010), p. 053601. DOI: 10.1103/PhysRevLett.105.053601.
- [74] Brian Julsgaard. "Brian Julsgaard - PhD." PhD thesis. 2003.
- [75] Klemens Hammerer. "Quantum Information Processing with Atomic Ensembles and Light." PhD thesis. Jan. 31, 2006.
- [76] J. M. Geremia, John K. Stockton, and Hideo Mabuchi. "Tensor polarizability and dispersive quantum measurement of multilevel atoms." In: *Physical Review A* 73.4 (Apr. 24, 2006). DOI: 10.1103/PhysRevA.73.042112.
- [77] Brian Julsgaard, Alexander Kozhekin, and Eugene S. Polzik. "Experimental long-lived entanglement of two macroscopic objects." In: *Nature* 413.6854 (Sept. 27, 2001), pp. 400–403. DOI: 10.1038/35096524.
- [78] J. Borregaard, M. Zugenmaier, J. M. Petersen, H. Shen, G. Vasilakis, K. Jensen, E. S. Polzik, and A. S. Sørensen. "Scalable photonic network architecture based on motional averaging in room temperature gas." In: *Nature Communications* 7 (Apr. 14, 2016), p. 11356. DOI: 10.1038/ncomms11356.
- [79] Daniel A. Steck. *Alkali D Line Data*. Cesium D Line Data. Jan. 2, 2004. URL: <http://steck.us/alkalidata/>.
- [80] Bruce W. Shore. *The theory of coherent atomic excitation*. New York, 1990.

- [81] Rodney Loudon. *The quantum theory of light*. 3rd ed. Oxford science publications. Oxford ; New York, 2000.
- [82] D. M. Brink and G. R. Satchler. *Angular momentum*. Oxford : New York, 1993.
- [83] Florentin Reiter and Anders S. Sørensen. "Effective operator formalism for open quantum systems." In: *Physical Review A* 85.3 (Mar. 9, 2012), p. 032111. DOI: 10.1103/PhysRevA.85.032111.
- [84] Victor V. Albert and Liang Jiang. "Symmetries and conserved quantities in Lindblad master equations." In: *Physical Review A* 89.2 (Feb. 21, 2014), p. 022118. DOI: 10.1103/PhysRevA.89.022118.
- [85] V. Popkov and R. Livi. "Manipulating energy and spin currents in non-equilibrium systems of interacting qubits." In: *New Journal of Physics* 15.2 (2013), p. 023030. DOI: 10.1088/1367-2630/15/2/023030.
- [86] K. Hammerer, M. Aspelmeyer, E. S. Polzik, and P. Zoller. "Establishing Einstein-Poldosky-Rosen Channels between Nanomechanics and Atomic Ensembles." In: *Physical Review Letters* 102.2 (Jan. 12, 2009), p. 020501. DOI: 10.1103/PhysRevLett.102.020501.
- [87] *Quantum Mathematica Add-On* by Jose Luis Gómez-Muñoz. 2016. URL: <http://homepage.cem.itesm.mx/lgomez/quantum/>.